Department of Physics
Indian Institute of Technology Guwahati
Ph.D. Thesis

Study of hysteresis and dynamic phase transition in kinetic Ising ferromagnet on regular, disordered, and fractal lattices

Sourav Chattopadhyay

Supervisor: Prof. Sitangshu Bikas Santra
March, 2021.

Study of hysteresis and dynamic phase transition in kinetic Ising ferromagnet on regular, disordered, and fractal lattices

A thesis submitted by

Sourav Chattopadhyay

to

Indian Institute of Technology Guwahati
in partial fulfillment of the requirements
for the award of the degree of
Doctor of Philosophy in Physics

Department of Physics
Indian Institute of Technology Guwahati
Guwahati - 781039, Assam, India

Statement

The work contained in the thesis, entitled "*Study of hysteresis and dynamic phase transition in kinetic Ising ferromagnet on regular, disordered, and fractal lattices*", has been carried out by me at the Department of Physics, Indian Institute of Technology Guwahati, India, under the supervision of Prof. Sitangshu Bikas Santra. The material of this thesis has not been submitted elsewhere for any other degree.

(Sourav Chattopadhyay)
Department of Physics
Indian Institute of Technology Guwahati
Guwahati - 781039, India

March 06, 2021

Certificate

It is certified that the work contained in the thesis entitled "*Study of hysteresis and dynamic phase transition in kinetic Ising ferromagnet on regular, disordered, and fractal lattices*" by Mr. Sourav Chattopadhyay, a Ph.D. student of the Department of Physics, Indian Institute of Technology Guwahati for the award of Doctor of Philosophy has been carried out under my supervision. This work has not been submitted elsewhere for the award of any degree.

(Prof. Sitangshu Bikas Santra)
Department of Physics
Indian Institute of Technology Guwahati
Guwahati - 781039

March 06, 2021

To my parents...

Acknowledgements

I express my sincere gratitude and indebtedness to my supervisor Prof. Sitangshu Bikas Santra, for his invaluable guidance, constant supervision, creative ideas, and continuous encouragement throughout my research work. I will remain ever grateful to him for his generous assistance in making this thesis possible. I share several memories with him that I will cherish long.

I want to thank my doctoral committee members, Prof. Ananthakrishnan Srinivasan, Prof. Saurabh Basu and Prof. Ashok Kumar Dasmahapatra, for valuable discussions whenever I needed it. I am thankful to other faculty members of the Department of Physics, IIT Guwahati, for their help and encouragement.

I wish to thank the Indian Institute of Technology Guwahati for providing the necessary computational facilities, excellent library, and various computational resources and state of the art sports facility. I am thankful to all the departmental staffs, especially Mr. Basab Bijoy Purkayastha, for his numerous help. My special thanks go to my senior, Dr. Jahir Abbas Ahmed, Dr. Bappadiyta Roy, for helping me in innumerable ways. A special thanks to Dr. Himangsu Bhaumik for helping me to understand various small but essential aspects of my research work and the Biriyani and all those late-night discussions at his place. I want to thank all juniors for their help and cooperations, especially Sagarika, Srikrishna, Sheuly, Karuna, Shilpi, and Sayandeep.

I have been fortunate to have a few fantastic friends who have always extended their helping hand, without whom life would be bleak. My special thanks go to Ashis, Koushik, Ramiz, Kallol, Sudin, Abhijit, Anabil, Rahul, Biswajit, Shibananda and Dr Tapas, for their help and encouragement. I greatly indebted to them for listening to my complaints and frustrations and for believing in me always.

This thesis is dedicated to my parents, my father, Mr Pradip Chattopadhyay and my mother, Mrs Binapani Chattopadhyay. Their unconditional love, support, encouragement to fulfil my dreams, and honest and pointed advice during my graduate life's most challenging stages have helped me complete my degree. I am deeply indebted to my family members for their unconditional love, immense support and constant encouragement.

Finally, I would like to thank the Ministry of Human Resource Development, Government of India, for providing scholarship and financial support to carry out the present thesis work.

- Sourav.

Abstract

The Ising ferromagnet is a bistable system below the critical temperature (T_c) of ferromagnet to paramagnet transition and has two symmetry broken ordered phases. An external oscillating field can push the system to either of the equivalent ordered phases, and the other ordered phase remains metastable. There are two competing time scales present in the system, the time period (P) of the external field and the mean metastable lifetime $\langle\tau\rangle$ of the system. The average metastable lifetime ($\langle\tau\rangle$) of a system is the mean time spent in a metastable phase after a sudden reversal of the static field applied in the system. There exists a critical period P_c, at which the half period ($P_{1/2}$) of the field becomes comparable with $\langle\tau\rangle$, the Ising ferromagnet undergoes a dynamic phase transition (DPT) from dynamic ordered phase (DOP) to dynamic disordered phase (DDP). If the period of the oscillating field is small ($P < P_c$), the system will remain in one of the metastable wells over a full period, and the system is said to be in a DOP. Whereas for a higher period ($P > P_c$), the system will be able to move from one free energy well to the other and vice versa as the field changes sign and the system is said to be in a DDP. The dynamic order parameter or period average magnetization $Q = \frac{1}{P}\int_0^P m(t)dt$ changes from a finite value in DOP to zero in DDP. Also, the asymmetric hysteresis loop in DOP becomes symmetric in DDP. A spontaneous breaking of the symmetry of the hysteresis loop occurs at $P = P_c$.

Such a system is well studied applying pulse as well as sinusoidal fields varying period and keeping temperature fixed and vice verse. However, there exists controversy about the nature of DPT. Once it is claimed to be a discontinuous type phase transition due to stochastic resonance below a tricritical point. In another series of articles, it has been shown that the DPT is a continuous type phase transition and follows finite size scaling (FSS) with the same critical exponents of the 2d zero field equilibrium Ising model. Such an issue is taken afresh in this thesis and, a detailed analysis of DPT in Ising ferromagnet on 2d square lattice is performed on an extended system in the high field regime. A novel technique is developed to analyze

hysteresis loop properties.

Apart from the above issues, the equilibrium Ising ferromagnet, as well as the kinetic Ising ferromagnet, are not well studied on disordered (or site diluted) lattices. The effect of site dilution on Ising ferromagnet is intriguing to explore. At different site dilution concentrations, the magnetic properties of Ising ferromagnet, hysteresis, and DPT are explored in this thesis.

The situation is going to more dramatic if the Ising ferromagnet is defined on a fractal lattice such as percolation cluster or percolation backbone. Both the equilibrium phase transition and DPT are rarely reported in the literature. A thorough investigation has been performed on the nature of phase transition and critical behaviour of the Ising ferromagnet defined on percolation cluster as well as on percolation backbone. Interesting novel results are obtained and reported in this thesis.

The thesis presents extensive Monte Carlo simulation results. Detailed FSS analysis is performed for the data obtained. Systems are studied with various concentrations of disorder, field amplitudes, periods, temperature, and system sizes. Far below the static equilibrium phase transition temperature T_c, DPT is studied either by varying temperature keeping the period fix or varying the period keeping the temperature fixed. A new methodology is developed to determine the hysteresis loop properties.

Contents

Chapter 1

Introduction

A phase is a state of matter in thermodynamic equilibrium. A system can be found in different phases according to the macroscopic conditions viz. pressure, temperature, external field, etc. of the system. An everyday example is ice-water-vapour, three different forms of a collection of H_2O molecules. The phase of a system is often changed by tuning a parameter such as temperature T of the system. Phase transition is observed in a wide variety of systems viz. liquid to gas, paramagnet to ferromagnet, paraelectric to ferroelectric, normal conductor to the superconductor, normal-fluid to superfluid, percolation, and many others. Most of the phase transitions are either first order or second order in nature. The macroscopic properties of the system in the vicinity of the critical point can be obtained by constructing a suitable free energy function of the system. According to Ehrnfest's criteria, nth order phase transition corresponds to the discontinuity or divergence of the nth derivative of the free energy function. Thus, the first derivative of the free energy at the transition point becomes discontinuous in a first order phase transition, whereas the second derivative of the free energy becomes discontinuous or diverges at the transition point or critical point. Criticality refers to the cooperative behaviour of an extended system at a phase transition point.

1.1 Equilibrium Phase transition and Ising Model

The critical behavior in magnetic systems is of central interest in condensed matter physics research [1–4] until today for several reasons, such as complexity in magnetic interaction among the magnetic ions; different materials exhibit varied novel features, etc. The simplest model to capture features of a ferro-to-paramagnetic transition is the spin-1/2 Ising model. The Ising model is a remarkably successful

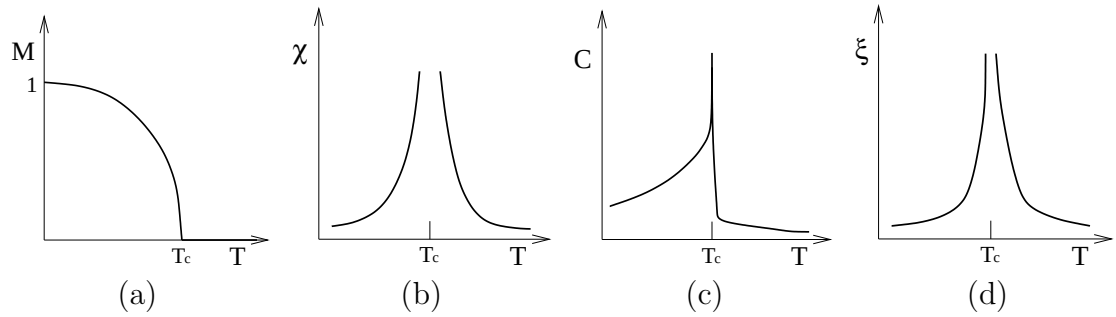

Figure 1.1: Temperature T variation of (a) magnetization M, (b) magnetic susceptibility χ, (c) specific heat C and (d) correlation length ξ.

model to mimic a variety of two states interacting thermodynamic systems for understanding phase transitions in those systems. We briefly present the Ising model on a two-dimensional (2d) square lattice of size L. All the lattice sites are occupied by Ising spins $S_i = \pm 1$ corresponding to up and down spins where i is lattice site index. Each spin interacts with its nearest neighbor spins with ferromagnetic interaction strength $J(> 0)$. The Hamiltonian of the Ising model is given by

$$\mathcal{H} = -J \sum_{\langle ij \rangle} S_i S_j - \mu H \sum_{i}^{L^2} S_i \tag{1.1}$$

where H is a constant external magnetic field, and μ is the magnetic moment associated with each spin. In the absence of an external field ($H = 0$), the model exhibits a second order phase transition at a critical temperature T_c ($k_B T_c/J = 2.269185$) below which long range order appears and above which no long range order exists. The phase with long range order is the ferromagnetic phase, and the phase with no long range order is the paramagnetic phase. The ferromagnetic phase has a non-zero spontaneous magnetization, and the paramagnetic phase has zero spontaneous magnetization.

There exists a well defined prescription in equilibrium statistical mechanics for studying critical phenomena in a magnetic system [5–9]. The characteristic features of a second order phase transition at the critical point are: order parameter continuously goes to zero, response function diverges, fluctuations in spin orientation appear at all length scales, long range order appears in spin-spin correlation (or divergence of correlation length), etc.

The thermodynamic parameters of a magnetic system can be derived from the Gibbs free energy $G(H, T)$ where T is the temperature, and H is the external magnetic field. The spontaneous magnetization M, isothermal susceptibility $\chi(T)$

and specific heat at constant field C_H are defined as $M = -(\partial G/\partial H)_T$, $\chi_T = (\partial M/\partial H)_T = -(\partial^2 G/\partial H^2)_T$ and $C_H = T(\partial S/\partial T)_H = -T(\partial^2 G/\partial T^2)_H$ respectively. There exists a critical temperature T_c below which the system is in the ferromagnetic phase and above in the paramagnetic phase. At $T = T_c$, a second order or continuous phase transition from ferro to paramagnet occurs. The ferromagnetic phase has a net spontaneous magnetization M, whereas it is zero in the paramagnetic phase. As the temperature T is increased from below T_c, the spontaneous magnetization M continuously goes to zero at $T = T_c$, and hence M is the order parameter of the magnetic transition. As $T \to T_c$, the thermodynamic quantities exhibit singularities in the form of power laws. It is customary to study the singular behavior in terms of the reduced temperature ϵ defined as $\epsilon = (T - T_c)/T_c$. The singularities of the thermodynamic quantities are given by:

$$M \sim (-\epsilon)^{\beta}, \chi_T \sim |\epsilon|^{-\gamma} \quad \text{and} \quad \mathrm{C_H} \sim |\epsilon|^{-\alpha} \tag{1.2}$$

where β, γ and α are the critical exponents associated with M, χ_T and C_H respectively. The behavior of these quantities around the critical point is schematically shown in Fig.1.1(a), (b) and (c), respectively. The critical isotherm at $T = T_c$ is given by

$$H \sim M^{\delta} \tag{1.3}$$

where δ is an exponent that describes the degree of the critical isotherm. The correlation between the spins is measured in terms of fluctuations of spin values away from their mean values, and a correlation function $\Gamma(r)$ is defined as

$$\Gamma(r) = \langle s_i s_j \rangle - \langle s_i \rangle \langle s_j \rangle = r^{-(d-2+\eta)} \exp(-r/\xi) \tag{1.4}$$

where r is the distance between s_i and s_j, ξ is the correlation length, d is the space dimension and η is some exponent. The correlation length ξ is the distance between any two up (or down) spins within the same domain. As $T \to T_c$, the correlation length ξ diverges as

$$\xi \sim |\epsilon|^{-\nu} \tag{1.5}$$

where ν is a critical exponent, and ϵ is the reduced temperature. The divergence of correlation length ξ is shown in Fig.1.1(d). Since at the criticality ξ diverges to infinity, the correlation function $\Gamma(r)$ follows a power law decay as

$$\Gamma(r) \sim r^{-\tau} \tag{1.6}$$

where $\tau = d - 2 + \eta$ is the decay exponent.

However, the critical exponents are not all independent. As all the thermodynamic quantities are derived from the Gibbs free energy, the critical exponents must be related to each other, and it is found that only two of them are independent. Considering the Gibbs free energy $G(T, H)$ as a generalized homogeneous function and other hyperscaling, a set of scaling relations are obtained:

$$\beta(\delta - 1) = \gamma, \quad \alpha + 2\beta + \gamma = 2, \quad 2 - \alpha = d\nu \quad \text{and} \quad (2 - \eta)\nu = \gamma \tag{1.7}$$

It has been observed that the critical exponents have identical values if the number of components of the order parameter and the space dimension d of the system are the same. The values of the critical exponents do not depend on the type of interaction or the lattice structure. The values of the critical exponents, the scaling relations among them, and the form of the scaling function then determine the universality class of a system.

Exact results of the 2d Ising model in the absence of external field H were obtained by Onsager [10]. The exact values of the critical exponents of the equilibrium 2d zero field Ising model are given in the table below.

Table 1.1: Critical exponents of 2d Ising model

α	β	γ	δ	ν	η
0	1/8	7/4	15	1	1/4

1.2 Hysteresis and Dynamic Phase Transition

Nonequilibrium phase transitions in interacting many-body systems are far less understood in comparison to its equilibrium counterpart. Equilibrium critical phenomena have well established results for a range of interacting systems, whereas such systems at out of equilibrium situations are difficult to solve. Continuous phase transitions also take place at far from equilibrium situations and are characterized by a set of critical exponents as it is done in equilibrium situations. Absorbing state phase transitions [11, 12] and phase transitions in driven diffusive systems [13, 14] are a few examples of continuous nonequilibrium phase transition. However, the classification of nonequilibrium phase transitions into different universality classes still remains incomplete.

The nonequilibrium phase transition in bistable systems is an interesting field of

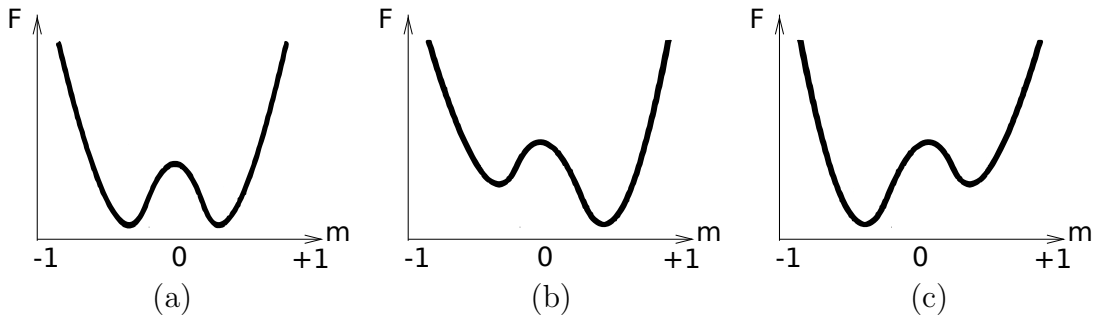

Figure 1.2: Free energy landscape of a bistable system in (a) without any field, (b) a small positive field brings the stable minima corresponding to the positive metastable phase down, and (c) a small negative field lowers the minima corresponding to the negative metastable phase.

research for the last three decades. An external time varying field can drive the system between two metastable phases of the system. The system follows the external field continuously without reaching any equilibrium. The free energy landscape of a bistable system the absence and presence of an external field are depicted in Fig.1.2. A system that undergoes the nonequilibrium phase transition has two competing timescales, the relaxation time of the system, and the time period of the external field. Usually, the system response has some delay while following the field that causes hysteresis. Hysteresis [15] is a characteristic feature of a non-equilibrium dynamical system. Ferromagnets [16–20], ferroelectrics [21, 22], liquid crystals [23], etc, are a few examples that exhibit metastability and hysteresis.

The Ising ferromagnet is a bistable system below the critical temperature (T_c) of ferromagnet to paramagnet transition and has two symmetry broken ordered phases. An external oscillating field can push the system to either of the equivalent ordered phases, and the other ordered phase remains metastable. There are two competing time scales present in the system, the time period (P) of the external field and the mean metastable lifetime $\langle\tau\rangle$ of the system. The average metastable lifetime ($\langle\tau\rangle$) of a system is the mean time spent in a metastable phase after a sudden reversal of the static field applied in the system. The value of $\langle\tau\rangle$ depends on the system size (L), amplitude (h_0) of the applied field, and the temperature (T) of the system [24]. Such a bistable system will try to be in one of the ordered phases for a fixed T and h_0. There exists a critical period P_c, at which the half period ($P_{1/2}$) of the field becomes comparable with $\langle\tau\rangle$, the Ising ferromagnet undergoes a dynamic phase transition (DPT) from dynamic ordered phase (DOP) to dynamic disordered phase (DDP) for the first time. If the period of the oscillating field is small ($P < P_c$), the system will remain in one of the metastable wells over a full period, and the system is said

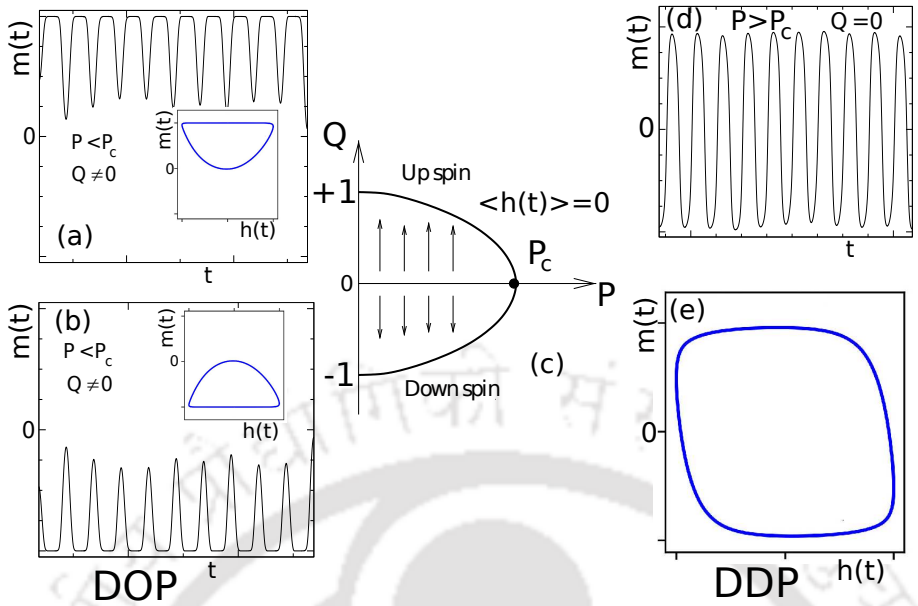

Figure 1.3: Plot of magnetization $m(t)$ with MC time t in DOP, for an initial state (a) all spins up, (b) all spins down, and (d) DDP. The respective asymmetric hysteresis loops in DOP are shown in the inset. The symmetric hysteresis loop in DDP is shown in (e), which is independent of the choice of the initial state. The system does not get enough time for $P_{1/2} < \langle\tau\rangle$ in DOP, and $m(t)$ does not change the sign in a half period. But in DDP $P_{1/2} > \langle\tau\rangle$ and $m(t)$ changes its sign in each cycle. (c) Period averaged magnetization Q is plotted with period P. The Q becomes zero in DDP above P_c, but the Q can have two different values in DOP corresponds to two possible ordered phases. This demonstrative data are obtained on a small lattice of size $L = 128$ for temperature $T = 0.8$, and amplitude of the external magnetic fields $h_0 = 1.0$.

to be in a DOP. Whereas for a higher period ($P > P_c$), the system will be able to move from one free energy well to the other and vice versa as the field changes sign and the system is said to be in a DDP. Different phases of the system are explained in Fig.1.3. In Fig.1.3(a) and (b), the two DOPs corresponding to two metastable states of Ising ferromagnet. In Fig.1.3(a), the magnetization time series is shown when the initial system was in a state of all spins up, and the system was driven by a sinusoidal field of period $P(< P_c)$. It could be seen that the magnetization decreases as the field changes sign, but the external field cannot overturn the whole system before the next cycle starts. As a result, the period average magnetization remains positive.

$$Q = \frac{1}{P}\int_0^P m(t)dt \tag{1.8}$$

However, if the initial system was in a state of all spins down, and the system was by the same field (period $P < P_c$), the magnetization did not become positive, and

the period average magnetization Q remains negative. Thus the system remains in one of the metastable states of the system, the ordered phases. The hysteresis loops are asymmetric in DOP, as shown in the insets of Fig.1.3(a) and (b). On the other hand, irrespective of the initial state configuration, if the system is driven by a sinusoidal field of period $P > P_c$, the magnetization of the system will change sign as the external field changes sign with a phase lag as shown in Fig.1.3(d). The period average magnetization Q becomes zero. The system is in DDP. The hysteresis loop becomes symmetric (Fig.1.3(e)) about the center of the loop. Thus DOP is characterized by finite Q and asymmetric hysteresis loop, whereas the DDP is characterized by zero Q value and symmetric hysteresis loop [24–26]. A spontaneous breaking of symmetry in the hysteresis loop occurs at the critical period $P = P_c$. In Fig.1.3(c), the period average magnetization Q is plotted against the period P. The variation of Q with P of a sinusoidal field ($\langle h(t) \rangle = 0$) is very similar to the variation of m with T at the equilibrium zero field ferro-para phase transition in an Ising system.

An all spin up state has finite positive magnetization in a metastable phase below the critical temperature (T_c) of the system. A droplet of down spins is formed when a small opposite magnetic field is applied. The droplet grows radially with time. Given enough time, the magnetization jumps to a negative value in the other metastable phase. For a very small field (h_0) on a small lattice size, only one supercritical droplet will be formed that will grow and cover the whole lattice. On the other hand, many such supercritical droplets will be formed simultaneously on larger lattices, and consequently, they grow and coalesce [27–32]. The metastable phase in the kinetic Ising model can decay following two different mechanisms. The free energy has a bistable shape below the critical point. The metastable state is the higher minimum point of free energy for a small external field. A critical field by which the metastable minimum disappears is called the spinodal point [33]. A spinodal point is a marginal point between the metastable and unstable regions for a finite system. For $h_0 < h_{DSP}$, the dynamic spinodal field, which depends on T and L, the mean lifetime τ of the metastable phase becomes comparable to the standard deviation of the lifetime distribution. This field regime is known as the stochastic or single-droplet (SD) region as the decay of the metastable phase proceeds by random nucleation of a single critical droplet of the stable phase. On the other hand, for $h_0 > h_{DSP}$, the mean lifetime of the metastable phase becomes much greater than the standard deviation of the lifetime distribution. This field region is called the deterministic or multidroplet (MD) region because of the decay of the metastable

phase proceeds by the nucleation, growth, and coalescence of many droplets of the stable phase [24, 27, 34–37].

1.2.1 Literature survey

Tome and Oliviera first reported non-equilibrium dynamic phase transition [38], solving the master equation governed by the Glauber stochastic process under an external sinusoidal field using the fourth order Runge-Kutta method and replacing the interaction by mean-field approximation. DPT is studied here, varying the temperature T below the critical temperature T_c of the Ising model, keeping the frequency of the external field fixed. It was found that there exists a critical temperature θ_c at which Q becomes zero from a finite non-zero value as T is varied from below θ_c to above θ_c. They also reported a dynamic phase boundary in the field amplitude and temperature phase plane $(h_0 - T)$ where a tricritical point (h_{tr}, T_{tr}) separates discontinuous and continuous phase transitions. It was shown that the transition is of discontinuous for $h_0 > h_{tr}$. However, it was reported later that they did not consider microscopic fluctuations in their master equation which can take the system from one free energy well to the other. Consequently, the magnetization was purely deterministic, and the transition they reported was not a completely true dynamic transition [39]. Rao *et al.* study [40] hysteresis in interacting spin systems in a continuum model specified by Langevin equation in three-dimensional $(\Phi^2)^2$ model with $O(N)$ symmetry in the large-N limit. This model considered thermal fluctuations in order to bring stochasticity under consideration. They employed both mean field calculations and Monte Carlo simulation to study hysteresis loop properties. A scaling relation between hysteresis loop area A, amplitude h_0, and frequency ω of the magnetic field was suggested as $A \sim h_0^{\alpha}\omega^{\beta}$ with $\alpha = \frac{2}{3}$ and $\beta = \frac{1}{3}$ for low amplitude and frequency of the magnetic field. After that, Lo and Pelcovits [41] observe the dynamic transition in the kinetic Ising model in a Monte Carlo study. They analyze hysteresis loops with varied amplitude and frequency in the presence of a sinusoidally oscillating magnetic field and reported the same scaling behavior of hysteresis loop area with field amplitude and frequency. Dhar and Thomas found two different types of scaling form for hysteresis loops at high and low frequency regime under sinusoidal field in N-vector model[42] for space dimension $d > 2$. They also reported critical frequency as a function of h_0. Chakrabarty and Acharyya studied [25] ferromagnetic Ising system solving the mean field equation of motion in space dimension $d = 1$ to 4 as well as using the Monte Carlo method

in the 2 dimension. They studied the variation of magnetization, dynamic order parameter, ac susceptibility, and hysteresis loop area for a range of frequency and field values. They also report the existence of a tricritical point in the detailed phase diagram. After that, Acharyya reported several mean field and Monte Carlo studies on susceptibility [43], critical slowing down, specific heat [44], hysteresis loop area, and dynamic correlation [45–47] in the kinetic Ising model. Initially, the DPT was believed to be discontinuous on the basis of the bimodal distribution of the dynamic order parameter (along with a weak third peak at the center) and negative fourth-order Binder cumulant.

Parallelly in another series of papers, it has been shown that the DPT is a continuous phase transition [24, 34–37, 48–50]. It was shown that the discontinuous transition observed previously was essentially a crossover to stochastic resonance at high field regimes in smaller systems that does not exist in the large systems, and the continuous DPT persists. Stochastic resonance is a phenomenon where a weak periodic signal can be amplified and optimized by the assistance of noise to overcome an energetic activation barrier [51]. In stochastic resonance, the response of the system undergoes resonance-like behavior as a function of the noise level. This claim was based on detailed Monte Carlo simulations and finite size scaling (FSS) analysis. Acharyya further investigated the dynamic phase transition (DPT) in the kinetic Ising model [52] and reported the existence of the stochastic resonance. It was further found that the DPT has the same critical exponents as that of the 2d zero field equilibrium Ising model. Sides *et al.* show the existence of deterministic or multidroplet (MD) and stochastic or single droplet (SD) decay regimes [35] based on droplet theory [34] of decay of metastable phases. They found that the SD and MD regimes depend on temperature, field strength, and system size. They introduce a size dependent spinodal field that separates these two SD and MD regimes. They also investigate amplitude and frequency dependence of the distribution of hysteresis loop area and dynamic order parameter. In another study [36] they report the evolution of hysteresis loops in SD and MD regime. They also report the distribution of the dynamic order parameter becomes a double hump in DOP from a single hump in DDP. Acharyya and Stauffer also reported in a separate study [27] on nucleation in the Ising model in different dimensions. They observed a size dependent crossover from coalescence to nucleation regime in all dimensions.

Park and Pleimling studied the critical behavior of the kinetic Ising model with surface [53]. They found that the bulk system undergoes a continuous non-equilibrium phase transition characterized by exponents of the equilibrium Ising

model, but the nonequilibrium surface exponents do not coincide with those of the equilibrium critical surface. Also, in the three dimensions, the surface phase diagram of the nonequilibrium system differs markedly from that of the equilibrium system. In another DPT study [54] in the three dimensional Ising model under time varying external field Park et al. reported that the the nonequilibrium phase transition belongs to the universality class of the equilibrium three-dimensional Ising model. They determined the critical exponents using finite size scaling.

Buendia and Rikvold reported non-equilibrium phase transition under square wave oscillation [48] using soft Glauber dynamics for which both nucleation and interface propagation are slower and the interfaces are smoother in comparison to the standard Glauber dynamic. They observed a critical point when the half period of the external field is approximately equal to the metastable lifetime of the system, and critical exponents are found to be consistent with the universality class of the two-dimensional equilibrium Ising model. They concluded that DPT is independent of the choice of underlying stochastic dynamics.

E. Vatansever *et al.* reported DPT in ferromagnetic thin-films[55]. They have estimated variations of surface, bulk, and total dynamical order parameters with temperatures for different thickness. They have reported the effects of quenched disorder on the dynamic phase transitions of kinetic spin models in two dimensions[56] in a more recent study.

Many theoretical and numerical studies have been performed in order to understand the origin of DPT and hysteretic response in bistable Ising ferromagnet. Theoretical and numerical studies include mean-field studies [57, 58], time dependent Ginzburg-Landau theory [59, 60] and effective field theory [61]. Buendia and Rikvold studied DPT under pulse field using soft Glauber dynamics [62] and concluded that the nature of DPT remains almost the same irrespective of the underlying stochastic dynamics. Sides *et al.* study finite size scaling and hysteresis in spin-1/2 kinetic Ising model [37, 63], stochastic resonance [24] with dimensionless frequency as the tuning parameter consistent with the droplet theory.

There are several experimental works related to DPT. He and Wang reported [64] dynamic scaling of magnetic hysteresis in mono layers of Fe/Au(001) film. The collapse was found to be consistent with numerical results by Rao [40]. Similar scaling was also reported [65] by Jiang *et al.* in epitaxially grown ultra-thin Co films on a Cu(001) surface, by Suen *et al.* [66] on thin Fe films. Choi *et al.* reported [67] dynamic magnetization reversal behavior of poly-crystalline $Ni_{80}Fe_{20}$ films. They also found the hysteresis loop area can be scaled with certain scaling

relation $A \sim h_o^{\alpha}\Omega^{\beta}T^{-\gamma}$ with $\alpha \approx 0.9$, $\beta \approx 0.8$, and $\gamma \approx 0.38$. So far, these experimental evidence for DPT was limited to qualitative observations of hysteresis loop collapse in studies of hysteresis-loop area scaling. Robb *et al.* presented significantly stronger experimental evidence of the DPT in a $[Co/Pt]_3$ multilayered system with strong perpendicular anisotropy [68]. They measure the out-of-plane magnetization time series to produce non-equilibrium phase diagrams that were found to be very similar to the calculated magnetization time series in simulations in a kinetic Ising model under similar situation. Berger *et al.* studied the time dependent magnetic behavior of uniaxial cobalt films [69] in the vicinity of the dynamic phase transition as a function of the period P and bias H_b of an oscillating magnetic field. They observed the DPT at a critical period P_c. Later, Berger *et al.* reported [70] the existence of anomalous metamagnetic fluctuations in the vicinity of the dynamic phase transition point that did not take place in the corresponding thermodynamic behavior of a ferromagnetic system. Buendia and Rickvold [71] presented a numerical study explaining Berger's finding [70]. They reported that stochastic resonance is responsible for such anomalous behavior with no counterpart in the corresponding thermodynamic phase transition.

1.3 Research motivation and description of chapters

The Ising ferromagnet is a bistable system below the critical temperature (T_c) of ferro to paramagnetic transition and has two symmetry broken ordered phases. Driving such a system by an external sinusoidal field, hysteresis, and dynamic phase transition (DPT) is extensively studied in the literature, as summarized above. However, there exists a long standing controversy that DPT is a discontinuous or continuous type phase transition. In certain cases, characteristic features of discontinuous phase transition such as the bimodal distribution of the dynamic order parameter (along with a weak third peak at the center) and negative fourth-order Binder cumulant appears due to stochastic resonance below a tricritical point. It is, however, shown that the discontinuous transition observed previously was essentially a crossover to stochastic resonance [51] at high field regimes in smaller systems that does not exist in the large systems, and the continuous DPT persists.

Apart from the above issue, the equilibrium Ising ferromagnet, as well as the kinetic Ising ferromagnet, are not well studied on disordered (or site diluted) lattices. The effect of site dilution on Ising ferromagnet is intriguing to explore. At different site dilution concentrations, the magnetic properties of Ising ferromagnet, hysteresis,

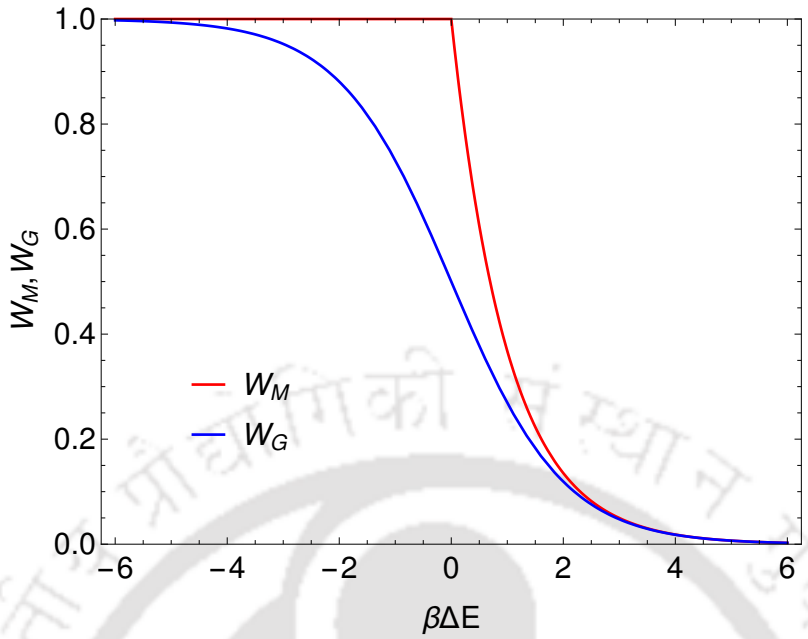

Figure 1.4: Variation of Metropolis (in red) and Glauber (in blue) acceptance probabilities with change in energy ($\Delta E = E_B - E_A$) in a move.

and DPT are explored in this thesis.

The situation is going to more dramatic if the Ising ferromagnet is defined on a fractal lattice such as percolation cluster or percolation backbone. Both the equilibrium phase transition and DPT are rarely reported in the literature. A thorough investigation has been performed on the nature of phase transition and critical behavior of the Ising ferromagnet defined on percolation cluster as well as on percolation backbone. Interesting novel results are obtained and reported in this thesis.

All the static phase transitions are studied using Metropolis single spin flip dynamics [72]. The Metropolis acceptance probability of getting a state B from state A is given by

$$W_{\mathrm{M}}(A \to B) = \mathrm{Min}\left[1, \exp(-\beta(E_B - E_A))\right] \tag{1.9}$$

where, $\beta = 1/(k_B T)$, E_A and E_B are the energy of the states A and B respectively. Glauber dynamics [73] is used to study the DPT on different lattices. The Glauber acceptance probability of getting a state B from state A is

$$W_{\mathrm{G}}(A \to B) = \frac{e^{-\beta(E_B - E_A)}}{1 + e^{-\beta(E_B - E_A)}} \tag{1.10}$$

A comparison of Metropolis and Glauber acceptance probabilities is shown in Fig.1.4. The nature of the transition does not depend on the dynamical rule of evolution.

The dynamical rules allow us to generate an ensemble of configurations for a given thermodynamic condition (h_0, P, and T for the present problem) in a Monte Carlo (MC) simulation following ergodicity and detailed balance condition [74]. Both the Metropolis and the Glauber dynamical rules are very efficient in case of high temperatures. As shown in Fig 1.4 for $\Delta E \leq 0$, the spin flip occurred with unit probability in the case of the Metropolis algorithm. Whereas the spin is flipped with the right Boltzmann weight for the Glauber algorithm. However, these two algorithms follow very different paths through configuration space. In the case of equilibrium phase transition, very often Metropolis algorithm is chosen for its comparatively lower computational cost. In dynamic phase transition (DPT), the Glauber dynamical rule is widely used in low temperatures as the ensemble averaged values are found to be smoother than that of Metropolis algorithm. That is why we preferred to use Glauber dynamics over the Metropolis algorithm. However, there are reports where the Metropolis algorithm is also used to study the DPT.

The thesis presents extensive Monte Carlo [72–75] simulation results. Detailed FSS analysis is performed for the data obtained. Systems are studied with various disorder concentrations, field amplitudes, periods, temperature, and system sizes. Far below the static equilibrium phase transition temperature T_c, DPT is studied either by varying temperature keeping the period fix or varying the period keeping the temperature fixed. A new methodology is developed to determine the hysteresis loop properties.

The thesis will be organized in the following manner:

In Chapter-I, a general introduction to the equilibrium and non-equilibrium phase transition is given. After a brief review of the static equilibrium phase transition, features of dynamic phase transition (DPT) and hysteresis in bistable Ising ferromagnet are discussed. A thorough survey of existing literature is made on the studies of critical phenomena and DPT in magnetic systems. Finally, the problems undertaken in this thesis are proposed and discussed with sufficient motivation.

In chapter-II, hysteresis and DPT in kinetic Ising ferromagnet is studied under a sinusoidal oscillating magnetic field on a regular square lattice in 2-dimensions. DPT is usually studied varying period P of the applied field keeping temperature T fixed far below the critical temperature $T_c = 2.269185$ of the equilibrium 2d zero-field Ising model. However, We study the system keeping the period P and the amplitude h_0 of the field fixed and tuning the temperature T of the system below T_c. Results of extensive Monte Carlo simulation are reported. Hysteresis loop properties and DPT are analyzed by finite size scaling (FSS) analysis.

Diluted or disordered kinetic Ising ferromagnet is considered in Chapter-III. The presence of the disorder adds extra complexity in the magnetic phase transition. This chapter will deal with physical disorder or spin dilution where a few magnetic ions or spins are missing at random or replaced with non-magnetic elements on a regular lattice. Due to the presence of disordered sites (or missing spins), the interactions among the magnetic ions are going to be strongly affected. As a result, the critical behavior of DPT and its hysteresis properties are found to be different from that of the regular lattice. The values of the critical exponents are obtained, and their scaling relations are verified.

In chapter-IV, fractal Ising ferromagnet is considered. Two random fractals, a large spanning percolation cluster obtained at the percolation threshold ($p_c = 0.59278$) and the percolation backbone extracted from the percolation cluster [76–79], are considered for this study. The Ising spins are embedded at the sites of a spanning percolation cluster or that of a percolation backbone obtained on a 2d square lattice. The fractal dimensions of the percolation cluster and the percolation backbone $d_f = 1.89$ and $d_B = 1.64$ respectively [80]. Static magnetic phase transition and DPT are studied on both the fractal Ising ferromagnets. First, the static equilibrium phase transition is studied to get an estimation of the critical temperature (T_c) and the associated critical exponents. The DPT is observed below T_c, where the ferromagnet has two metastable phases. A strong influence of the fractal geometry is observed on the nature of phase transitions and the variation of critical exponents.

Finally, in Chapter-V, an overall summary, conclusions, and future prospects of the field are described. To summarize, this chapter addresses and highlights the findings of the thesis viz. the nature of DPT in a ferromagnetic system under a sinusoidal external field of different amplitudes on several system sizes, the methodology to study DPT from the geometry of hysteresis loops. How random physical disorder affects DPT on a ferromagnetic system and its critical behavior are the central part of this thesis. The fractal geometry and dilution of the lattice sites or spins have a non-trivial impact on the static and dynamic phase transitions and hysteresis.

Chapter 2

Hysteresis and DPT in Kinetic Ising Ferromagnet on $2d$ regular lattices

Dynamic phase transition (DPT) is rigorously studied on regular lattices, and there are many results [24, 25, 27, 34–37, 40–42, 81]. However, there exists a long term controversy on the nature of DPT, whether it is discontinuous or continuous type. In some literature, the DPT is claimed to be a discontinuous type phase transition due to stochastic resonance below a tricritical point [26, 39, 45, 52] as the system displays the bimodal distribution of the dynamic order parameter (along with a weak third peak at the center) and negative fourth-order Binder cumulant. On the other hand, it has also been claimed that the DPT is a continuous type phase transition [49, 50] and follows finite size scaling (FSS) with the same critical exponents of the zero field equilibrium Ising model. Later it was found that the discontinuous transition observed previously was essentially a crossover to stochastic resonance [51] at high field regimes in smaller systems that do not exist in the large systems, and the continuous DPT persists. In most of the cases, the finite-size effect on DPT were studied either by varying the period of the applied sinusoidal field at a fixed temperature [24, 37, 48] or by tuning the temperature of the system under a pulse-field of a fixed period [50].

In this chapter, we study hysteresis and DPT in kinetic Ising ferromagnet on 2d regular square lattice applying a sinusoidal oscillating magnetic field $h(t) = h_0 \sin(2\pi t/P)$. We tune the temperature T of the system (far below the $T_c = 2.269185$ of the equilibrium 2d zero-field Ising model) for a fixed period P and amplitude h_0 of the field. As the temperature T of the system varies, the metastable lifetime $\langle\tau\rangle$ of the system varies accordingly as the value of $\langle\tau\rangle$ depends on T besides system size (L) and amplitude (h_0) of the applied field [24]. The DPT occurs at

a temperature θ_c ($\ll T_c$) when $\langle\tau\rangle$ becomes comparable with the half period $P_{1/2}$ of the applied field. We present the results of an extensive Monte Carlo simulation study of the model on systems of different sizes L. A finite size scaling (FSS) analysis of data has been performed. We aimed to resolve the above issue and try to find the regime of the field intensity and system size with no stochastic resonance. Below we present the model and details of the numerical simulations. First, we will describe the hysteresis loop properties employing a new methodology, and then we characterize the DPT performing a detailed FSS analysis at different field amplitudes h_0.

2.1 Model and Simulation

A kinetic Ising model is developed on a two-dimensional square lattice of size L. All the lattice sites are occupied by Ising spins $S_i = \pm 1$. Each spin can interact with its nearest neighbor spins under periodic boundary condition with ferromagnetic interaction strength $J(> 0)$. An external time varying sinusoidal oscillating magnetic field $h(t)$ given by

$$h(t) = h_0 \sin(2\pi t/P) \tag{2.1}$$

where h_0 is the amplitude and P is the time period of the oscillating field, is applied to the system. The Hamiltonian of the kinetic Ising model under the external field $h(t)$ can be expressed as,

$$\mathcal{H} = -J \sum_{\langle ij \rangle} S_i S_j - h(t) \sum_{i}^{L^2} S_i \tag{2.2}$$

where $\langle ij \rangle$ represents the sum over the nearest neighbors only. The field amplitude h_0 is taken in the unit of J.

In order to equilibrate the system with the heat bath at a temperature T, the system is evolved without magnetic field following Glauber Monte Carlo (MC) single spin-flip dynamics. According to the Glauber [73, 74, 82, 83] MC dynamics, the S_i to $-S_i$ spin-flip acceptance ratio W is given by

$$W(S_i \to -S_i) = \frac{e^{-\Delta E/k_B T}}{1 + e^{-\Delta E/k_B T}} \tag{2.3}$$

where ΔE is the change in energy due to spin flip in the presence of the external field, and k_B is the Boltzmann constant. Assuming $J = 1$, ΔE for a single spin (S_i)

flip at time t can be obtained as

$$\Delta E = 2S_i\Sigma + 2S_i h(t) \tag{2.4}$$

where Σ is the sum of the nearest neighbor spins of the spin S_i. The value of the transition probability $W(S_i \to -S_i)$ is then estimated, setting Boltzmann constant $k_B = 1$ and measuring the temperature T in energy units. A random number z, uniformly distributed between 0 and 1, is called. If $z \leq W(S_i \to -S_i)$, the spin is flipped; otherwise, it remains in the same state.

Extensive Monte Carlo (MC) simulation has been performed following Glauber single spin-flip dynamics on two-dimensional square lattices of size varying from $L = 128$ to $L = 1024$. One MC step corresponds to updating on an average each spin of the system once. The initial state is taken as either all spins up $S_i = +1$ state or all spins down $S_i = -1$ state. The system is iterated for 10^6 MC time steps to thermalize it at a given temperature T in the absence of the external field. A number of equilibrium states with constant magnetization are then generated at a given T in the absence of the external field. As the system achieves a constant magnetization in equilibrium at a given temperature T, the external time-dependent magnetic field $h(t)$ is applied to a randomly chosen equilibrium state at a given temperature T. In a MC step, L^2 spins are randomly chosen and updated using Glauber acceptance ratio W in which ΔE is calculated using the full Hamiltonian (Eq.2.2). One cycle of the applied field of period P consists of P number of MC steps. The system is further evolved to achieve stable dynamical states in the presence of the applied field over 256 cycles, more than 10^5 MC steps, before collecting data. The system is further evolved for another 10^6 MC steps for data collections [37, 49, 50, 71, 84]. Eight randomly chosen equilibrium configurations are taken as initial samples, and measurements are made on the 1024 stable cycles (selected from all over the time series) for each sample. All the dynamical quantities are averaged over the cycles and configurations, leading to an ensemble of size 8192. Simulations are repeated for three values of field amplitudes $h_0 = 1.0$, 2.0 and 3.0.

2.2 Metastable lifetime and critical point

As the mean metastable lifetime $\langle\tau\rangle$ corresponds to the half-period $P_{1/2}$ at the dynamic phase transition point [24], we estimate an approximate critical temperature θ_c of DPT before starting the main simulations. The metastable lifetime is the time

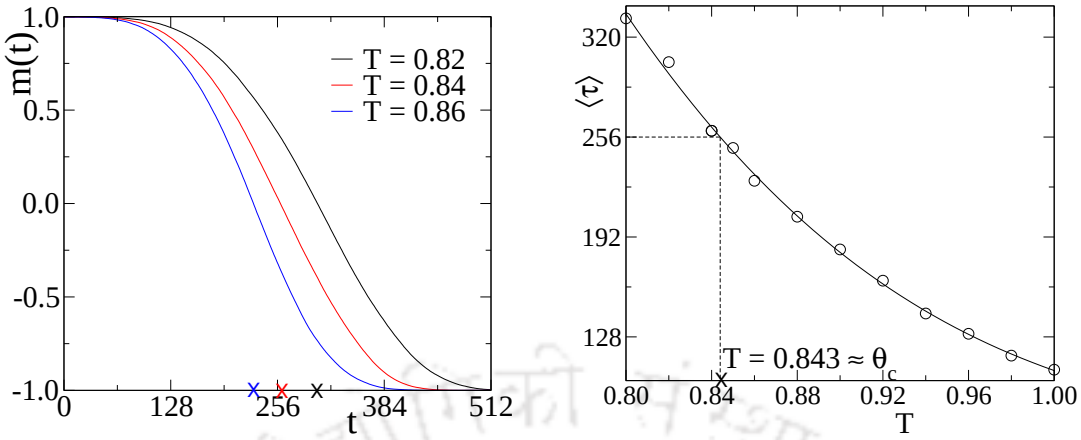

Figure 2.1: (a) Plot of $m(t)$ versus t over a constant field reversal from $+h_{\rm rms}$ to $-h_{\rm rms}$, $h_{\rm rms} = h_0/\sqrt{2}$ for $h_0 = 1.0$. (b) Plot of $\langle\tau\rangle$ against T on a system size $L = 512$.

spent in a metastable phase after a sudden field reversal. It depends on the temperature and the intensity of the applied field. In order to measure metastable lifetime, the system is evolved at a constant external field of intensity h_0 at a given temperature T. As the system achieves a constant magnetization $m(t)$, the field is suddenly reversed to $-h_0$, and the number of MC steps are counted for the magnetization to become zero. The number of MC steps represents the metastable lifetime. Taking an average over several such field reversals, the mean metastable lifetime $\langle\tau\rangle$ of a system is evaluated. Since a sinusoidal field of amplitude h_0 is used for the study of DPT here, the root mean square (rms) value of the field amplitude $h_{\rm rms} = h_0/\sqrt{2}$ is taken as the constant field [37]. In Fig.2.1(a), variation of magnetization $m(t)$ for three different temperatures are plotted against MC steps t for $h_{\rm rms} = 1/\sqrt{2}$ corresponding to $h_0 = 1.0$ only and fixed period $P = 512$. The magnetization $m(t)$ is estimated on a system of size $L = 512$. The system is evolved with $h_{\rm rms}$, and a constant magnetization is reached. Time is set to $t = 0$ when the sign of the constant field $h_{\rm rms}$ is changed from positive to negative. The metastable lifetime corresponding to $m(t) = 0$ for different values of T are marked by crosses on the time axis. Taking an average over several such field reversals, the mean metastable lifetime $\langle\tau\rangle$ is determined. In Fig.2.1(b), variation of $\langle\tau\rangle$ against temperature T is shown $h_{\rm rms} = 1/\sqrt{2}$ (corresponding to $h_0 = 1.0$). As we will be using an external field of fixed period $P = 512$, the temperature corresponding to $\langle\tau\rangle = P_{1/2} = 256$ should be the DPT critical temperature θ_c for a given h_0, P and L. The value of approximate $\theta_c \approx 0.843$ ($\ll T_c = 2.269185$) for $h_0 = 1.0$, $P = 512$ and system of size $L = 512$ is marked by a cross on the T axis. A more accurate value of θ_c

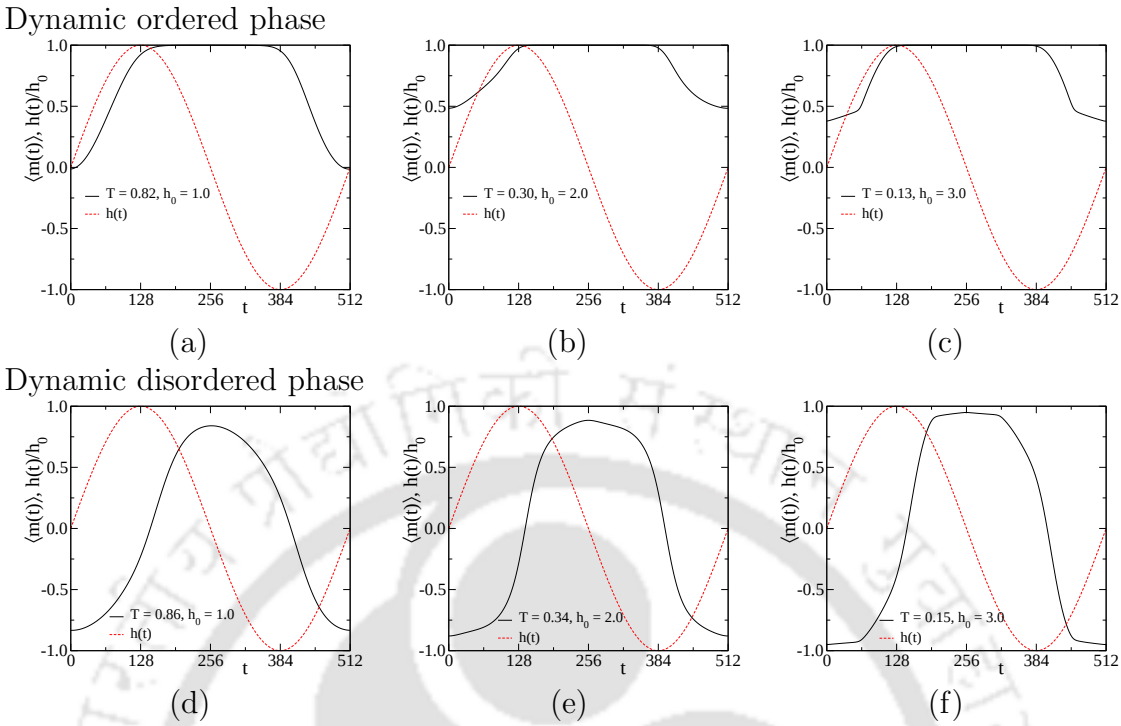

Figure 2.2: Average instantaneous magnetization $\langle m(t)\rangle$ with MC step t over a complete cycle (time period $P = 512$) of the magnetic field $h(t) = h_0 \sin(2\pi t/P)$ for (a) $T = 0.82$, (b) 0.30 and (c) 0.13 in DOP and (d) for $T = 0.86$, (e) 0.34 and (f) 0.15 for different field amplitudes $h_0 = 1.0$, 2.0 and 3.0 respectively on a square lattice of size $L = 512$. The dashed line in red represents the external field $h(t)/h_0 = \sin(2\pi t/P)$, with $P = 512$.

will be determined later. The value of θ_c will decrease further with the increase in field amplitude h_0. Thus, if the system is driven with an external field of fixed period, $\langle\tau\rangle$ is greater than $P_{1/2}$ for $T < \theta_c$ and the system will be in either of the metastable states. On the other hand, $\langle\tau\rangle$ is less than $P_{1/2}$ for $T > \theta_c$, and the system continuously moves from one metastable state to the other.

2.3 Magnetization, Spin configuration and Hysteresis

The hysteresis loop appears due to the phase lag between the instantaneous magnetization and the applied field because of the delayed response of the spins [26, 85, 86]. The sample average instantaneous magnetization for a given cycle is defined as

$$\langle m(t)\rangle = \langle \frac{1}{L^2}\sum_i S_i(t)\rangle \tag{2.5}$$

where $S_i(t)$ represents the value of the spin at the ith lattice site at time t and $\langle \cdots \rangle$ represents the ensemble average. The variation of $\langle m(t) \rangle$ is shown against MC time step t over a full period in Fig.2.2 for three different field of amplitudes $h_0 = 1.0$, 2.0 and 3.0 (in black continuous line) whereas variation of $h(t)/h_0$ is shown by a dashed red line. The period of the field is taken $P = 512$ for all three amplitudes. The systems presented in this plot are evolved starting from the all spin up ($S_i = +1$) configuration. Fig.2.2(a), (b), and (c) has plots correspond to lower temperatures than θ_c whereas the plots in Fig.2.2(d), (e) and (f) correspond to higher temperatures than θ_c. Firstly, the magnetization lags behind the magnetic field at all temperatures and field amplitudes. Such an effect will lead to hysteresis. Secondly, for the plots in Fig.2.2(a), (b) and (c) at low temperatures, the magnetization remains positive and at $+1$ for most of the time as the initial state was all spins up ($S_i = +1$) state. However, it could be negative, and at -1 for most of the time if they were started from the all spins down ($S_i = -1$) configurations. Such configurations corresponding to two metastable states are verified over the long magnetization time series up to 10^6 MC steps. In contrast, it is continuously varying from a positive to a negative value and vice versa at higher temperatures (Fig.2.2(d), (e), and (f)). It can be noted that the behavior is independent of the initial choice of spin configurations. This means that the system moves from one metastable state to the other continuously for $T \geq \theta_c$ and remains in either of the metastable states for $T < \theta_c$. A period average magnetization Q now can be defined as

$$Q = \frac{1}{P} \int_0^P \langle m(t) \rangle dt \tag{2.6}$$

where P is the time period of the external field. The system then will have a non-zero Q (either +ve or −ve) at lower temperatures, but it will be zero at higher temperatures. The system then moves from a non-zero Q to $Q = 0$ as the temperature T is increased from a lower value to a higher value far below the ferro-para transition temperature $T_c (\approx 2.269185)$ of the zero-field Ising model in 2d. This indicates the existence of two distinct dynamic phases; one is called the dynamic ordered phase or DOP with a finite Q, and the other is called the dynamic disordered phase or DDP with $Q = 0$. A phase transition from DOP to DDP occurs at a temperature θ_c far below T_c.

It is known that the magnetization response is different in DOP and DDP. It will be interesting to know how the spin configurations change over a stable period of the external field. Let us take a look at the spin configuration snapshots for both

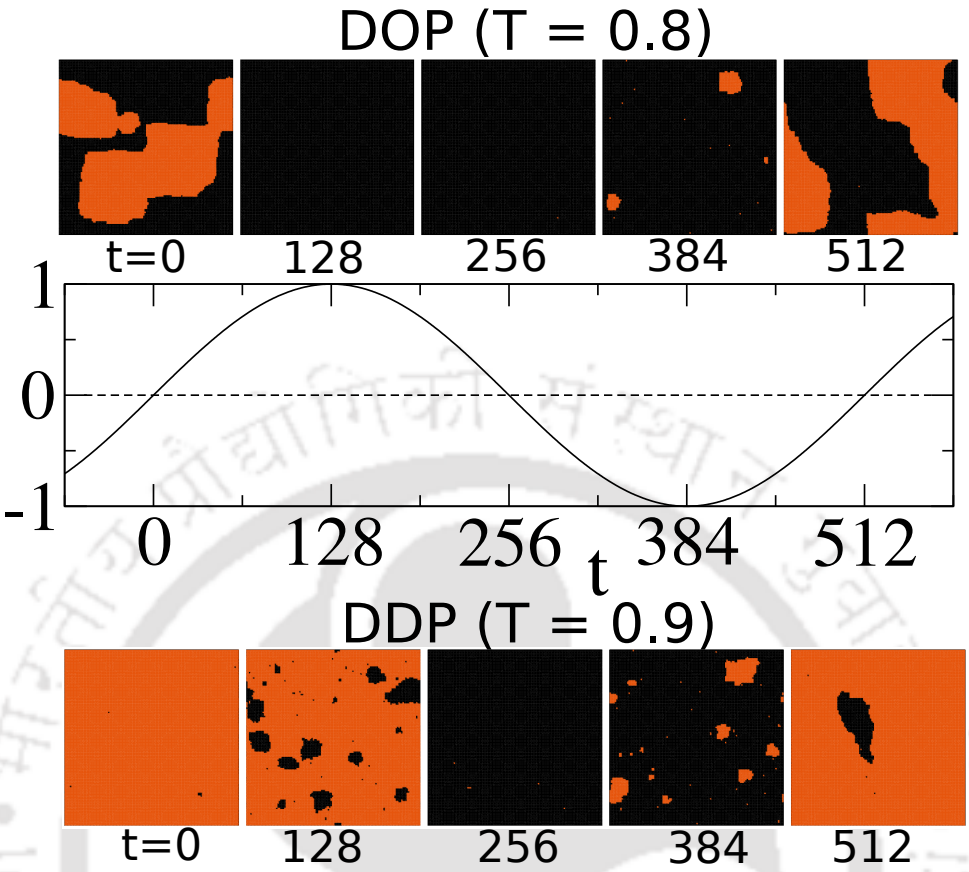

Figure 2.3: Time evolution of spin configurations over a stable cycle of external field $h(t) = h_0 \sin(2\pi t/P)$ in both DOP and DDP on a square lattice of size $L = 128$ with $P = 512$, $h_0 = 1.0$. Black and Saffron dots represent up and down spins respectively.

DOP and DDP taken at a different time of the period shown in Fig.2.3. The top and bottom panel shows the system morphology at time $t = 0, 128, 256, 384$ and 512 of the period $P = 512$ in DOP ($T = 0.8$) and DDP ($T = 0.9$) respectively. The field $h(t) = h_0 \sin(2\pi t/P)$ is shown in the middle. The initial spin configuration was all spins up. Let us first describe the top panel configurations in DOP. The spin configuration reached at $t = 0$, $h(t = 0) = 0$ passing through a gradually decreasing negative field of the previous cycle. So, down spin block formation was favorable up to or before $t = 0$. We can see several down spin blocks have coalesced and formed a giant down spin domain (periodic boundary) inside up spin domain. The $m(t = 0)$ is nearly zero as there are almost equal number of up and down spins in the system (see Fig.2.2(a)). The field increases from zero to $+h_0$ in between $t = 0$ to $t = 128$ and down spin domains overturns and entire lattice is covered by up spin and $m(t) \approx 1$ (see Fig.2.2(a)). After that field decreases to zero at $t = 256$. A few down spins appear among the up spin domain. These down spin domains nucleates and grows

in size as the field further decreases to $-h_0$ from zero. We can see a few down spin islands in the up spin domain at $t = 384$, magnetization still remains around its saturation value. The field remains negative but going to zero in the last quarter of the field from $t = 384$ to $t = 512$. The negative spin blocks coalesce and form a big down spin block at $t = 512$ around the up spin domain. The corresponding $m(t)$ becomes zero from its saturation value (see Fig.2.2(a)). Throughout DOP, the system remains in one (here, positive well) free energy metastable well and could not go to the other well as $P_{1/2} < \langle\tau\rangle$. The field changes its sign before the system could make an opposite spin block large enough to take the system to the other metastable phase. On the other hand, $P_{1/2} > \langle\tau\rangle$ in DDP. The field can take the system from one metastable well to the other in each half period. The first system image in DDP at $t = 0$ in the bottom panel starts with a situation where the previous negative field overturned almost all the spins to down state and $m(t)$ is negative (see Fig.2.2(d)). As the field increases to $+h_0$, several up spin blocks nucleate and appear inside the down spin domain around $t = 128$. Then the positive field continues up to $t = 256$ and becomes zero. Meanwhile, all the spins become up, forming a big up spin block, and we can see maximum positive $m(t)$ in Fig.2.2(d) at this time. The field again changes sign, and small down spin blocks appear at $t = 384$ and $m(t)$ becomes close to zero. The field continues to remain negative up to $t = 512$, and the down spin blocks coalesce and span the entire lattice. The $m(t)$ takes large negative value (see Fig.2.2(d)).

To visualize the hysteresis loop at different temperatures and field amplitudes, $\langle m(t)\rangle$ are plotted against the field $h(t)$ in Fig.2.4(a) for $T = 0.82$, (b) 0.30, and (c) 0.13 for low temperatures ($T < \theta_c$) and in Fig.2.4(d) for $T = 0.86$, (e) 0.34, and (f) 0.15 for high temperatures ($T > \theta_c$) at all three field amplitudes $h_0 = 1.0$, 2.0 and 3.0. It can be seen that the hysteresis loops about the zero magnetization line are asymmetric for lower temperatures, whereas they are symmetric at higher temperatures. At lower temperatures, the center of the hysteresis loops (period average magnetization Q) is positive if the initial configurations are taken as all spins up ($S_i = +1$) state, and it is negative if the initial configurations are taken as all spins down ($S_i = -1$) state. Thus as the temperature decreases from a higher temperature, the symmetry of the hysteresis loops breaks at a critical temperature θ_c. The phase corresponding to the asymmetric hysteresis loop with finite Q is the DOP, and the phase corresponding to the symmetric hysteresis loop with $Q = 0$ is the DDP. The shape, orientation, and symmetry of the hysteresis loops are found to change continuously as the temperature T is varied from below θ_c to above θ_c for

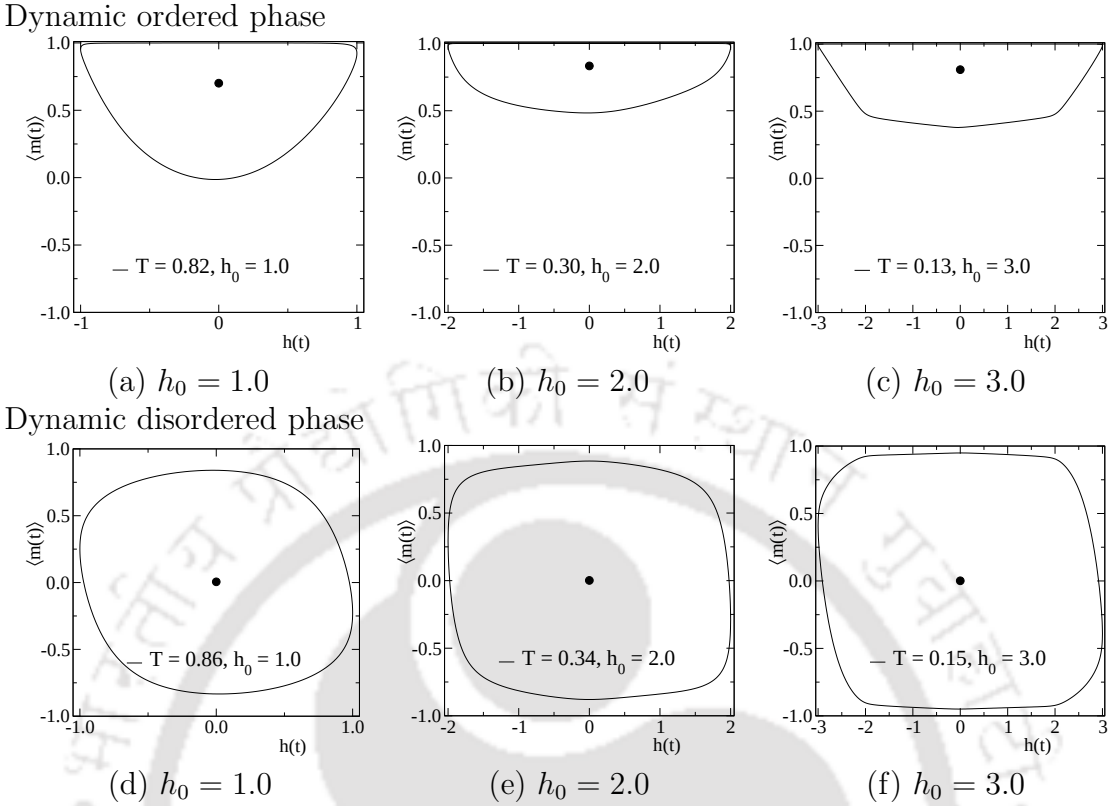

Figure 2.4: Hysteresis loops, $\langle m(t)\rangle$ versus $h(t)$, over a complete cycle of the field $-h_0$ to $+h_0$ (time period $P = 512$) on a square lattice of size $L = 512$ for different field amplitudes $h_0 = 1.0$, 2.0 and 3.0 for temperatures (a) $T = 0.82$, (b) 0.30 and (c) 0.13 in DOP and at (d) $T = 0.86$, (e) 0.34 and (f) 0.15 in DDP respectively. The solid circles represent the centers of the hysteresis loops.

each field amplitude. In the following, we develop a simple tool to estimate such quantities and study their behavior as a function of temperature.

A hysteresis loop tensor $\overleftrightarrow{T}$ is constructed to quantitatively describe the geometric properties of the hysteresis loops such as shape, size, and orientation etc. The loop is defined by the P number of points in the $h-m$ plane, where P is the period of the field. The coordinate of the tth point on the loop is given by (h_t, m_t) where $m_t = \langle m(t)\rangle$ corresponding to the field $h_t = h(t)$. The center of the loop $(\langle h(t)\rangle, Q)$ is given by

$$\langle h(t)\rangle = \frac{1}{P}\sum_{t=1}^{P} h_t = 0, \quad Q = \frac{1}{P}\sum_{t=1}^{P} m_t \tag{2.7}$$

where the period averaged value of $h(t)$ is zero for a sinusoidal field, and that of the magnetization is represented by Q. A two-dimensional hysteresis loop tensor (or

matrix) then can be defined as

$$\overleftrightarrow{T} = \begin{bmatrix} T_{hh} & T_{hm} \\ T_{mh} & T_{mm} \end{bmatrix} \tag{2.8}$$

The diagonal elements T_{hh} and T_{mm} are given by

$$T_{hh} = \frac{1}{P}\sum_{t=1}^{P} h_t^2, \quad T_{mm} = \frac{1}{P}\sum_{t=1}^{P} (m_t - Q)^2 \tag{2.9}$$

and the off diagonal elements are given by

$$T_{hm} = T_{mh} = \frac{1}{P}\sum_{t=1}^{P} h_t\,(m_t - Q) = \frac{1}{P}\sum_{t=1}^{P} h_t m_t, \tag{2.10}$$

as $\langle h(t)\rangle = 0$. The eigenvalues λ_1 and λ_2 of $\overleftrightarrow{T}$ are given by

$$\lambda_{1,2} = \frac{1}{2}\left[(T_{mm} + T_{hh}) \pm \sqrt{D}\right] \tag{2.11}$$

where $D = (T_{mm} - T_{hh})^2 + 4T_{mh}^2$, plus sign corresponds to the largest eigenvalue λ_1 and minus sign corresponds to the smallest eigenvalue λ_2. The corresponding orthonormal eigenvectors $|e_1\rangle$ and $|e_2\rangle$ along the principal axes are also estimated, solving the eigenvalue equations. Note that, $\sqrt{\lambda_1}$ and $\sqrt{\lambda_2}$ represent approximately half of the height and width of the loop along the principal axes. As the hysteresis loop becomes more and more symmetric with increasing temperature, not only the principal axes rotate but also the values of λ_1 and λ_2 change. Thus the eigenvalues and eigenvectors of the hysteresis loop tensor keep vital information of the evolution of the loop with temperature.

The evolution of shape, size and orientation of the hysteresis loops with T (below T_c) for the field intensity $h_0 = 1.0$ is shown in Fig.2.5 for a system defined on a square lattice of size $L = 512$. The $m(t)$ has a very small variation over the period at very low temperatures. The respective asymmetric hysteresis loops are found to be narrow, having a very small width along the magnetization axis at low temperatures in Fig.2.5(a) and (b). The $m(t)$s changes significantly with the variation of the external field as temperature rises in DOP. The asymmetric loops then acquire some width along the magnetization axis, and the area gradually increases Fig.2.5(c) to (f). Near the DPT hysteresis loops become symmetric Fig.2.5(g) when the $m(t)$s start following field in each cycle. The hysteresis loop area keeps on increasing for a

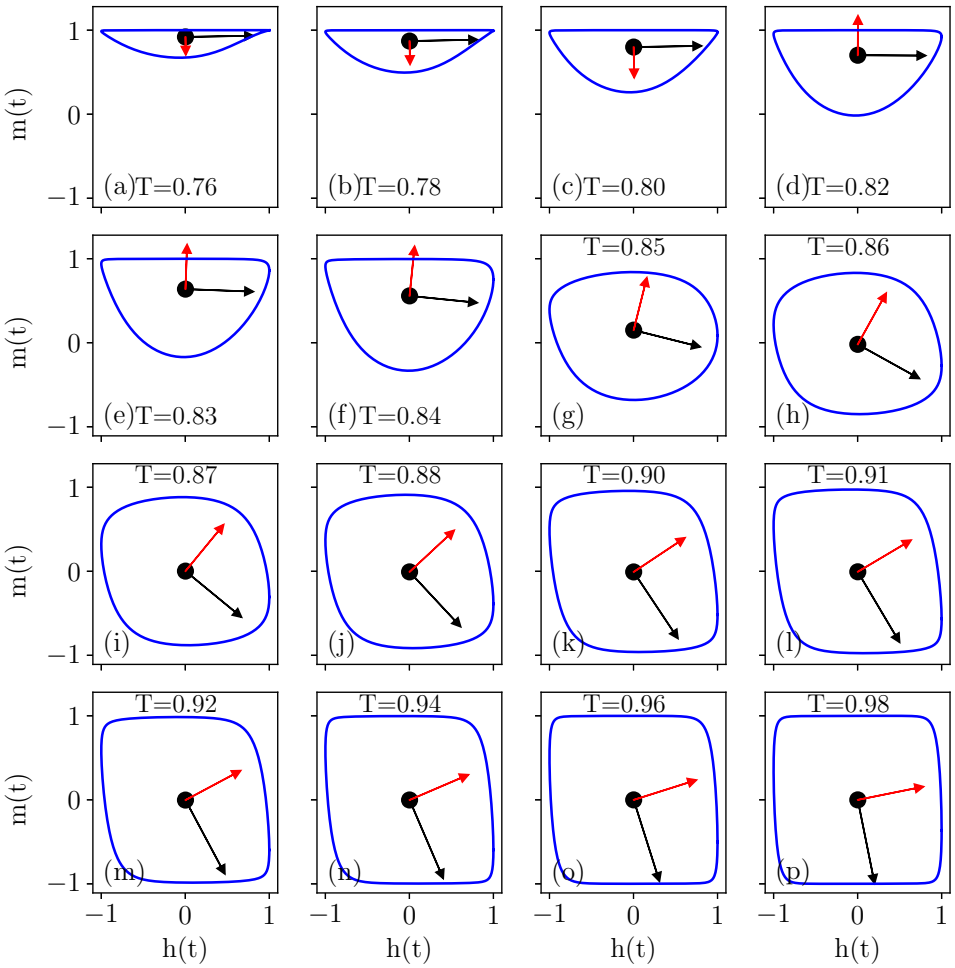

Figure 2.5: Evolution of average hysteresis loops with temperature T over a complete cycle of field (time period $P = 512$) on a square lattice of size $L = 512$ for field amplitude $h_0 = 1.0$. The two eigenvectors are shown in each sub figure, in black and red corresponding to larger (λ_1) and smaller (λ_2) eigenvalues, respectively. The hysteresis loop area, shape, and orientation change as the temperature of the system increases.

little while even after the DPT Fig.2.5(h) to (p). The other interesting observations are how the loops rotate while changing their area and shape with increasing temperature. The two eigenvectors corresponding to the two eigenvalues are shown in each loop. The black arrow represents the vector ($\vec{e_1}$) corresponding to the largest eigenvalue λ_1 and the red one ($\vec{e_2}$) corresponding to the smaller eigenvalue λ_2. The $\vec{e_1}$ rotates continuously from the first quadrant to the fourth quadrant in a clockwise direction. On the other hand, The $\vec{e_2}$ starts in the fourth quadrant comes to the first quadrant after a jump at $T = 0.82$ when part of the hysteresis loop acquires some negative $m(t)$ in DOP. After that, the $\vec{e_2}$ continuously decreases to smaller values as the T increases.

Two quantities of interest are the area A of the hysteresis loop and the dynamic correlation C. The area A of the loop, the average loss in magnetic energy over a cycle, is given by

$$A = -\oint m(t)dh(t) \tag{2.12}$$

where $h(t)$ is time dependent external field. However, an approximate loop area A can be obtained in terms of the eigenvalues of the hysteresis loop as

$$A \approx 4\sqrt{\lambda_1 \lambda_2}. \tag{2.13}$$

However, the estimate of A from Eq.2.13 is always less than equal to that of estimated from Eq.2.12 and the largest difference occurs at the maximum loop area. The dynamic correlation C is defined as

$$C = \langle m(t)h(t)\rangle - \langle m(t)\rangle\langle h(t)\rangle. \tag{2.14}$$

Since $\langle h(t)\rangle = 0$ over the period P, C can be obtained as

$$C = \frac{1}{P}\oint m(t)h(t)dt = T_{hm} \quad (\text{or } T_{mh}) \tag{2.15}$$

which is nothing but negative of the time averaged spin-field interaction energy per lattice site over a complete cycle. Apart from the area and dynamic correlation, we have introduced two new quantities, the orientation and shape of the hysteresis loop for further characterization. Both the orientation and the shape of the loop can be determined in terms of the eigenvectors and eigenvalues of the hysteresis loop tensor. The orientation of the hysteresis loop can be estimated by the angle of rotation of one of the principal axes or the eigenket $|e_1\rangle$ or $|e_2\rangle$. The orientation α can be defined as the angle made by $|e_1\rangle$ corresponding to the eigenvalue λ_1 with the horizontal axis corresponding to field amplitude. The orientation α of the loop with respect to the field axis is then given by

$$\alpha = \tan^{-1}\left(\frac{e_m}{e_h}\right) \tag{2.16}$$

where e_h and e_m are the components of $|e_1\rangle$ along magnetic field and magnetization axes respectively. The shape of the loop can be studied by measuring the aspect

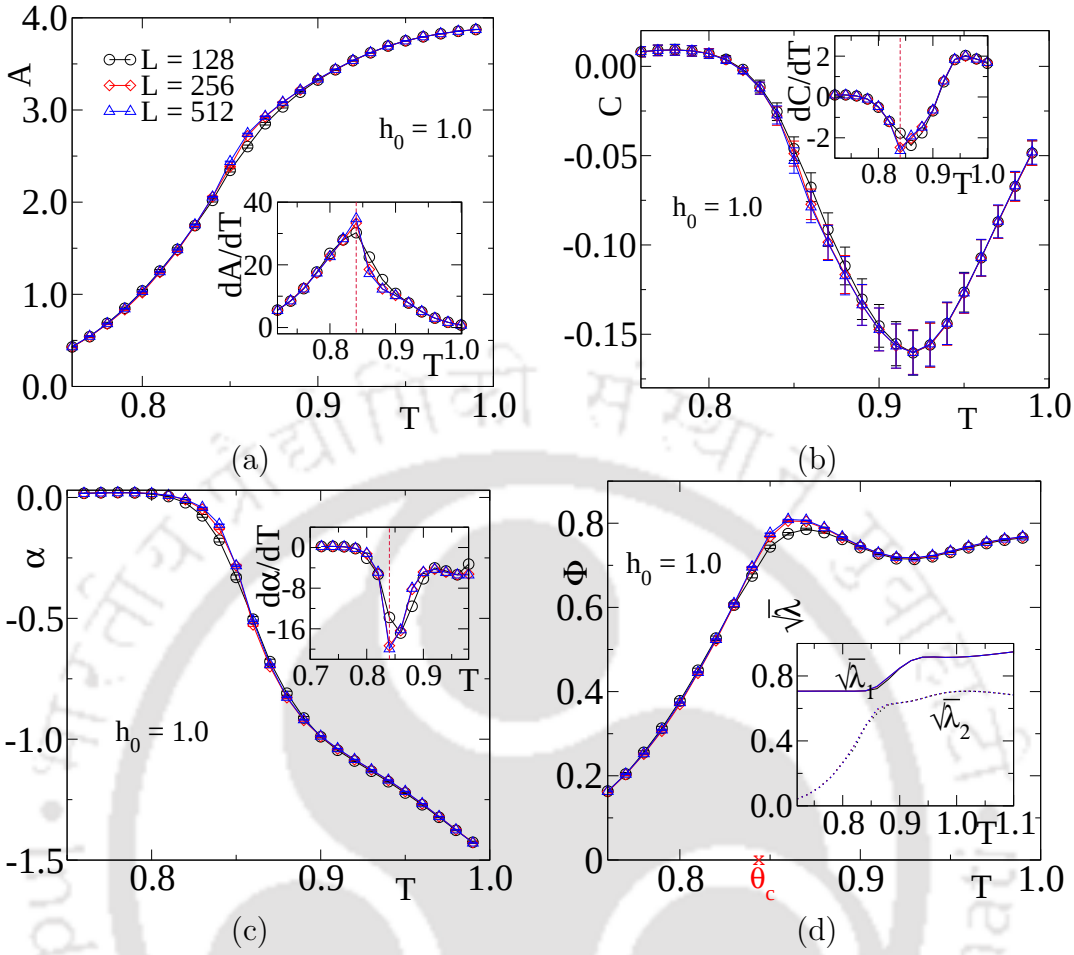

Figure 2.6: (a) Hysteresis loop area A, (b) dynamic correlation C, (c) orientation α and (d) aspect ratio Φ are plotted against temperature T for $h_0 = 1.0$ and $P = 512$ for different system sizes $L = 128(\bigcirc), 256(\diamond)$, and $512(\triangle)$. Derivatives of the quantities are shown in the respective inset. They have got a sharp peak and deep at the transition point except for Φ. The vertical bars with the data points represent the statistical error of each point.

ratio of the loop. The aspect ratio Φ of the loop is defined as

$$\Phi = \sqrt{\frac{\lambda_2}{\lambda_1}} \tag{2.17}$$

in terms of λ_1 and λ_2. Note that for a circular loop $\Phi = 1$ as both the dimensions of the circle are same. As Φ decreases, the loop is expected to be of elliptic shape. Qualitatively, Φ would describe the variation of the shape of the hysteresis loop with temperature and field amplitude.

Effect of field amplitude on loop area A, dynamic correlation C, orientation α and aspect ratio Φ are studied for $h_0 = 1.0$, 2.0 and 3.0. First, we describe the results for $h_0 = 1.0$. The variation of loop area A, dynamic correlation C, orientation α

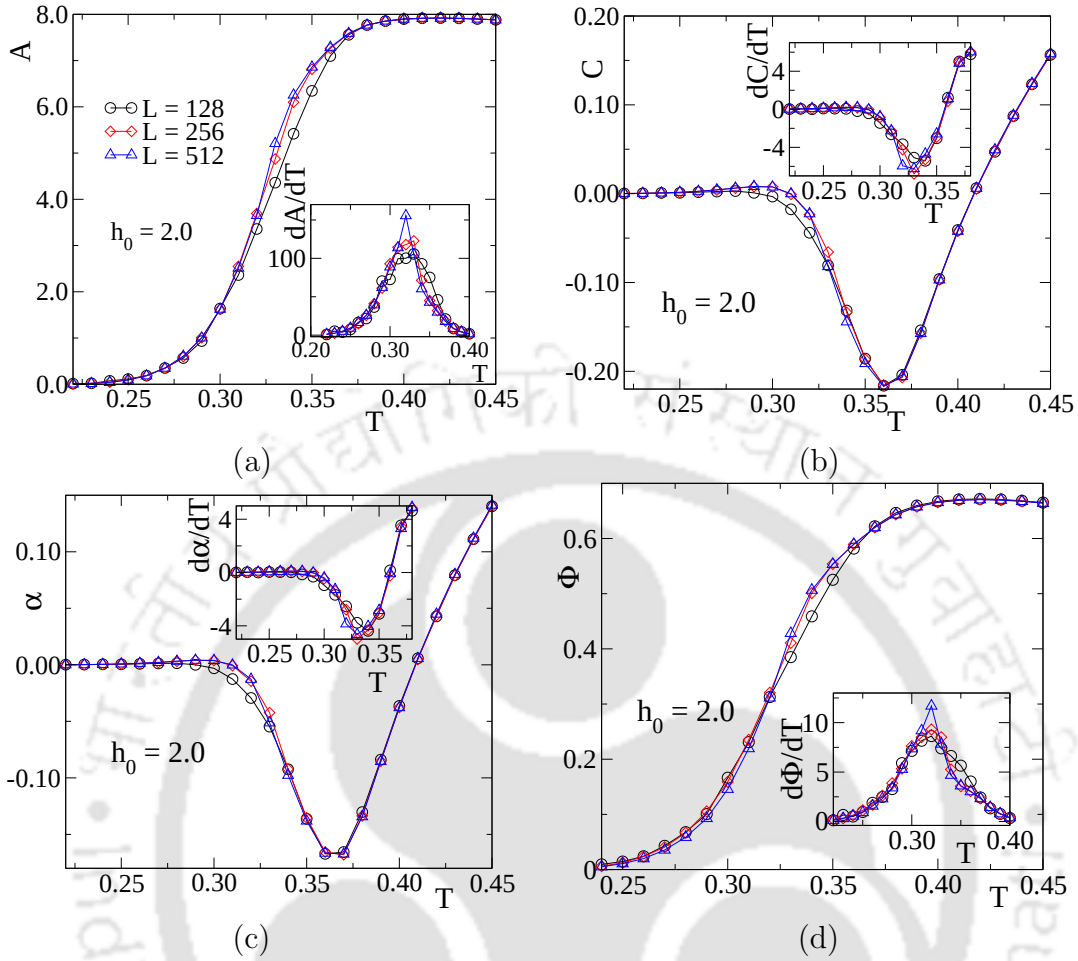

Figure 2.7: (a) Hysteresis loop area A, (b) dynamic correlation C, (c) orientation α and (d) aspect ratio Φ are plotted against temperature T for $h_0 = 2.0$ and $P = 512$ for different system sizes $L = 128(\bigcirc), 256(\diamond)$, and $512(\triangle)$. Derivatives with respect to T of respective quantities are shown in the inset. They have sharp peak or deep at the transition point θ_c.

and aspect ratio Φ against temperature T (below T_c) are shown in Fig.2.6(a), (b), (c) and (d) respectively for several system sizes taking field amplitude $h_0 = 1.0$ and period $P = 512$. The derivatives of A, C, and α are plotted against T in the respective insets. It can be seen that dA/dT has a maximum whereas dC/dT and $d\alpha/dT$ have minima at a critical temperature $\theta_c \approx 0.843$. At θ_c, rapid change in loop area, as well as the maximum change in spin-field interaction energy occur. The maximum loss of magnetic energy and large spin-field interaction occurs at a higher temperature after the transition [45]. Below θ_c the loops are asymmetric, and above θ_c, the loops are symmetric. At θ_c, the hysteresis loop quickly orients itself from an asymmetric to a symmetric one. The loop, however, continues rotating in the same direction after the transition in this temperature range. Whereas the aspect

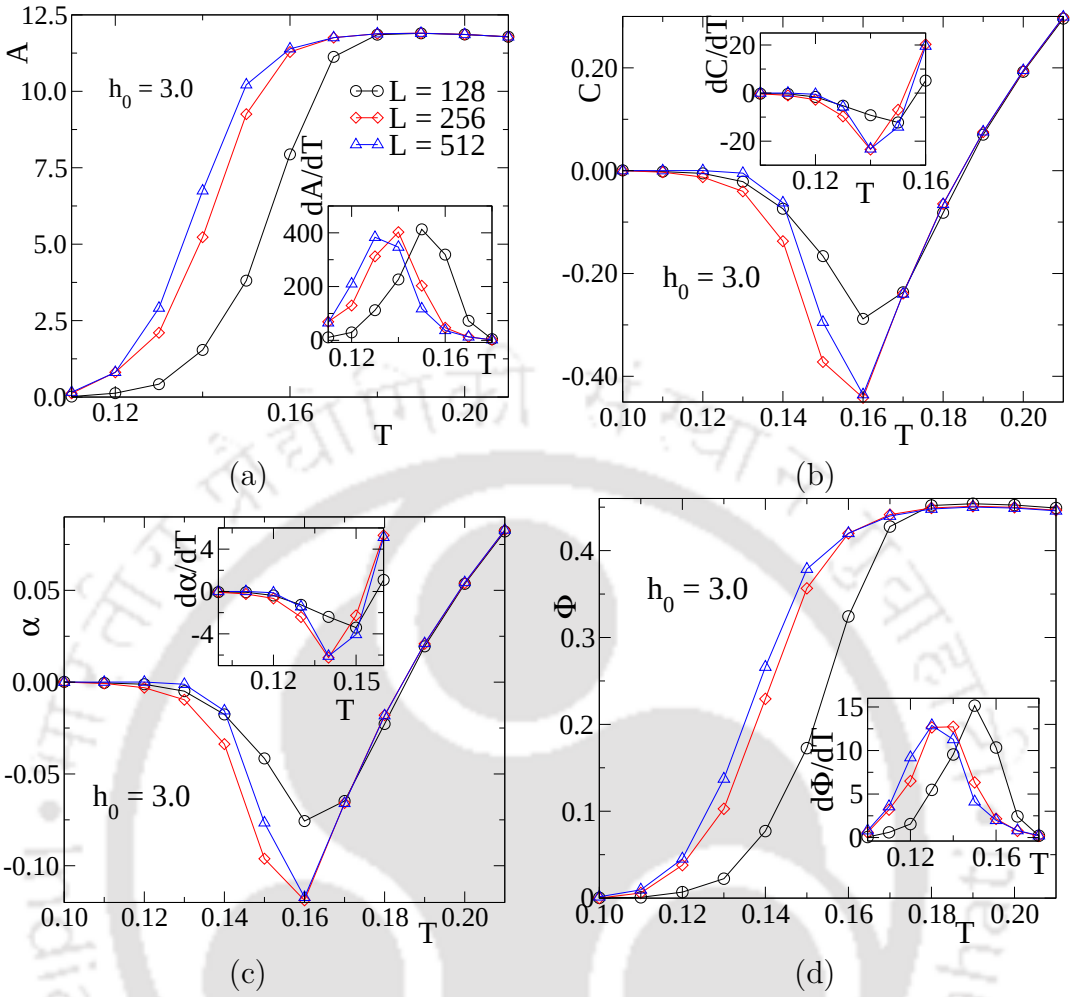

Figure 2.8: (a) Hysteresis loop area A, (b) dynamic correlation C, (c) orientation α and (d) aspect ratio Φ are plotted against temperature T for $h_0 = 3.0$ and $P = 512$ for different system sizes $L = 128(\bigcirc), 256(\diamond)$, and $512(\triangle)$. Derivatives with respect to T of respective quantities are shown in the inset. They have sharp peak or deep at the transition point θ_c. The θ_cs are found to be different depending on system size for high field amplitude.

ratio Φ increases with temperature T and achieves a maximum then saturates to a definite value as seen from Fig.2.6(d). The transition from DOP to DDP occurs just before Φ achieves its maximum value. Thus, a transition from asymmetric DOP to symmetric DDP occurs around θ_c. Just after the transition, A, C, α, and Φ all have a weak finite system size (L) dependence.

The variations of A, C, α and Φ with T at higher field amplitudes $h_0 = 2.0$ and 3.0 remain almost the same as those of $h_0 = 1.0$. However, there are some notable differences in the behaviour of A, C, α and Φ at higher field intensities plotted against T for $h_0 = 2.0$ in Fig.2.7 and those for $h_0 = 3.0$ are plotted in Fig.2.8 respectively. The finite size effect is found to be increasingly prominent with

higher and higher field amplitudes. The evolution of Φ is smooth in comparison to $h_0 = 1.0$. It seems the evolution of the hysteresis loop is more controlled by the temperature for lower field amplitudes, whereas the field controls it at higher field amplitudes. The derivatives of both A, C, α, and Φ would have maxima or minima corresponding to the transition temperature θ_c, which are now strongly dependent on system size (L).

2.4 Dynamic phase transition

As the bistable system is driven by a field of constant period (or frequency) here, the system moves from an asymmetric dynamic ordered phase (or DOP) to a symmetric dynamic disordered phase (or DDP) as the temperature T of the system (below the critical temperature T_c of equilibrium Ising model) is increased from below θ_c to above θ_c, a critical temperature at which DPT occurs. In DOP, the system remains in one of the metastable states, whereas, in DDP, the system moves from one metastable state to the other in a complete cycle. The period average magnetization $Q = \frac{1}{P}\int_0^P \langle m(t)\rangle dt$ is defined in Eq.3.6 (also in Eq.2.7) is taken as the dynamic order parameter of DPT. As Q could have both positive and negative values in DOP corresponding to two metastable states, it continuously goes to zero in DDP. We describe a finite size scaling (FSS) theory considering the absolute order parameter $|Q|$. Following the theory of thermal critical phenomena [5, 7], the finite size scaling (FSS) form of $|Q|$ is assumed to be

$$|Q| = L^{-\beta/\nu}\widetilde{Q}[\varepsilon L^{1/\nu}] \tag{2.18}$$

where $\varepsilon = (T-\theta_c)/\theta_c$ is the reduced temperature and $\widetilde{Q}$ is a scaling functions. The order parameter exponents β is defined as $|Q| \sim (-\varepsilon)^{\beta}$ and the correlation length exponents ν is defined as $\xi \sim |\varepsilon|^{-\nu}$, where ξ is the correlation length. Following the formalism of equilibrium critical phenomena [87], the probability distribution of $|Q|$ is taken as

$$P_L(|Q|) = L^{\beta/\nu}\widetilde{P}_L[|Q|L^{\beta/\nu}] \tag{2.19}$$

where $\widetilde{P}_L$ is a universal scaling function, for a given system of size L. The susceptibility χ of the system then can be estimated from the fluctuation of dynamic order parameter $|Q|$ as

$$\chi = L^d(\langle |Q|^2\rangle - \langle |Q|\rangle^2) \tag{2.20}$$

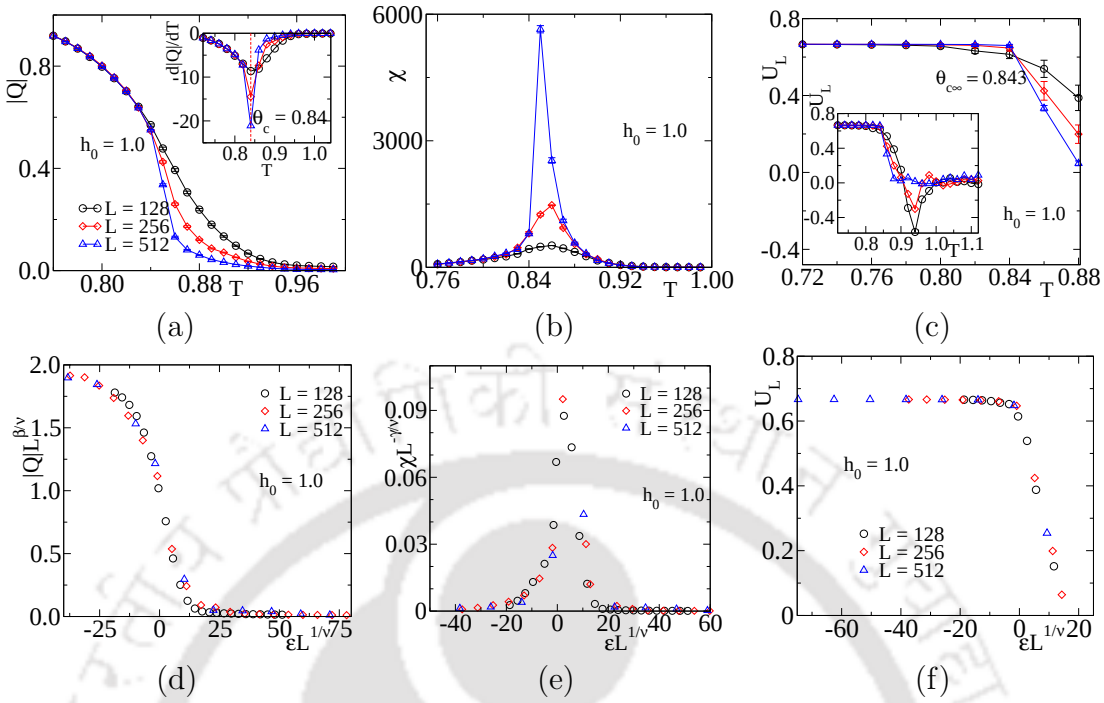

Figure 2.9: Plot of (a) order parameters $|Q|$, (b) susceptibility χ and (c) Binder cumulant U_L against temperature T for $h_0 = 1.0$ and $P = 512$ for system sizes $L = 128(\bigcirc)$, $256(\diamond)$ and $512(\triangle)$. The vertical bars with the data points represent the statistical error of each point. $d|Q|/dT$ is plotted against T in the inset of (a) and variation of U_L is shown for wide range of T in the inset of (c). The scaled parameters, $|Q|L^{\beta/\nu}$, $\chi L^{-\gamma/\nu}$ and U_L are plotted against the scaled variable $\varepsilon L^{1/\nu}$ in (d), (e) and (f) respectively taking the values of the critical exponents $\beta = 1/8$, $\gamma = 7/4$ and $\nu = 1$ as that of 2d equilibrium Ising model.

where $\langle |Q|^n \rangle = \int |Q|^n P_L(|Q|) d|Q|$ and $d = 2$ for two dimensions. The FSS form of χ is then given by

$$\chi = L^{\gamma/\nu} \widetilde{\chi}[\varepsilon L^{1/\nu}] \tag{2.21}$$

where $\widetilde{\chi}$ is a scaling function and $\gamma/\nu = d - 2\beta/\nu$ as both $\langle Q^2 \rangle$ and $\langle |Q| \rangle^2$ goes as $L^{-2\beta/\nu}$. The susceptibility exponent γ is defined as $\chi \sim |\varepsilon|^{-\gamma}$.

The fourth order Binder cumulant is defined as,

$$U_L = 1 - \frac{\langle Q^4 \rangle}{3\langle Q^2 \rangle^2} \tag{2.22}$$

and its FSS form is given by

$$U_L = \widetilde{U}[\varepsilon L^{1/\nu}] \tag{2.23}$$

where $\widetilde{U}$ is a universal scaling function.

First, we present data for $h_0 = 1.0$, and then we will compare it with the data

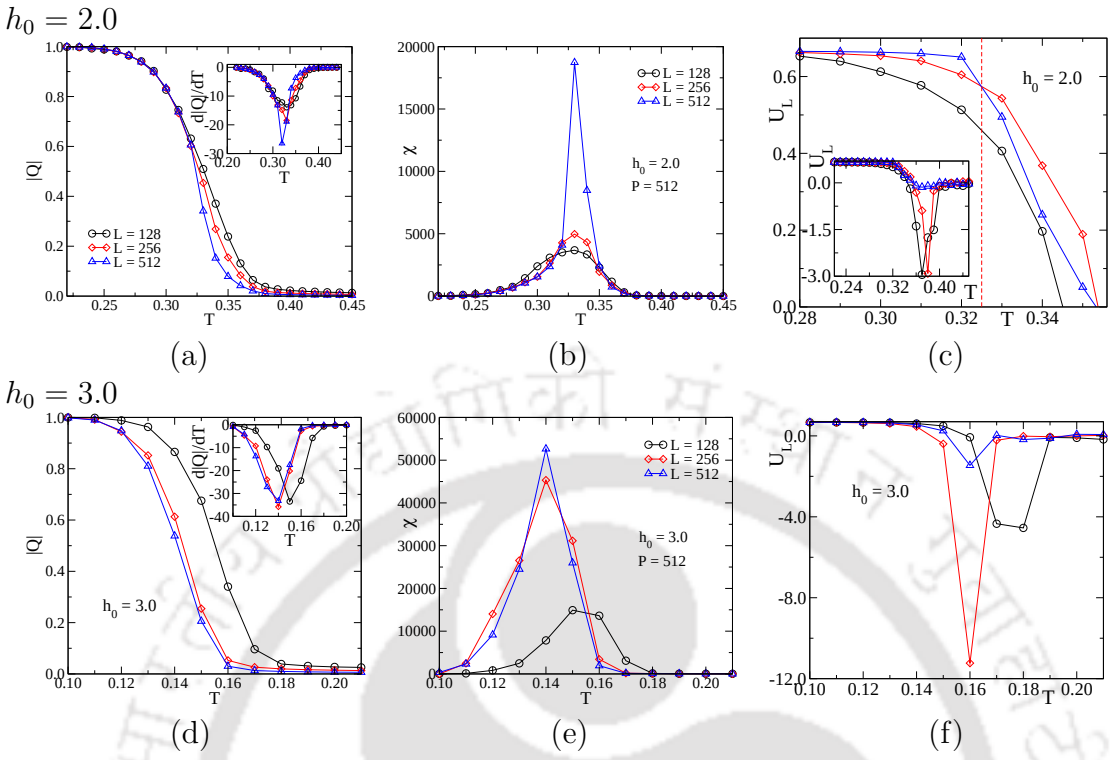

Figure 2.10: Plot of (a) order parameters $|Q|$, (b) susceptibility χ and (c) Binder cumulant U_L against temperature T for $h_0 = 2.0$ and $P = 512$ for system sizes $L = 128(\bigcirc)$, $256(\diamond)$ and $512(\triangle)$. In the inset of (a), $d|Q|/dT$ is plotted against temperature. In the inset of (c), variation of U_L is shown for wide range of T. The same is shown in bottom row for $h_0 = 3.0$

obtained at higher field amplitudes. The variation of $|Q|$, χ, and U_L against temperature T are shown In Fig.2.9(a), (b) and (c) respectively for $h_0 = 1.0$ and $P = 512$ for different values of L. The statistical errors of the data points are indicated by vertical bars with the data points. The plots in Fig.2.9(a) show that order parameter $|Q|$ has a finite size dependence around the transition. The transition point is determined by estimating $d|Q|/dT$. As shown in the inset of Fig.2.9(a), it has a dip at $T = \theta_c = 0.84$ corresponding to the DOP to DDP transition. It seems that the value of θ_c is almost independent of the system size L for the field intensity $h_0 = 1.0$. The susceptibilities χ for different L are shown in Fig.2.9(b), have peaks at θ_c, and the height of the peak increases with the system size L. The plots of U_L against temperature T in Fig.2.9(c) for different values of L cross each other at a temperature ≈ 0.843, little higher than θ_c. The temperature corresponding to such crossing indicates the phase transition temperature of the system in the thermodynamic limit. The value of U_L at the crossing is found to be $U^* \approx 0.61$, close to the already known estimates for the 2d the equilibrium zero field Ising model

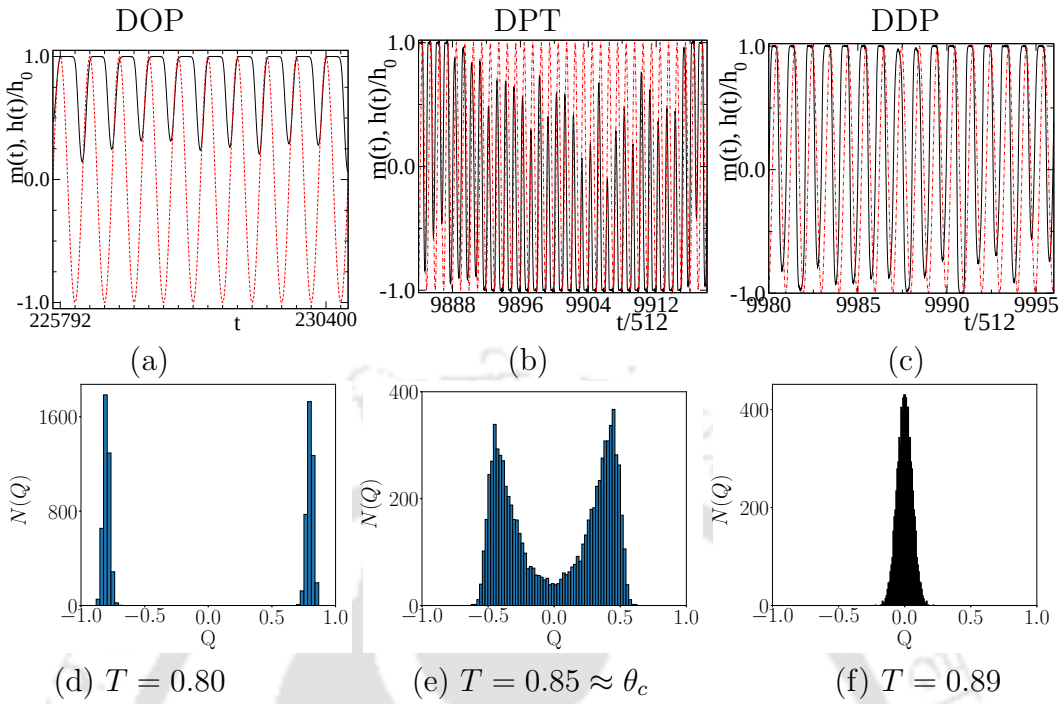

Figure 2.11: Plot of magnetization time series $m(t)$ against MCS (t) at different temperatures (a) $T = 0.80$ (DOP), (b) $T = 0.85$ (DPT) and (c) $T = 0.89$ (DDP) on a system of size $L = 512$ for $h(t) = h_0 \sin(2\pi t/P)$, with $h_0 = 1.0$ and $P = 512$. The corresponding distribution of Q are given in (d), (e) and (f) respectively. Histograms are obtained for 8192 order parameters Q over 60 equispaced bins.

[24, 88, 89]. It is also as per the U^* value for the DPT reported in Ref.[24]. Though U_L remains positive within this temperature range, the values of the smaller lattice sizes once become negative and then come back to zero at higher temperature as shown in the inset of Fig.2.9(c). Now we verify the FSS forms of $|Q|$, χ and U_L taking the scaling exponents as that of the 2d equilibrium Ising model critical exponents, *i.e.*, $\beta = 1/8, \gamma = 7/4$ and $\nu = 1$. As $\nu = 1$, the values of β/ν and γ/ν remain as that of β and γ respectively. The scaled order parameter $|Q|L^{\beta/\nu}$, the scaled susceptibility $\chi L^{-\gamma/\nu}$ and U_L are plotted against the scaled variable $\varepsilon L^{1/\nu}$ in Fig.2.9(d), (e), (f) respectively. A good collapse of data occurred with the chosen values of the critical exponents. It is interesting to note that the non-equilibrium DPT is characterized by the exponents exactly that of the equilibrium zero field Ising model in 2d, far below the critical temperature T_c of the equilibrium model. The dynamic phase transition from DOP to DDP is then characterized by a set of critical exponents and follows the FSS hypothesis as that of a continuous phase transition [37, 48, 49, 63]. Though the surface criticality of the kinetic Ising model with surface undergoes non-equilibrium transition with surface exponents different

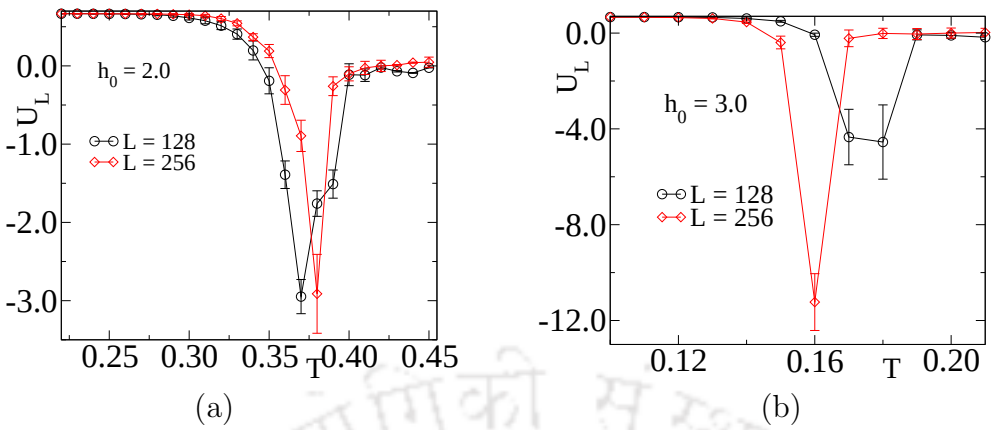

Figure 2.12: Plot of fourth order cumulant U_L against T for systems of size $L = 128(\bigcirc)$ and $L = 256(\diamond)$ at (a) $h_0 = 2.0$ and (b) $h_0 = 3.0$. The period of the applied field $P = 512$ remains same for all the field amplitudes. The vertical bars with the data points represent statistical error of each point.

from those of the equilibrium critical surface [53], the corresponding bulk systems undergo a continuous non-equilibrium phase transition with exponents that of the equilibrium 3d Ising model [54].

The variation of $|Q|$, χ and U_L with T remains almost same for higher field $h_0 = 2.0$ and 3.0. The finite size effect becomes more prominent or higher field amplitudes, and θ_c depends on system size with increasing field amplitudes as shown in Fig.2.10. It is not possible to have data collapse for these quantities with any known critical exponent values. Thus, the underlying nature of the transition at higher field amplitudes ($h_0 = 2.0$ and 3.0) on system size $L = 128, 256$ and 512 is not the same as the case of $h_0 = 1.0$. The nature of DPT may appear different due to the finite size effects. We must check results on larger systems to reach a conclusion about the nature of the DPT at higher field amplitudes.

The transition from DOP to DDP can be better understood by studying the magnetization time series and the order parameter distribution. In Fig.2.11, the selected portion of magnetization time series $m(t)$ (solid line) and the order parameter distribution are plotted at different temperatures (a) $T = 0.80$, (b) $T = 0.85 \approx \theta_c$ and (c) $T = 0.89$ corresponding to DOP, DPT and DDP on a system of size $L = 512$ for $h_0 = 1.0$ and $P = 512$. In DOP, the $\langle\tau\rangle$ is always larger than the half period $P_{1/2}$. As a result, the system remains in one of the free energy wells depending on the starting configuration and can not come out from the metastable well it is already in. Fig.2.11(a) represents magnetization time series of a system of all spins up ($S_i = +1$) initial configuration and $m(t)$ shows a small fluctuation about a finite non-zero value but does not cross zero. The corresponding distribution (histogram)

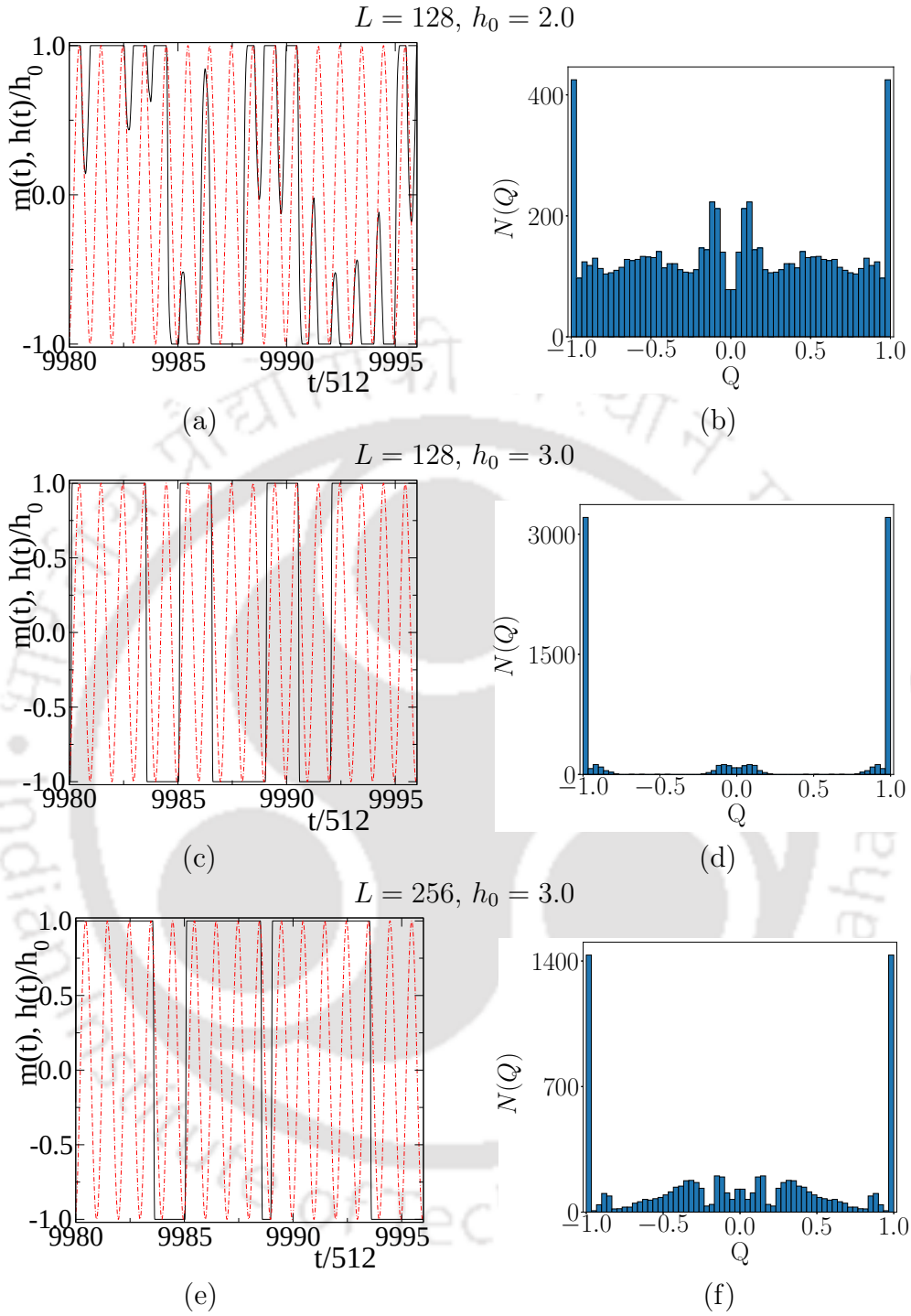

Figure 2.13: Magnetization time series and histograms of 8192 order parameter Q values over 60 equispaced bins are shown for the system of size $L = 128$ at the field intensities $h_0 = 2.0$ (a) and (b) and at $h_0 = 3.0$ (c) and (d). The same plots for $L = 256$ and $h_0 = 3.0$ are given in (e) and (f). The period P is kept constant at 512. The systems are at their respective DPT temperatures $\theta_c \approx 0.33$ and 0.14 for $h_0 = 2.0$ and 3.0 respectively.

of the order parameter Q is shown in Fig.2.11(d). The peak corresponding to positive Q represents systems with $m(t) > 0$, and the peak corresponding to negative Q represents systems with $m(t) < 0$. It is evident from the distribution that the system remains trapped in either of the wells. As temperature increases, the average metastable lifetime $\langle \tau(T, h_0) \rangle$ becomes comparable with the half period of the external field $P_{1/2}$ and DPT occurs. The situation is described in Fig.2.11(b) and (e). The $m(t)$ varies from a positive value to a negative value (or negative to positive) and crosses zero as shown in Fig.2.11(b). Note that $m(t)$, however, does not reach a value $+1$ or -1. The distribution of Q (Fig.2.11(e)) have peaks around $\pm|Q|_c$. At this point, when the cycle average magnetization is still finite, the external field can move the system from one well to the other smoothly. Usually, in large systems, it corresponds to the MD regime [34, 36, 90]. The scaling form of $P_L(|Q|)$ given in Eq.2.19 is verified for different system sizes $L = 128$, 256 and 512 near the transition temperature $T = 0.85$ for $h_0 = 1.0$. The unimodal distributions had a reasonable collapse of data with the value $\beta/\nu = 1/8$. In DDP, $\langle \tau \rangle$ is smaller than the $P_{1/2}$, $m(t)$ follows the external field with certain phase lag changes from close to $+1$ to close to -1 as shown in Fig.2.11(c). Most of the states arise at $Q = 0$ and the distribution $N(Q)$ has a single peak around zero Q as it can be seen in Fig.2.11(f). At lower field intensity like $h_0 = 1.0$, the smaller systems like $L = 256$ and 128 also behave similarly and found to exhibit continuous DPT.

2.5 Higher field results and system size dependence

Now, we present data obtained at higher field amplitudes $h_0 = 2.0$ and $h_0 = 3.0$ keeping the period of the applied filed $P = 512$, as before. First, we will consider the smaller system sizes at higher field amplitudes and then the larger system sizes at the same field amplitudes. The behavior of the smaller systems at higher field intensities such as $L = 256$ at $h_0 = 3.0$ and $L = 128$ at $h_0 = 2.0$ and $h_0 = 3.0$ are quite different from those obtained for these systems at low field intensities. The transition temperatures for these systems are determined from the deep of $d|Q|/dT$ plots (not shown), and they are found to be $\theta_c \approx 0.32$ and $\theta_c \approx 0.14$ for $h_0 = 2.0$ and $h_0 = 3.0$ respectively. The Binder cumulants U_L for $L = 256$ and 128 at $h_0 = 2.0$ and for $h_0 = 3.0$ are plotted in Fig.2.12(a) and in Fig.2.12(b) respectively. The statistical errors of the data points are indicated by vertical bars with the data points. For both the field amplitudes $h_0 = 2.0$ and 3.0, (i) the U_Ls corresponding to $L = 128(\bigcirc)$ and $L = 256(\diamond)$ do not intersect each other throughout the temperature range and (ii)

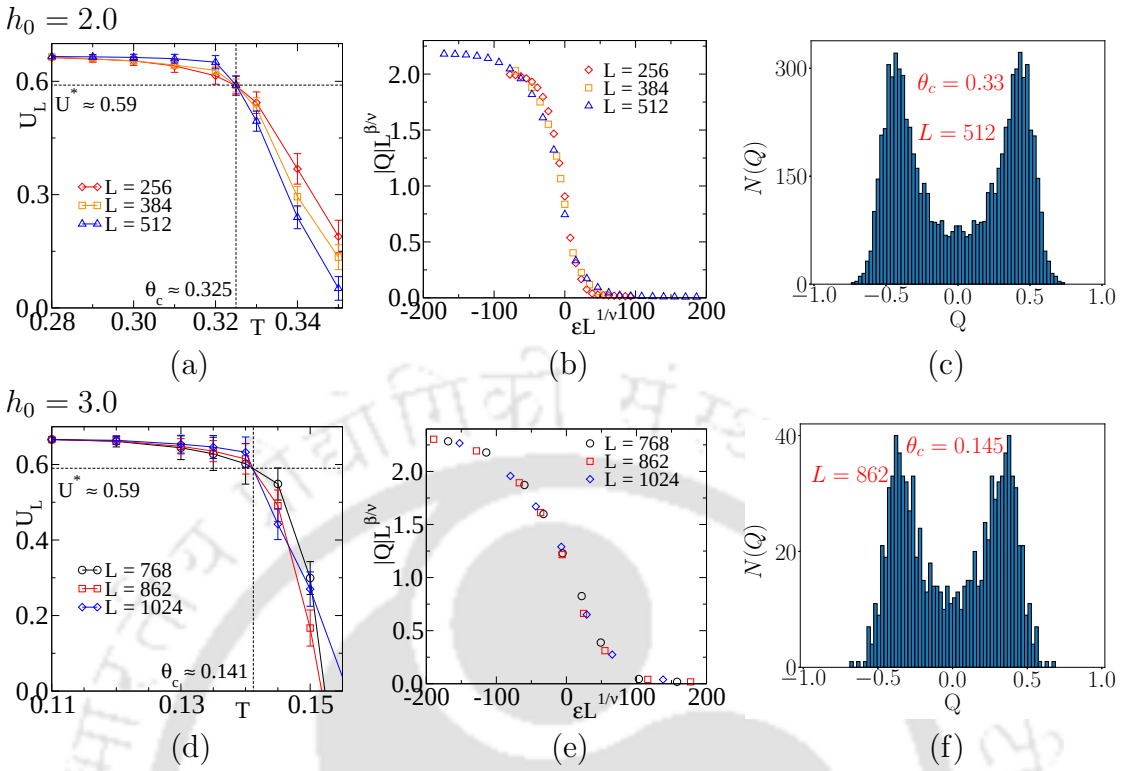

Figure 2.14: For $h_0 = 2.0$ and the system sizes $L = 256$, 384 and 512: Plot of (a) Binder cumulant U_L versus T, (b) $|Q|L^{\beta/\nu}$ versus $\varepsilon L^{1/\nu}$ and (c) $N(q)$ versus Q at θ_c of $L = 512$. The same plots for $h_0 = 3.0$ and system sizes $L = 768$, 862 and 1024 are given in (d), (e) and (f) at θ_c of $L = 1024$ respectively. The vertical bars with the data points in (a) and (d) represent statistical error of each point. The whole range of Q are divided over 60 equal bins in both the histograms. There are total 8192 samples for $L = 512$ in (c) and 1024 samples for $L = 862$ in (e).

the U_Ls corresponding to $L = 128$ and 256 become negative at certain temperatures and come back to zero at a higher temperature. The values of U_L become more negative at $h_0 = 3.0$ as it can be seen in Fig.2.12(b). Thus, it indicates that the transitions occurring in smaller systems at higher field amplitudes are very different from those obtained at lower field intensities.

The nature of transitions in these systems is now analyzed by looking into the magnetization time series $m(t)$ and distribution of order parameter Q. The variation of $m(t)$ against t and the histograms $N(Q)$ (distribution of 8192 values of Q over 60 equal bins) are shown in Fig.2.13 for the system sizes $L = 128$ and 256 at the field amplitudes $h_0 = 2.0$ and 3.0 around their respective transition points θ_c. In all three situations, ($L = 128$, $h_0 = 2.0$; $L = 128$, $h_0 = 3.0$; $L = 256$, $h_0 = 3.0$), once the system is in one of the well $+1$ (or -1), it tries to stay there for a longer time and makes a few attempts to cross to the other well -1 (or $+1$). The field $h(t)$ and

temperature T are the external noise that pushes the system from one ordered phase to the other. The period of the applied field is still so small for the given situation that the process takes a long time and occurs only at a good chance. As a result, most of the states appear with Q value either $+1$ or -1 and a fewer states with intermediate values of Q appear in the system as shown in Fig.2.13. The situation becomes more prominent at the higher field amplitudes such as $h_0 = 3.0$. Such a situation is called stochastic resonance. It usually occurs at higher field amplitudes h_0 for smaller systems.

It is now important to clarify that for a given field intensity, whether the stochastic resonance observed at a smaller system size will disappear with the increasing system size or not. To verify the existence of continuous DPT in larger system sizes in the high field regime, we have performed FSS study for higher system sizes: for $h_0 = 2.0$ we have considered $L = 256$, 384 and 512; for $h_0 = 3.0$ the system sizes considered are $L = 768$, 862 and 1024. In Fig.2.14, the binder cumulant U_L against temperature T, scaled order parameter $|Q|L^{\beta/\nu}$ against the scaled temperature $\varepsilon L^{1/\nu}$ and the histogram $N(Q)$ of order parameter Q are shown for $h_0 = 2.0$ and $h_0 = 3.0$. For both the field amplitudes, the Binder cumulants cross each other at the critical point θ_c and $U^* \approx 0.61$, known for DPT [24]. The vertical bars with the data points represent the statistical errors. The scaled order parameter collapses onto a single curve when plotted against the scaled temperature for the values of the exponents $\beta = 1/8$ and $\nu = 1$ as that of the zero-field equilibrium 2d Ising model. The histograms $N(Q)$ of Q at θ_c have a bimodal distribution picked around $\pm Q_c$ of these systems. All these properties indicate a continuous DPT for larger systems at higher field amplitudes. Note that at such high field amplitudes, the smaller systems displayed stochastic resonance with negative Binder cumulant. Thus negative Binder cumulant and bimodal distribution of order parameter in the stochastic resonance regime of these systems does not necessarily represent a discontinuous transition [52] as the transition becomes continuous in the $L \to \infty$ limit [50].

2.6 Summary and Conclusion

The kinetic Ising ferromagnet, a bistable system, is studied under a sinusoidal oscillating field $h(t)$ of fixed period $P = 512$ and amplitude $h_0 = 1.0$, 2.0 and 3.0 tuning the temperature T of the system far below the ferro to paramagnetic transition temperature T_c of the equilibrium 2d zero field Ising model. The system undergoes a dynamic phase transition at a temperature θ_c ($\ll T_c$) at which the mean

metastable lifetime $\langle\tau\rangle$ becomes comparable to the half period of the applied field. The system also possesses strong hysteresis effects. The hysteresis loops are found to be symmetric above θ_c and asymmetric below θ_c. A spontaneous breaking of the symmetry of the hysteresis loop occurs right at $T = \theta_c$. The asymmetric loop part is associated with the dynamic ordered phase (DOP), and the symmetric loop part is associated with the dynamic disordered phase (DDP). The hysteresis properties are evaluated employing a novel methodology that provides properties like loop area A, dynamic correlation C, as well as orientation α and aspect ratio Φ of the loop. For lower field intensity $h_0 = 1.0$, a weak finite size dependence of the loop properties is observed, whereas, at higher field intensities, a stronger finite size dependence of the loop properties is observed. The dynamic phase transition that occurs at θ_c is characterized by extensive FSS analysis at different field intensities. At $h_0 = 1.0$, the systems undergo a continuous DPT for the system sizes $L \geq 128$ with the critical exponents that of the equilibrium zero-field Ising model in 2d. From the study of magnetic time series and order parameter histogram, the system of size $L = 128$ at $h_0 = 2.0$ and the system of sizes $L = 128$ and 256 at $h_0 = 3.0$ are found to be in the stochastic resonance regime at their respective transition temperatures. It is further demonstrated for higher field amplitudes that the systems of larger sizes ($L \geq 256$ for $h_0 = 2.0$ and $L \geq 768$ for $h_0 = 3.0$) display continuous DPT with the critical exponents that belong to the same universality class of 2d Ising model. Hence, at high field intensities, the stochastic resonance occurring in smaller systems disappears in the large system size limit, and they display continuous DPT.

Chapter 3

Hysteresis and DPT in diluted kinetic Ising ferromagnet

Pure materials are rare, and impurities are inevitable. A real magnetic material can have several kinds of disorder present in it. The disorder always adds extra complexity to its physical behavior. The presence of disorder not only changes the regular lattice morphology of a pure material, but also the interactions among the magnetic ions are strongly affected in the presence of disorder. The most common type of physical disorder corresponds to a situation where a few magnetic ions or spins are physically missing at random or replaced by non-magnetic elements in a regular magnetic material [4]. It is expected that a magnetic system with the disorder will show distinctive critical properties and phase transition in comparison to a pure magnetic substance. In the Ising model, impurities are implemented by replacing a magnetic spin with a non-magnetic entity, and the model is called site diluted Ising model [91–95]. Impurities can also be implemented by removing interaction among two nearby spins, and such a model is called bond diluted Ising model [96–101]. Annealed site diluted Ising model is known to exhibit critical behavior of that of the pure Ising model [102, 103]. However, the critical behavior of the quenched site diluted Ising model is less understood and extensively studied both theoretically [104, 105] and experimentally [106–108]. The main aim of these studies was to know how the disorder influences the critical behavior of the system and its universality class. According to Harris criterion [109], if the specific heat critical exponent α of a pure system is positive, the values of the critical exponents change with the introduction of weak disorder in the system, and consequently, disorder changes the universality class. On the other hand, there will be no change in the values of the critical exponents with the increase in disorder in the system if $\alpha < 0$

for the corresponding pure system. The site diluted 2d equilibrium Ising model is particularly interesting as it corresponds to a marginal case, as $\alpha = 0$ for the pure 2d Ising model. There exists a controversy between the strong universality hypothesis [95] which claims that the critical exponents remain unchanged with the disorder. However, scaling has multiplicative logarithmic corrections and the weak universality hypothesis [91, 110–112], which favors the dilution dependent critical exponents. However, hysteresis and dynamic phase transition in diluted Ising ferromagnets are rarely reported [56, 113, 114].

It will be interesting to know how nonequilibrium dynamic phase transition (DPT) dynamics get affected by the underlying diluted lattice morphologies. This chapter will discuss extensive Monte Carlo study results to describe nonequilibrium phase transitions on diluted lattices. First, we will study the hysteresis and nonequilibrium DPT in the presence of an external sinusoidal field, far below the respective $T_c(q)$ of the diluted kinetic Ising ferromagnet at different concentrations of dilution $q = 0.1, 0.2$ on the 2d square lattices for several systems sizes L. We will explore the DPT in both ways: tuning the temperature T below $T_c(q)$ keeping the period P of the field fixed and also varying the period P of the external field, keeping the temperature of the system fixed below $T_c(q)$. The model, details of the numerical simulations, and results are described below.

3.1 Dynamic phase transition in diluted kinetic Ising model

Diluted Ising ferromagnets are also bistable systems below the respective ferro to paramagnetic phase transition temperature $T_c(q)$, q is the concentration of dilution. Such a system is expected to show hysteresis effects and nonequilibrium phase transition under external time varying field. Estimates of $T_c(q)$, the phase transition temperature in diluted Ising model are reported for several values of q [93, 110]. Since we are only interested for weak disorder below we quote the values of $T_c(q)$ for $q = 0.1$ and 0.2 in Table.3.1. An independent estimate of $T_c(q)$ is also performed, and it found that $T_c(q) = 1.90 \pm 0.02$, and 1.52 ± 0.02 for $q = 0.1$ and 0.2 respectively. Our estimates are very close to the reported values within error bars [93, 110]. It is further noticed that $T_c(q) \to 0$ as the q is increased upto $1 - p_c = 0.407254$ [115], where p_c is the percolation threshold (≈ 0.592746).

q	$T_c(q)$	β/ν	γ/ν
0.1	1.9095(5)	0.125(5)	1.76(2)
0.2	1.5046(10)	0.11(1)	1.78(2)

Table 3.1: The values of $T_c(q)$ at different dilution q from Ref [93, 110].

3.1.1 Model and Simulation

A diluted kinetic Ising model (DKIM) is developed on a two dimensional square lattice of size L. A site is either occupied by an Ising spin $S_i = \pm 1$ or remains empty. A site without a spin is called a disordered site; otherwise, it is a regular site. Disorder in the lattice is assigned randomly with concentration q by calling a uniformly distributed random number $r \in [0, 1]$ for each lattice site. If $r \leq q$, the site is not assigned any spin and marked as a disordered site. Otherwise, a spin is assigned to the site and marked as a regular site. Each spin can interact with its nearest neighbor spins, if available, under periodic boundary condition with ferromagnetic interaction strength $J(> 0)$. An external time varying sinusoidal oscillating magnetic field $h(t)$ given by

$$h(t) = h_0 \sin(2\pi t/P) \tag{3.1}$$

where h_0 is the amplitude and P is the time period of the oscillating field, is applied on the system. The Hamiltonian of the DKIM under the external field $h(t)$ can be expressed as,

$$\mathcal{H} = -J \sum_{\langle ij \rangle} c_i c_j S_i S_j - h(t) \sum_i c_i S_i \tag{3.2}$$

where h_0 is taken in the unit of J, the occupation index $c_i = 0$ corresponds to a disordered site, and $c_i = 1$ corresponds to a regular site.

In order to equilibrate the system with the heat bath at temperature T, the system is evolved without magnetic field following Glauber Monte Carlo (MC) single spin flip dynamics [73]. The T is also measured in the unit of J. The spin flip acceptance ratio W according to the Glauber MC dynamics is given by

$$W(S_i \to -S_i) = \frac{e^{-\Delta E/k_B T}}{1 + e^{-\Delta E/k_B T}} \tag{3.3}$$

where ΔE is the change in energy due to spin flip at any time t. It can obtained as

$$\Delta E = 2S_i \Sigma + 2S_i h(t) \tag{3.4}$$

where Σ is the sum of the nearest neighbor spins of the spin S_i. Both the value of J and Boltzmann constant k_B are taken to be 1 throughout the simulations.

Detailed Monte Carlo (MC) simulation has been performed following Glauber MC spin flip dynamics on two dimensional square lattices of size $L = 128, 256$ and 512 at different disorder $q = 0.1$ and 0.2 and regular lattice. One MC step corresponds to updating on an average each spin of the system once. A MC step is the calling and updating $(1 - q)L^2$ spins on a diluted square lattice of size L and dilution q, which is taken as one unit of time. The initial state is taken as either all spins up $S_i = +1$ state or all spins down $S_i = -1$ state. The system is iterated for 10^6 MC time steps to thermalize it at a given temperature T in the absence of the external field. A number of equilibrium states with constant magnetization are then generated at a given T in the absence of the external field. As the system achieves a constant magnetization in equilibrium at a given temperature T, the external time-dependent magnetic field $h(t)$ is applied to a randomly chosen equilibrium state at a given temperature T. In a MC step, $(1 - q)L^2$ spins are randomly chosen and updated using Glauber acceptance ratio W using the full Hamiltonian (Eq.3.2). One cycle of the applied field of period P consists of P number of MC steps. The system is further evolved to achieve the stable dynamic states in the presence of the applied field over 256 cycles, i.e., $\mathcal{O}(10^5)$ MC steps, before collecting data. Then the data is collected over the next 10^6 MC steps over the stable cycles. Eight randomly chosen equilibrium disordered configurations are taken as initial samples, and measurements are made on the 1024 stable cycles (selected from all over the time series) for each sample. All the dynamic quantities are averaged over the cycles and configurations, leading to an ensemble of size 8192. For a given disorder concentration q, the magnetic state of the system is defined by the values of field amplitude h_0, field time period P, and temperature T.

3.2 Temperature varied DPT

Let us first discuss the DPT varying the temperature T far below the respective ferro to para transition temperature $T_c(q)$ for a given dilution q on several system sizes $L = 128, 256$ and 512. The external field amplitude $h_0 = 0.75$, and period $P = 512$ are kept fixed throughout the temperature varied DPT study.

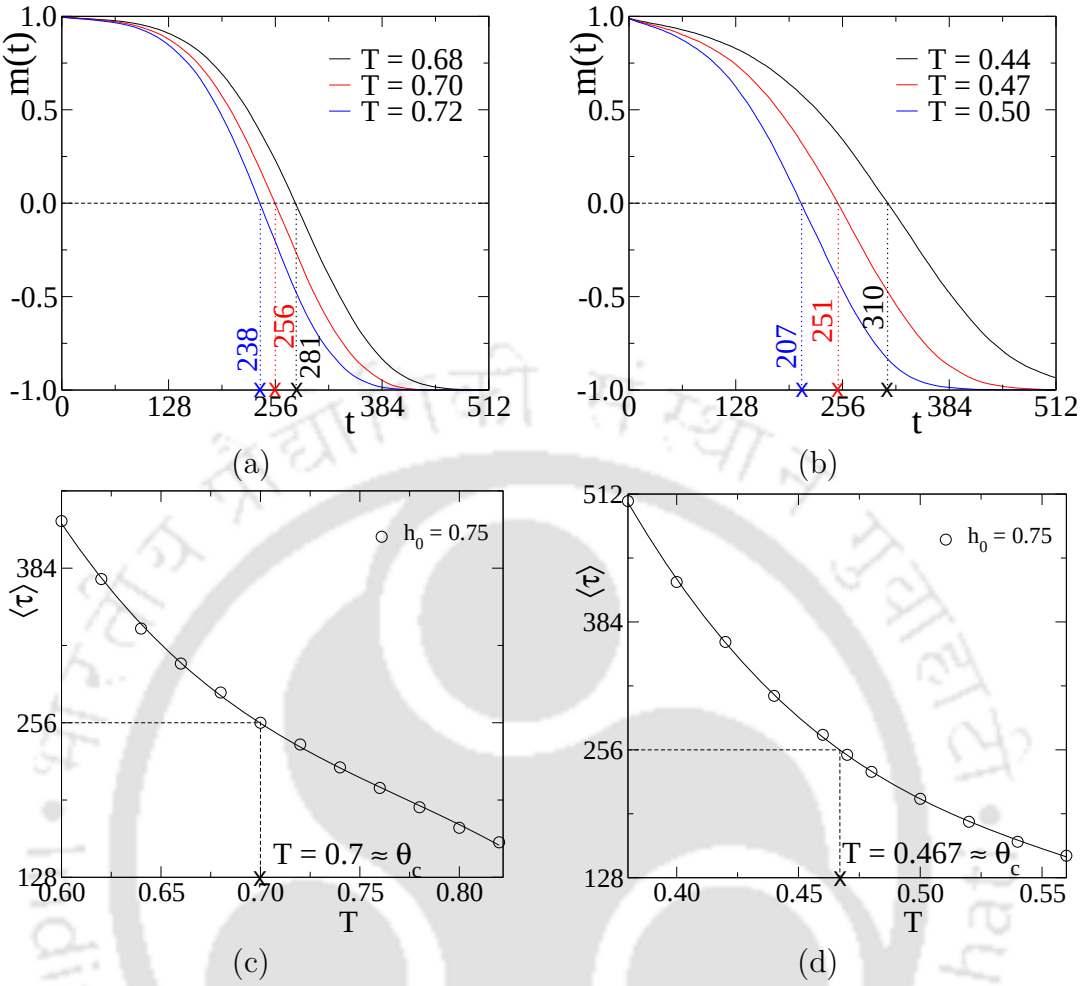

Figure 3.1: Variation of $m(t)$ with t after a constant field $+h_{\rm rms}$ overturns to $-h_{\rm rms}$ at $t = 0$, $h_{\rm rms} = h_0/\sqrt{2}$ for $h_0 = 0.75$ (a) $q = 0.1$ and (b) $q = 0.2$. Plot of $\langle\tau\rangle$ against T for (c) $q = 0.1$ and (d) $q = 0.2$ on a system size $L = 512$.

3.2.1 Metastable lifetime and critical point

We are in fact varying the mean metastable lifetime $\langle\tau\rangle$ of the system when tuning its temperature. The system is first evolved at a constant external field of intensity h_0 at a given temperature T and allowed to reach a constant magnetization $m(t)$. Then, we reverse the field to $-h_0$ and keep track of the count of MC steps it takes to reach zero magnetization. The number of MC steps represent the metastable lifetime. Such variations of $m(t)$ for three different temperatures is plotted with t in Fig.3.1(a) and (b) for $q = 0.1$ and 0.1 on a system of size $L = 512$ and $h_0 = 0.75$. The metastable lifetime corresponding to $m(t) = 0$ for different values of T are marked by crosses on the time axis. Taking an average over several such field reversals, the mean metastable lifetime $\langle\tau\rangle$ of a system is evaluated. Since sinusoidal field of

amplitude h_0 is used for the study of DPT here, the root mean square (rms) value of the field amplitude $h_{\rm rms} = h_0/\sqrt{2}$ is taken as constant field [37]. The variation of $\langle\tau\rangle$ against temperature T is shown for $q = 0.1$ and $q = 0.2$ in Fig.3.1(c) and (d) on $L = 512$. The $\langle\tau\rangle$ corresponds to the half-period $P_{1/2}$ at the dynamic phase transition point [24]. Thus, we can estimate an approximate critical temperature $\theta_c(q)$ of DPT corresponding to a $P_{1/2}$ or $\langle\tau\rangle$ value from the $\langle\tau\rangle$ versus T plot. The $\langle\tau\rangle = 256$ corresponds to temperatures 0.7 and 0.47 for disorder $q = 0.1$ and $q = 0.2$. Thus, the approximate value of $\theta_c(q)$ is 0.7 and 0.47 for disorder $q = 0.1$ and $q = 0.2$ respectively for $h_0 = 0.75$ and $P = 512$. For a fixed period, $\langle\tau\rangle$ is greater than $P_{1/2}$ for $T < \theta_c(q)$ and the system will be in either of the metastable states. On the other hand, $\langle\tau\rangle$ is less than $P_{1/2}$ for $T > \theta_c(q)$ and the system continuously moves from one metastable state to the other.

3.2.2 Hysteresis

There is phase lag between the per spin instantaneous magnetization and the applied field due to the delay in response of the spins. The ensemble average instantaneous magnetization for a given cycle is defined as

$$\langle m(t)\rangle = \langle \frac{1}{N_s}\sum_{i=1}^{N_s} S_i(t)\rangle \tag{3.5}$$

where $S_i(t)$ represents the value of the spin at the ith lattice site at time t and $\langle\cdots\rangle$ represents the ensemble average for a fixed disorder q. $N_s = \sum_{i=1}^{L^2} c_i$ is total number of spins. The variation of $\langle m(t)\rangle$ is shown against MC time step t over a full period in Fig.3.2 for regular lattice and different dilutions $q = 0.1$ and 0.2 for $h_0 = 0.75$ and the period $P = 512$. The systems presented in this plot are evolved starting from the all spins up ($S_i = +1$) configurations. Fig.3.2(a), (b), and (c) have plots at lower temperatures, whereas the plots in Fig.3.2(d), (e), and (f) have the same in higher temperatures. There are few observations, first, the magnetization lags behind the magnetic field at all temperatures and field amplitudes. This leads to hysteresis loss in the system.

Second, the magnetization remains at $+1$ (or -1 if started from the negative metastable phase) for most of the time at low temperatures. Whereas it is continuously varying from a positive to a negative value and vice versa at higher tempera-

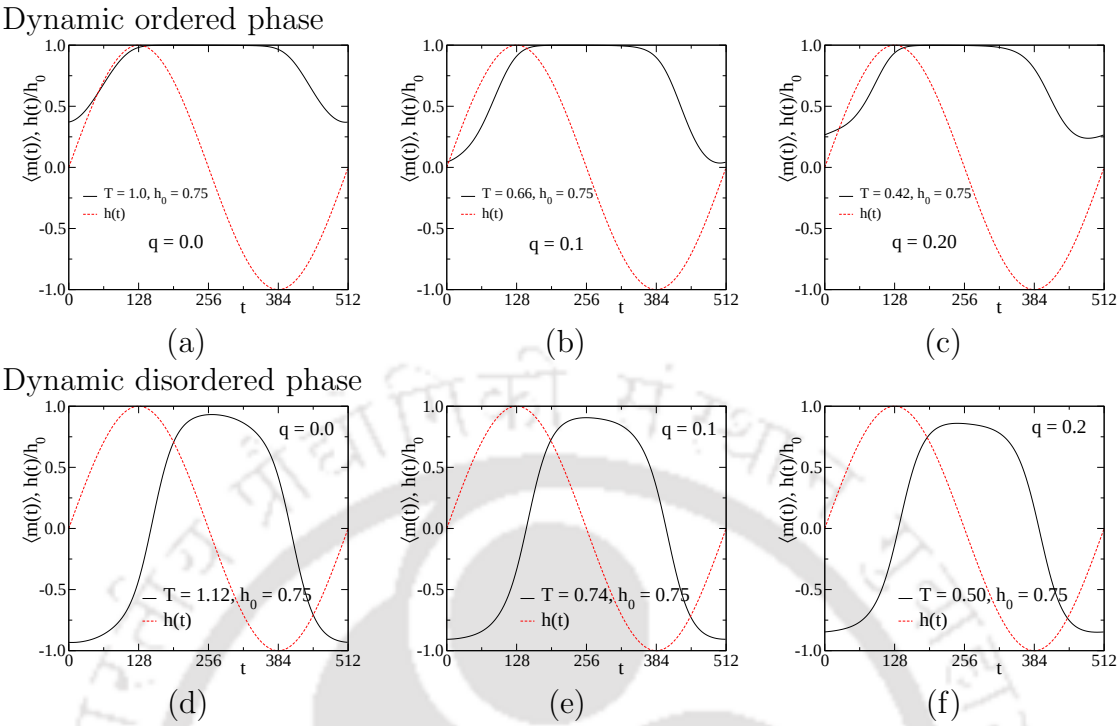

Figure 3.2: Instantaneous magnetization $\langle m(t)\rangle$ with MC step t over a complete cycle of the magnetic field $h(t) = h_0 \sin(2\pi t/P)$ for $h_0 = 0.75, P = 512$ for regular lattice and different concentrations of dilution $q = 0.1$, and 0.2 at temperatures (a) $T = 1.0$, (b) 0.66 and (c) 0.42 in DOP and (d) $T = 1.12$, (e) 0.74 and (f) 0.50 in DDP respectively on a square lattice of size $L = 512$. The dashed line in red represents the external sinusoidal field.

tures. A period average magnetization Q now can be defined as

$$Q = \frac{1}{P}\int_0^P \langle m(t)\rangle dt \tag{3.6}$$

where P is the time period of the external field. As a result, the system has a non-zero period average magnetization ($Q \neq 0$) (either +ve or −ve) at lower temperatures, but it will have a zero period average magnetization ($Q = 0$) at higher temperatures. The system then moves from a non-zero Q to $Q = 0$ as the temperature T is increased from a lower value to a higher value far below the respective zero field ferro-para transition temperature $T_c(q)$ for a particular q. This observation indicates the existence of two distinct dynamical phases, one called dynamic ordered phase (DOP) with a finite period average magnetization and the other called dynamic disordered phase (DDP) with zero cycle average magnetization. A phase transition from DOP to DDP occurs at a temperature $\theta_c(q)$ far below $T_c(q)$.

The magnetizations $\langle m(t)\rangle$ are plotted against the field $h(t)$ in Fig.3.3(a) $T = 1.0$,

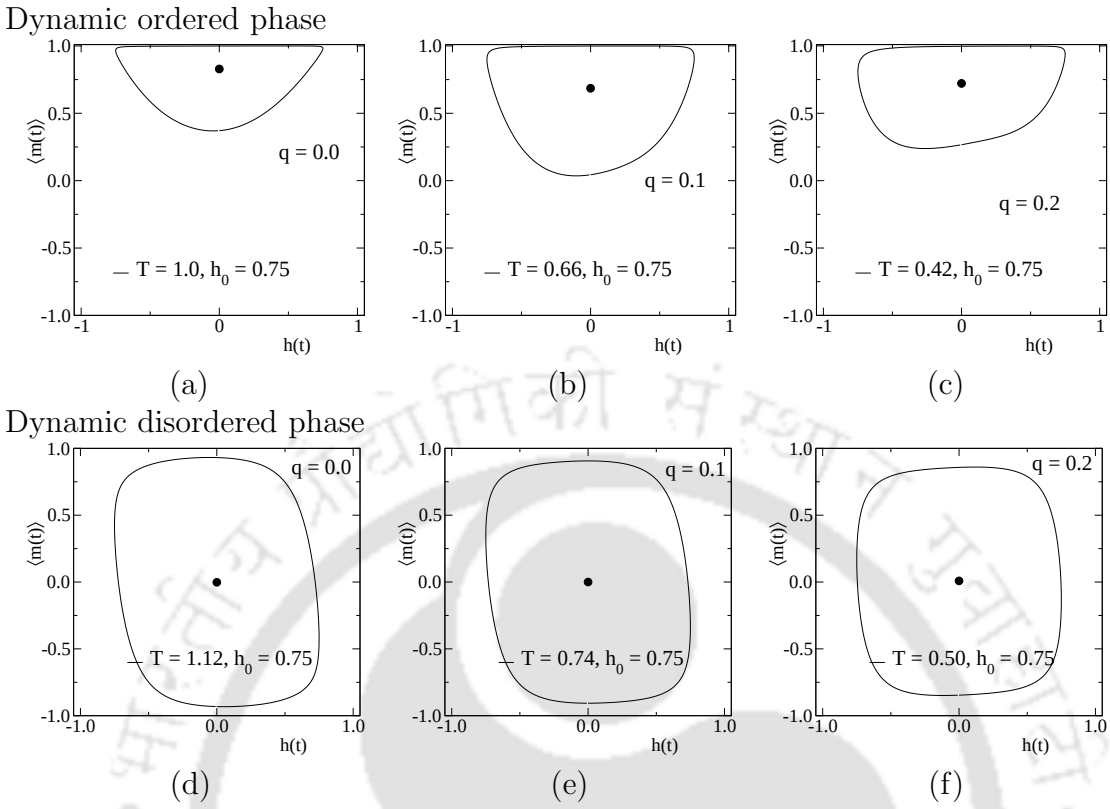

Figure 3.3: Hysteresis loops over a complete cycle of field (time period $P = 512$) on a square lattice of size $L = 512$ for regular lattice and different dilution $q = 0.1$ and 0.2 at temperatures (a) $T = 1.0$, (b) 0.66 and (c) 0.42 in DOP and (d) $T = 1.12$, (e) 0.74 and (f) 0.50 in DDP respectively. The solid circles represent the centers of the hysteresis loops.

(b) 0.66, and (c) 0.42, and in Fig.3.3(d) $T = 1.12$, (e) 0.74, and (f) 0.50 to visualize the hysteresis loop at different temperatures on regular lattice and dilution $q = 0.1$ and 0.2 for fixed field amplitude $h_0 = 0.75$. It can be seen that the hysteresis loops about the zero magnetization line are asymmetric for lower temperatures, whereas they are symmetric at higher temperatures. The shape, orientation, and symmetry of the hysteresis loop change as temperature T is increased for a fixed field. The center of the loop moves from a positive finite value to zero with increasing T. The phase corresponding to the asymmetric hysteresis loop, finite cycle average magnetization (represented by the center of the loop) is the DOP and the phase corresponding to symmetric hysteresis loop, zero cycle average magnetization is the DDP, the transition to DDP from DOP occurs at a temperature $\theta_c(q)$.

The asymmetric hysteresis loops remain very flat, almost like a horizontal line parallel to the field axis at very low temperatures. As the T increases in DOP, the loops acquire some width along the magnetization axis, and the area gradually increases. Near the DPT, hysteresis loops become symmetric for the first time. The

hysteresis loop area keeps on increasing for a little while, even after the DPT. The other interesting observation is that the loops rotate while changing their area and shape with increasing temperature. The hysteresis loop shows a jump or abrupt change in its orientation when part of the hysteresis loop reaches the other half with respect to the zero magnetization line, i.e., when $m(t)$ changes sign. The loop area A continuously decreases to smaller values as the T increases after reaching maximum after $\theta_c(q)$ [45].

The instantaneous magnetization lags behind the applied field in ferromagnetic systems [26]. As a result, the hysteresis loop appears in the system. The hysteresis loops area, shape, and orientation change with the increase in temperature of the system. A hysteresis loop tensor $\overleftrightarrow{T}$ can be constructed to quantitatively describe the geometric properties of the hysteresis loops as described in the previous chapter. The eigenvalues λ_1 and λ_2 of $\overleftrightarrow{T}$ are given by

$$\lambda_{1,2} = \frac{1}{2}\left[(T_{mm} + T_{hh}) \pm \sqrt{D}\right] \tag{3.7}$$

where $D = (T_{mm} - T_{hh})^2 + 4T_{mh}^2$, plus sign corresponds to the largest eigenvalue λ_1 and minus sign corresponds to the smallest eigenvalue λ_2. Where the diagonal elements T_{hh} and T_{mm} are given by $T_{hh} = \frac{1}{P}\sum_{t=1}^{P} h_t^2, T_{mm} = \frac{1}{P}\sum_{t=1}^{P}(m_t - Q)^2$ and the off diagonal elements are given by $T_{hm} = T_{mh} = \frac{1}{P}\sum_{t=1}^{P} h_t\,(m_t - Q) = \frac{1}{P}\sum_{t=1}^{P} h_t m_t$. The area A of the loop, the average loss in magnetic energy over a cycle, is given by $A = -\oint m(t)dh(t)$ where $h(t)$ is time dependent external field. However, an approximate loop area A can be obtained in terms of the eigenvalues of the hysteresis loop as $A \approx 4\sqrt{\lambda_1\lambda_2}$. The dynamic correlation C is defined as $C = \langle m(t)h(t)\rangle - \langle m(t)\rangle\langle h(t)\rangle$. The orientation of the hysteresis loop can be estimated by the angle of rotation of one of the principal axes or the eigenket $|e_1\rangle$ or $|e_2\rangle$.The orientation α can be defined as the angle made by $|e_1\rangle$ corresponding to the eigenvalue λ_1 with the horizontal axis corresponding to field amplitude. The orientation α of the loop with respect to the field axis is then given by $\alpha = \tan^{-1}\left(\frac{e_m}{e_h}\right)$ where e_h and e_m are the components of $|e_1\rangle$ along magnetic field and magnetization axes respectively. The shape of the loop can be studied by measuring the aspect ratio of the loop. The aspect ratio Φ of the loop is defined as $\Phi = \sqrt{\frac{\lambda_2}{\lambda_1}}$ in terms of λ_1 and λ_2.

The variation of hysteresis loop area A, orientation α, aspect ratio ϕ, and dynamic correlation C with temperature T are plotted in Fig. 3.4(a), (b), (c), and (d)

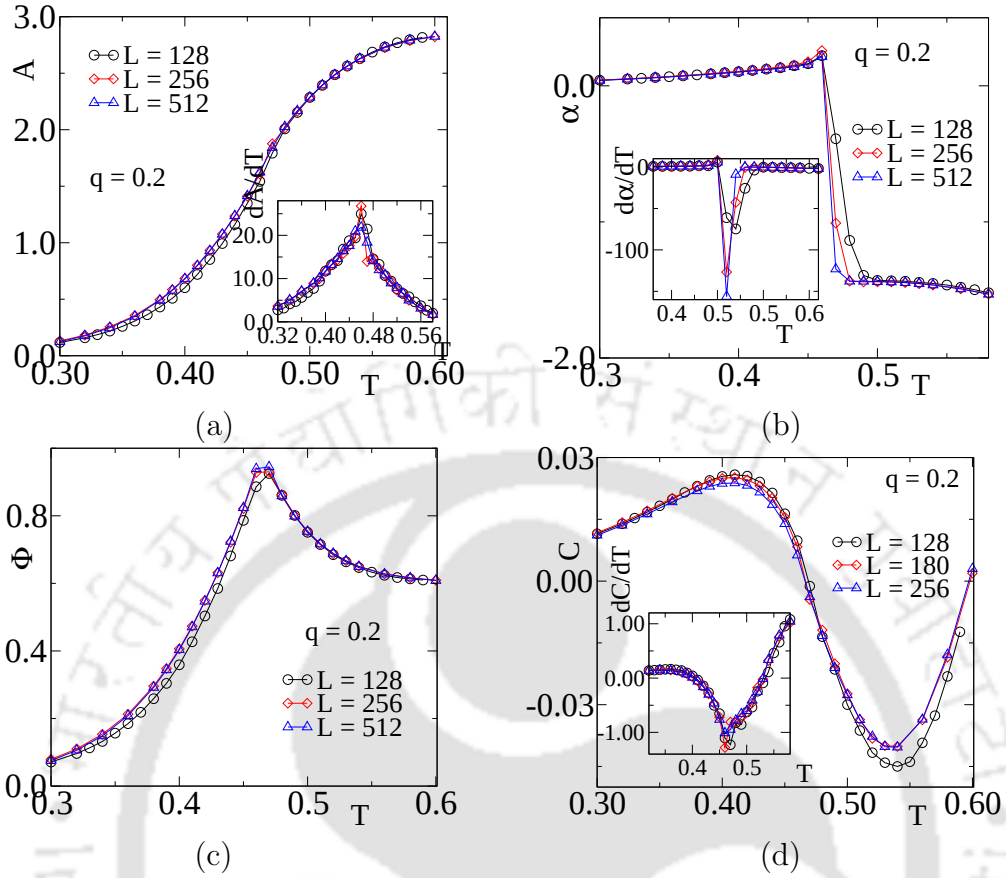

Figure 3.4: Plot of hysteresis loop (a) area A, (b) orientation α, (c) aspect ratio ϕ, and (d) dynamic correlation C with temperature T for $h_0 = 0.75$ and $P = 512$ on system sizes $L = 128(\bigcirc)$, $256(\diamond)$ and $512(\triangle)$ for $q = 0.2$.

for $h_0 = 0.75$, $P = 512$, and $q = 0.2$ on different system sizes $L = 128(\bigcirc)$, $256(\diamond)$ and $512(\triangle)$. All these hysteresis loop related quantities have almost no finite size effect except around the DPT point. The loop area A remains very small in DOP due to asymmetric hysteresis loops. Then, A increases with increasing T in DOP. The hysteresis loop areas keep increasing at $\theta_c(q)$, and the loop becomes symmetric for the first time. The symmetric loop area becomes maximum after the transition [45]. The A decreases after reaching the maximum value with a further increase in T. The $\frac{dA}{dT}$ is plotted with T in the inset of Fig.(a), where we can see the rate of increase in area or the loss in the system is maximum at $\theta_c(q)$. The change in orientation of hysteresis loop α with temperature T is shown in Fig.(b). The asymmetric hysteresis loops remain almost flat and parallel to the field axis in DOP at lower temperatures. The α then increases by a tiny amount as the asymmetric loop widens along the magnetization axis. Near the DPT $\theta_c(q)$ the loops tend to become asymmetric to symmetric. The α rotates in the opposite direction and having either

a point of inflection ($q = 0.1$) or a jump ($q = 0.2$) at DTP ($\theta_c(q)$). A $\frac{d\alpha}{dT}$ versus T has a trough at $\theta_c(q)$ shown in inset of Fig.(b). Finally, with further increase in T, the loop rotates in the same direction. The aspect ratio of hysteresis loop Φ with temperature T is shown in Fig.(c). The Φ is small in DOP, corresponding to asymmetric hysteresis loops. Φ increases as the loop area increase with T in DOP. Aspect ratio becomes maximum around $\theta_c(q)$ of DTP. The Φ decreases after DPT with an increase in T in DDP. The dynamic correlation C is plotted with temperature T in Fig.(d). C almost does not have any finite size effect except around the DPT point ($\theta_c(q)$). C shows a prominent finite size effect with the introduction of dilution, which was absent in regular lattice. The C is small in DOP, corresponding to asymmetric hysteresis loops. Next, C or the negative of spin-field interaction energy increases with the increases of loop area with T. C also shows a point of inflection at the DPT point $\theta_c(q)$, where $\frac{dC}{dT}$ has a trough. The nature of variation of A, α, ϕ, and C with increasing T in DOP and DDP are very similar for other dilution and regular lattices except their DOP to DDP transition temperature $\theta_c(q)$ decreases with increasing q for fixed h_0 and P.

Next, we will study how the behavior of hysteresis loop properties change with the disorder for fixed $h_0 = 0.75, P = 512$ on a lattice of size $L = 512$. The behavior of hysteresis loop area A, orientation α, aspect ratio ϕ, and dynamic correlation C with reduced temperature $\varepsilon = (T - \theta_c(q))/\theta_c(q)$ are plotted in Fig. 3.5(a), (b), (c), and (d) for $h_0 = 0.75$, $P = 512$ on square lattice of size $L = 512$ on regular lattice $q = 0.0(\bigcirc)$, and for different dilution $q = 0.1(\diamond)$ and $q = 0.2(\triangle)$. The $\theta_c(q)$ is different for regular lattice and different dilution q. So plots are shown with ε to have a comparative view. $\varepsilon = 0$ refers to the DPT temperature $\theta_c(q)$. It can be seen that the rate of increase in hysteresis loop areas or loss with ε is higher for smaller q value, and the rate of loss is lower for higher q. The spin-spin correlation becomes weak on diluted lattices as some of the spins are removed from the system. The field can more easily alter the spin orientations, and the rate of loss decreases. The rate of hysteresis loss increases when the spins in the system have a stronger correlation and oppose any change in spin configuration due to external field. The comparative behavior of orientation α shown in Fig.(b), remains almost similar in all cases except the amount of jump at the $\theta_c(q)$ is larger for higher q. The aspect ratio Φ reaches its maximum value near the transition point where the symmetric loops have their two dimensions (height and width) closest in the regular lattice, and diluted lattices are shown in Fig.(c). After $\theta_c(q)$ the Φ decreases with increase in T. The rate of increase of Φ with T as well as the rate of decrease $d\Phi/d\varepsilon$ is

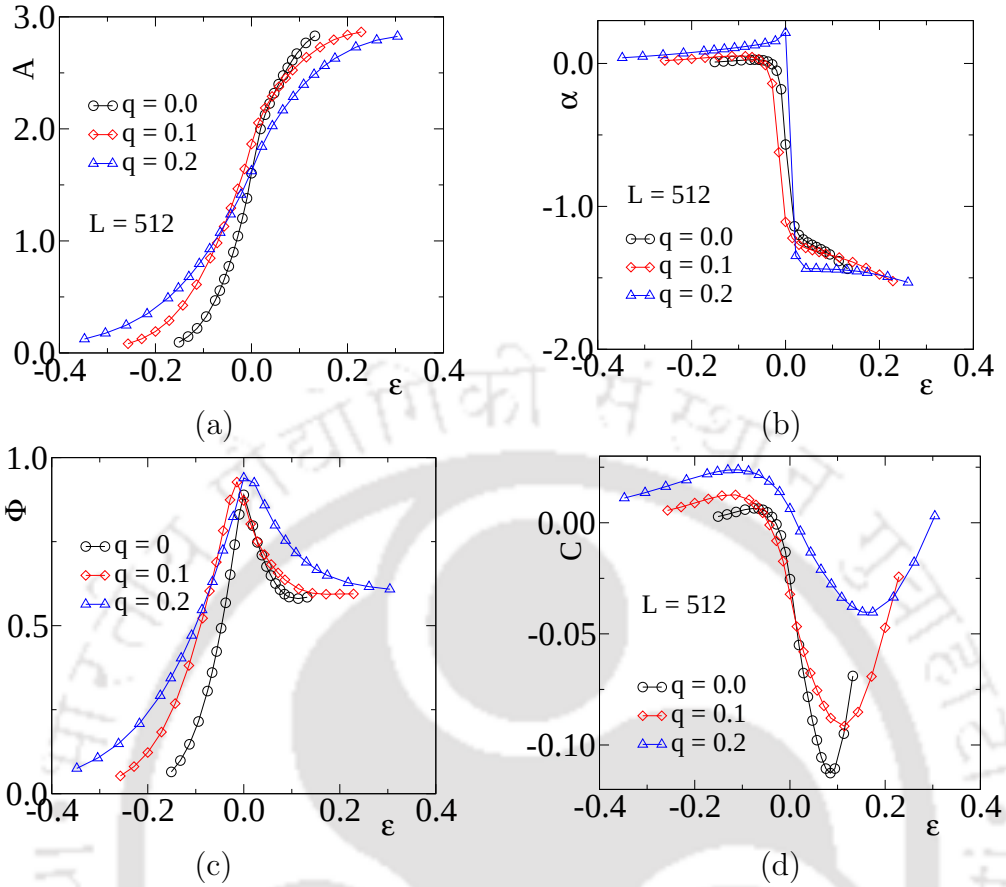

Figure 3.5: Plot of hysteresis loop (a) area A, (b) orientation α, (c) aspect ratio ϕ, and (d) dynamic correlation C with temperature T for $h_0 = 0.75$ and $P = 512$ on a lattice of size $L = 512$ for regular lattice ($\bigcirc$), $q = 0.1(\diamond)$ and $q = 0.2(\triangle)$.

highest in the case of the regular lattice. But $\pm d\Phi/d\varepsilon$ decreases with increase in q. The peak value of Φ is largest for $q = 0.2$ and smallest in regular lattices. In Fig.(d), the dynamic correlation C or the negative spin-field interaction energy is shown for different dilutions. It beautifully depicts the fact how dilution makes the system more vulnerable to the external field. In DOP, on a regular lattice, C is only a little positive as the external field has the least effect on the spin system. As the q increases, the spin-spin interaction decreases - the C value increases indicating a stronger field dominance. When the system reaches the transition point $\theta_c(q)$, the spin-spin interaction dominates over the field, more in the case of regular lattice and smallest in high dilution, the C value becomes negative. If the T is further increased, the field effect starts dominating again.

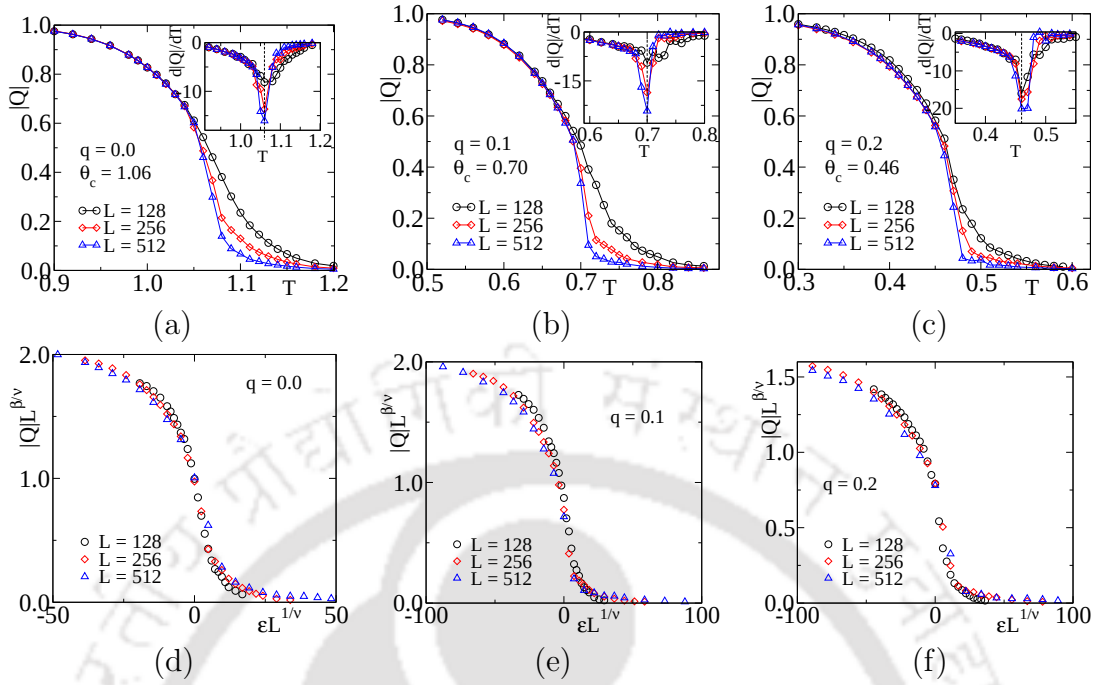

Figure 3.6: Plot of dynamic order parameters $|Q|$ with temperature T for $h_0 = 0.75$ and $P = 512$ on system sizes $L = 128(\bigcirc)$, $256(\diamond)$ and $512(\triangle)$ for (a) regular lattice, (b) $q = 0.1$, and (c) $q = 0.2$. $d|Q|/dT$ is plotted with T in each plot shown in the insets. The scaled order parameters, $|Q|L^{\beta/\nu}$ are plotted against the scaled variable $\varepsilon L^{1/\nu}$ in (d), (e) and (f) for respective q with corresponding critical exponents.

3.2.3 Finite size scaling study varying T

The ferro to paramagnetic phase transition temperature $T_c(q)$ for a diluted Ising system depends on the dilution concentration q. The diluted Ising ferromagnet is a bistable system below ferro to para equilibrium phase transition temperature $T_c(q)$. The magnetization response and the hysteresis loops under external time varying field are different while tuning the temperature T of the system for fixed h_0 and P. The system moves from an asymmetric dynamic phase (or DOP) to a symmetric dynamic phase (or DDP) as the temperature T of the system (below the critical temperature $T_c(q)$) is increased from below $\theta_c(q)$ to above $\theta_c(q)$, a critical temperature at which DPT occurs. In DOP, the system remains in one of the metastable states, whereas, in DDP, the system moves from one metastable state to the other in a complete cycle. The period average magnetization $Q = \frac{1}{P}\int_0^P m(t)dt$ is taken as the dynamic order parameter of DPT. Where P is the period of the applied field. As Q could have both positive and negative values in DOP corresponding to two metastable states, we describe a finite size scaling (FSS) theory here considering the absolute order parameter $|Q|$. Following the theory of thermal critical phenomena

[5, 7], the finite size scaling (FSS) form of $|Q|$ is assumed to be

$$|Q| = L^{-\beta/\nu}\widetilde{Q}[\varepsilon L^{1/\nu}] \tag{3.8}$$

where $\widetilde{Q}$ is a scaling function. The order parameter exponents β is defined as $|Q| \sim (-\varepsilon)^{\beta}$ and the correlation length exponents ν is defined as $\xi \sim |\varepsilon|^{-\nu}$, where ξ is the correlation length. Following the formalism of equilibrium critical phenomena [87], the susceptibility χ of the system then can be estimated from the fluctuation of dynamic order parameter $|Q|$ as $\chi = L^d(\langle|Q|^2\rangle - \langle|Q|\rangle^2)$ where $\langle|Q|^n\rangle = \int |Q|^n P_L(|Q|)d|Q|$ and $d = 2$ for two dimensions. The FSS form of χ is then given by

$$\chi = L^{\gamma/\nu}\widetilde{\chi}[\varepsilon L^{1/\nu}] \tag{3.9}$$

where $\widetilde{\chi}$ is a scaling function and $\gamma/\nu = d - 2\beta/\nu$ as both $\langle Q^2\rangle$ and $\langle|Q|\rangle^2$ goes as $L^{-2\beta/\nu}$. The susceptibility exponent γ is defined as $\chi \sim |\varepsilon|^{-\gamma}$. The fourth order Binder cumulant is defined as $U_L = 1 - \frac{\langle Q^4\rangle}{3\langle Q^2\rangle^2}$ and its FSS form is given by

$$U_L = \widetilde{U}[\varepsilon L^{1/\nu}] \tag{3.10}$$

where $\widetilde{U}$ is a universal scaling function. We have from Eq.4.18 at the $T = \theta_c$

$$U'_L = \frac{\widetilde{U'}[0]}{\theta_c} L^{1/\nu} \tag{3.11}$$

where $\widetilde{U'}$ is a universal scaling function, and $U'_L = \frac{dU_L}{dT}$.

The $|Q|$ is plotted with temperature T in the top row of Fig. 3.6 for regular lattice and on different values of disorder q on square lattice of sizes $L = 128(\bigcirc)$, $256(\diamond)$ and $512(\triangle)$. The $|Q|$s have strong finite system size dependence and change almost similarly for different q values except they have different $\theta_c(q)$. The value of $\theta_c(q)$ is estimated from the temperature where the change of Q with T *i.e.*, $d|Q|/OT$ is maximum. The $d|Q|/dT$ is plotted with T in all cases and the $\theta_c(q)$s are estimated from the trough in each plot shown in the inset. The values of $\theta_c(q)$ found to be 1.06 ± 0.01, 0.70 ± 0.01 and 0.46 ± 0.01 for regular lattice and $q = 0.1$ and 0.2 respectively. The fall of $|Q|$ appears to become more sharper as the dilution increases. Next, we verify the FSS forms of $|Q|$ by plotting the scaled order parameters $|Q|L^{\beta/\nu}$ against the scaled variable $\varepsilon L^{1/\nu}$ in Fig.3.6 (d), (e), (f) for different q. Good collapse of data occurred with the 2d equilibrium Ising model critical exponents, *i.e.*, $\beta = 1/8, \gamma = 7/4$ and $\nu = 1$ for regular lattice. We have estimated the equilibrium phase

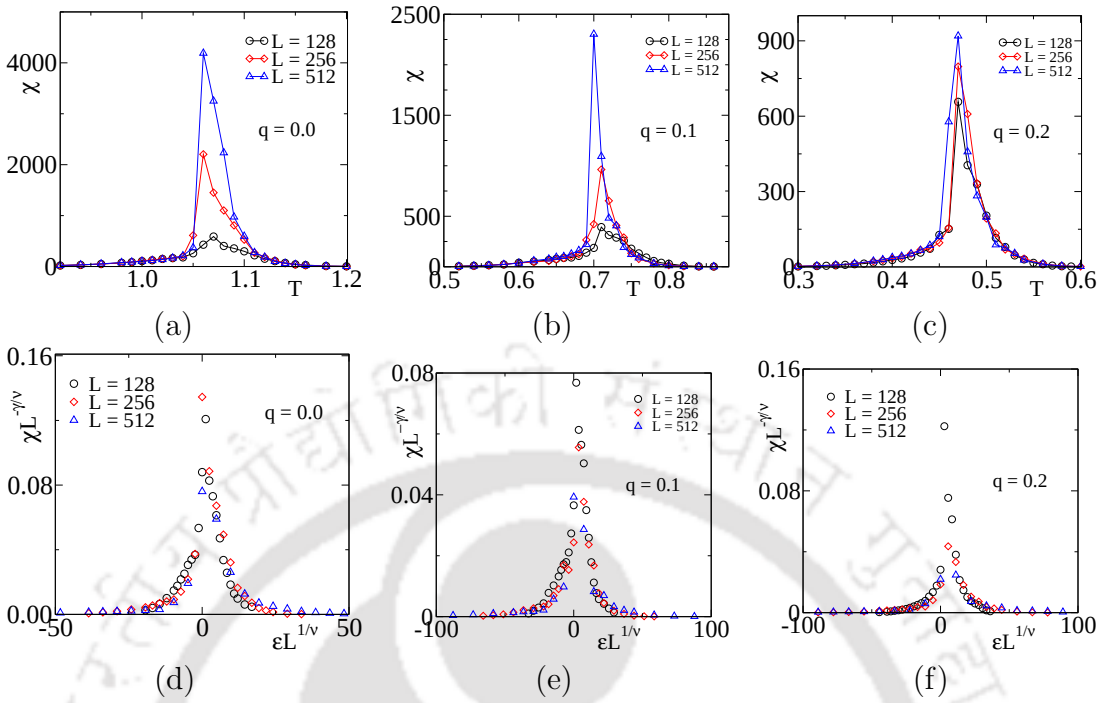

Figure 3.7: Plot of susceptibility χ with temperature T for $h_0 = 0.75$ and $P = 512$ on system sizes $L = 128(\bigcirc)$, $256(\diamond)$ and $512(\triangle)$ for (a) $q = 0.0$, (b) $q = 0.1$, and (c) $q = 0.2$. The scaled susceptibility $\chi L^{-\gamma/\nu}$ are plotted against the scaled variable $\varepsilon L^{1/\nu}$ in (d), (e) and (f) for different q with respective critical exponents.

transition critical exponents on 2d diluted Ising model and found the exponent values are slightly different from the regular lattice, $\beta/\nu = 0.118 \pm 0.004$, and $\gamma/\nu = 1.76 \pm 0.02$ for $q = 0.1$ and $\beta/\nu = 0.102 \pm 0.006$, and $\gamma/\nu = 1.78 \pm 0.02$ for $q = 0.2$ in accordance with the weak universality hypothesis [110, 116–118]. The scaling exponents satisfy the relation $2(\beta/\nu) + \gamma/\nu = 2$ approximately. A reasonably good data collapse is obtained for dilution $q = 0.1$, and 0.2 using the respective equilibrium critical exponents on 2d diluted Ising system. The value of $\nu = 1$ is taken for both the cases.

The appearance of a peak around the phase transition point is a general observation in the variation of susceptibility with temperature. The peak is the manifestation of the fact that the system goes through huge fluctuation near the phase transition. In other words, the peak in susceptibility indicates the phase transition point. The χ has strong finite size effects for different qs. The observations of χ with T shown in Fig.3.7 top row are obtained for $h_0 = 0.75$ and $P = 512$. In Fig.3.7(a), (b) and (c) χ is plotted for regular lattice, $q = 0.1$, and 0.2 respectively on different system sizes $L = 128(\bigcirc)$, $256(\diamond)$ and $512(\triangle)$. The largest χ value is corresponding to the largest system size in each case as the larger lattice consists of more spins and

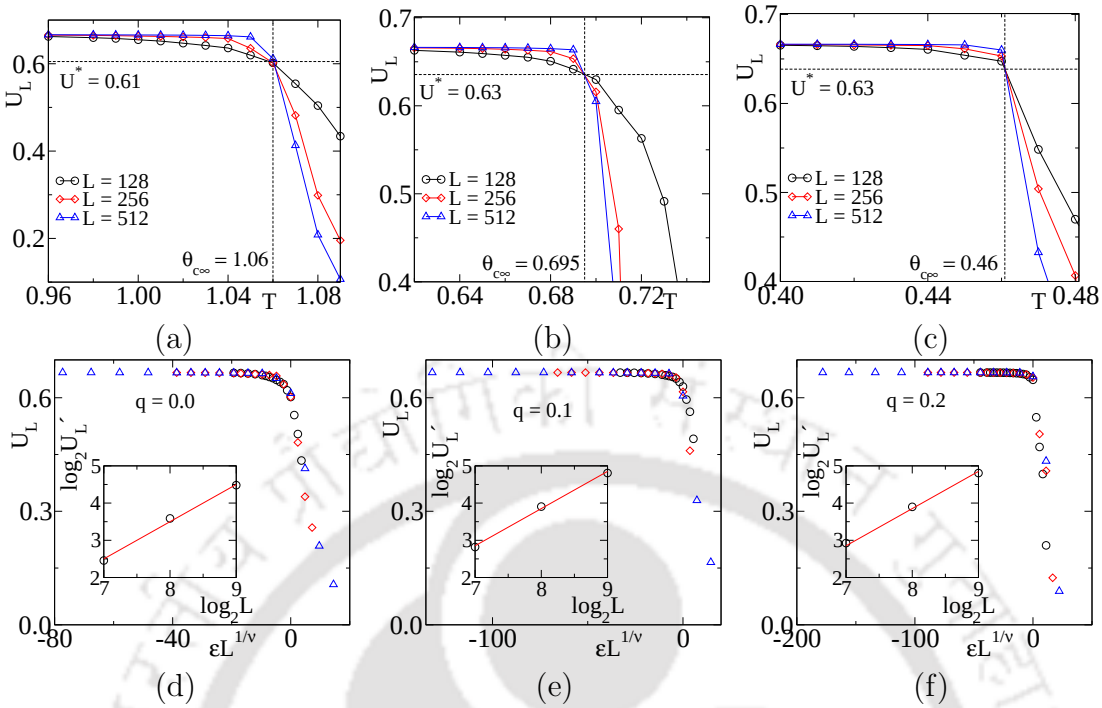

Figure 3.8: Plot of Binder cumulant U_L with temperature T for $h_0 = 0.75$ and $P = 512$ on system sizes $L = 128(\bigcirc)$, $256(\diamond)$ and $512(\triangle)$ for (a) $q = 0.0$, (b) $q = 0.1$, and (c) $q = 0.2$. The U_L are plotted against the scaled variable $\varepsilon L^{1/\nu}$ in (d), (e) and (f) for different q with respective critical exponents. The each inset in the bottom row shows variation of U'_L at $P_c(q)$ with L in double log plot. The exponent $\nu = 1$ is estimated, approximately for all qs.

contributes to maximum fluctuation. The other observation is that the maximum of χ decreases for the largest lattice ($L = 512$) as the dilution q increases. The χ/L^2 for different system sizes are not the same. It indicates the transition is not of the first order or discontinuous type. The FSS forms of χ are verified with the same set of critical exponents as described above for different disorders q under the weak universality hypothesis. The scaled susceptibility $\chi L^{-\gamma/\nu}$ are plotted against the scaled variable $\varepsilon L^{1/\nu}$ in Fig.3.7(d), (e), (f) for different q. A reasonable collapse of data occurred with the chosen respective values of the critical exponents.

The U_L is plotted against temperature T in Fig.3.8 for (a) regular lattice, (b) $q = 0.1$ and (c) $q = 0.2$ respectively for different values of L. In each case, U_L corresponding to different system sizes L cross each other at a temperature. The crossing points are found to be 1.06 ± 0.01, 0.70 ± 0.01 and 0.46 ± 0.01 for $q = 0, 0.1$, and 0.2 respectively which matches with the estimated $\theta_c(q)$ from the order parameter shown in Fig.3.6. The temperature $\theta_{c\infty}$ at which such crossing occurs indicates the phase transition temperature of the system in the thermodynamic

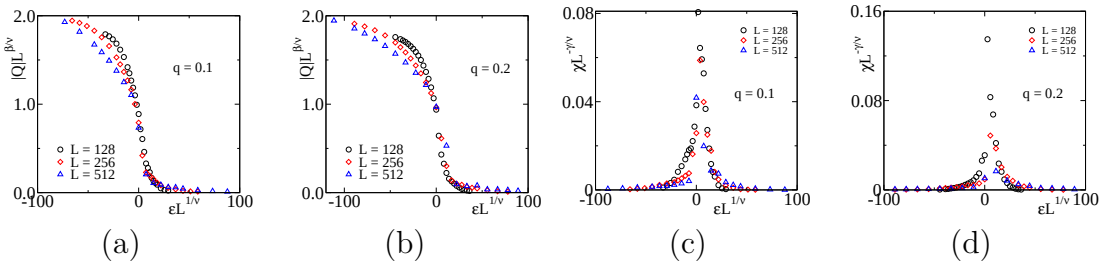

Figure 3.9: Data collapse of order parameter $|Q|$ and magnetic susceptibility χ with the respective FSS variables for $q = 0.1$, and $q = 0.2$ under the strong universality hypothesis.

limit. The value of U_L at the crossing is found to be $U^* \approx 0.61, 0.63$ and 0.63 for regular lattice, $q = 0.1$, and 0.2, close to the already known estimates for the 2d the equilibrium zero field Ising model [24, 88, 89, 110]. It is also as per the U^* value for the DPT reported in Ref.[24]. The U_L are plotted against the scaled variable $\varepsilon L^{1/\nu}$ in Fig.3.8(d), (e), (f) for different q. The FSS forms of U_L are verified with critical exponent $\nu = 1$ for all cases. A good collapse of data is observed. The U'_L at θ_c is plotted with different L in double logarithmic scale for regular lattice, $q = 0.1$, and 0.2 in the inset of Fig.3.8(d), (e) and (f) in symbols. The solid red line shown in each inset corresponds to $\nu = 1$ line.

q	$\theta_c(q)$	$\theta_{c\infty}(q)$	U^*
0.0	1.06 ± 0.01	1.06 ± 0.01	0.61
0.1	0.70 ± 0.01	0.70 ± 0.01	0.63
0.2	0.46 ± 0.01	0.46 ± 0.01	0.63

Table 3.2: DOP to DDP transition temperatures $\theta_c(q)$ at different dilution for $h_0 = 0.75$ and $P = 512$.

We have obtained good data collapse for $|Q|$, χ, and U_L plotting the respective FSS variables with slightly modified scaling exponents from that of the exact values for 2d Ising equilibrium. Let us now verify the FSS forms of the same quantities under the strong universality hypothesis, which assumes that the scaling exponents do not change with dilution. The temperature variation of $|Q|$ and χ for several q and system size L are shown in top rows of Fig.3.6 and 3.7 respectively. The corresponding FSS variables $|Q|L^{\beta/\nu}$ and $\chi L^{-\gamma/\nu}$ are plotted with a variable $\varepsilon L^{1/\nu}$ using the 2d equilibrium Ising critical exponents ($\beta = 1/8, \gamma = 7/4$, and $\nu = 1$) in Fig.3.9 for dilution $q = 0.1$ and 0.2. The data collapse is not satisfactory. The quality of collapse further deteriorates as the q increases. The temperature varied DTP in the diluted kinetic Ising model under the external sinusoidal field fits well with the weak universality hypothesis.

3.3 DPT by varying Period P at fixed T

There are a few drawbacks of studying DPT with varying system temperature T. The DPT occurs when $P_{1/2} \sim \mathcal{O}(\langle\tau\rangle)$. By tuning T keeping P fixed, we are indeed changing $\langle\tau\rangle$ and observing DPT when it matches with the half period $P_{1/2}$. The $\langle\tau\rangle$ also depends on h_0 and L apart from the T. It is observed that for a fixed P for higher field amplitude h_0 and strong dilution q, the $\theta_c(q)$ decreases drastically, and we may not reach the DOP at any non-zero finite temperature. On the other hand, we still could study DPT varying P of the external field keeping T fixed. The benefit is that the period varying DPT study at a constant T and h_0 allows us to explore a larger part of the phase space.

In this section, we are going to carry out a system size L dependent MC study on DPT in diluted Ising ferromagnet varying the period P of the external field, keeping the temperature and the field amplitude $h_0 = 1.0$ fixed far below the respective $T_c(q)$. The temperature T is fixed at 80% of respective $T_c(q)$ for each disorder, i.e., $T = 1.80, 1.50$ and 1.24 for regular lattice and $q = 0.1$ and 0.2 respectively. Here, the mean metastable lifetime $\langle\tau\rangle(h_0, T)$ remains fixed. We vary P and the system undergoes the DPT when $P_{1/2}$ matches the $\langle\tau\rangle$. The simulations are repeated for $L = 64, 128, 256$ and 512 for all lattices.

3.3.1 Finite size scaling study varying P

We have already discussed the finite size scaling forms for Q, χ, and U_L with reduced temperature ε. In this section, we will redefining those scaling forms with reduced period P^* to study the period varied DPT. The FSS form for $|Q|$ can be considered following the equilibrium thermal critical phenomena

$$|Q| = L^{-\beta/\nu}\widetilde{Q}[P^*L^{1/\nu}] \tag{3.12}$$

where, $P^* = (P - P_c(q))/P_c(q)$ is the reduced dimensionless period, and $\widetilde{Q}$ is a scaling function. The exponent β, and ν are the 2d Ising order parameter and correlation length exponents. The FSS form for χ is

$$\chi = L^{\gamma/\nu}\widetilde{\chi}[P^*L^{1/\nu}] \tag{3.13}$$

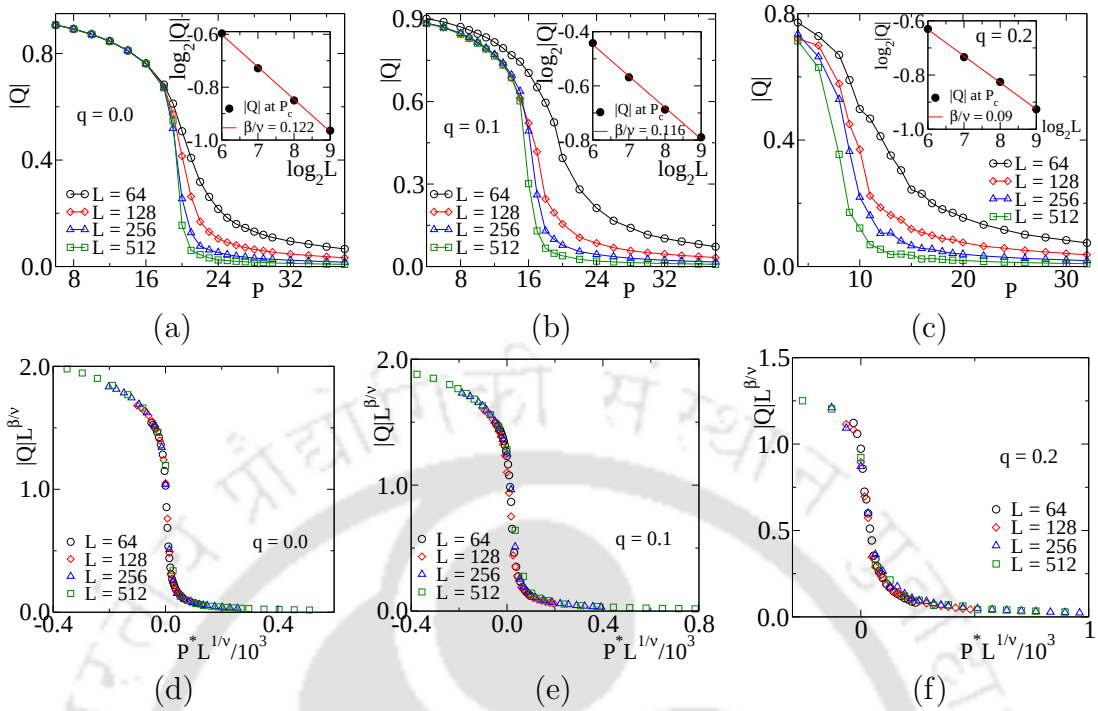

Figure 3.10: Plot of dynamic order parameters $|Q|$ with period P for $h_0 = 1.0$ and $T = 80\%$ of respective $T_c(q)$, $T = 1.80, 1.50$ and 1.24 for (a) regular lattice, (b) $q = 0.1$, and (c) $q = 0.2$ on system sizes $L = 64(\bigcirc)$, $L = 128(\diamond)$, $256(\triangle)$ and $512(\square)$. Critical exponents β is estimated from the double logarithmic plot of $|Q|$ at $P_c(q)$ with system size L for different q values shown in each inset. The bottom rows (d), (e) and (f) shows the data collapse corresponding to each $|Q|$ versus P plot of top row when plotted scaled order parameter $|Q|L^{\beta/\nu}$ with scaled variable $P^*L^{1/\nu}$ for different q with respective critical exponents.

where $\widetilde{\chi}$ is a scaling function and γ is the 2d Ising susceptibility exponent. The fourth order Binder cumulant has the following FSS form

$$U_L = \widetilde{U}[P^* L^{1/\nu}] \tag{3.14}$$

where $\widetilde{U}$ is a universal scaling function. We have from Eq.3.14 at the $P = P_c(q)$

$$U'_L = \frac{\widetilde{U'}[0]}{P_c(q)} L^{1/\nu} \tag{3.15}$$

where $\widetilde{U'}$ is a universal scaling function, and $U'_L = \frac{dU_L}{dP}$.

Dynamic order parameter $|Q|$ is plotted with period P in Fig. 3.10(a), (b) and (c) for different values of disorder q on square lattice of sizes $L = 64(\bigcirc)$, $L = 128(\diamond)$, $256(\triangle)$ and $512(\square)$ for fixed $h_0 = 1.0$ and $T = 1.80, 1.50$ and 1.24 (80% of respective $T_c(q)$). The $|Q|$s have strong finite system size dependence and

change almost similarly for different q values except they have different dynamic phase transition period $P_c(q)$. The value of $P_c(q)$ is estimated from the value of the period where the change of Q with P *i.e.*, $d|Q|/dP$ is maximum at the inflection point. The $d|Q|/dP$ is plotted with T in all cases, and the $P_c(q)$s are estimated from the trough in each plot. The values of $P_c(q)$ were found to be 19 ± 1, 15 ± 1 and 8 ± 1 for regular lattice, $q = 0.1$, and 0.2, respectively on the largest lattice $L = 512$. The fall of $|Q|$ appears to become more sharper as the dilution increases.

Now, the slope of a least square fit straight line in a double logarithmic plot of $|Q|$ with L should give us β/ν. In the inset of Fig.3.10 (a), (b), and (c) $|Q|$ is plotted with L in double logarithmic scale for different q. The slope gives us the β/ν for different q values. $\beta/\nu = 0.122 \pm 0.004, 0.116 \pm 0.007$, and 0.09 ± 0.005 for regular lattice, and $q = 0.1$, and 0.2 respectively. The exponents obtained above are very close to the values obtained for the equilibrium diluted Ising model in 2d [110]. Next, we verify the FSS forms of $|Q|$ using the scaling exponents obtained above under the weak universality hypothesis as the exponent values deviate from the regular system. The scaled order parameters $|Q|L^{\beta/\nu}$ are plotted against the scaled variable $P^*L^{1/\nu}$ in Fig.3.10(d), (e), (f) for different disorder with $\nu = 1$. A good collapse of data occurred with the chosen values of the critical exponents.

The susceptibility χ of the system is estimated from the fluctuation of dynamic order parameter $|Q|$ as $\chi = L^2(\langle|Q|^2\rangle - \langle|Q|\rangle^2)$. The χ also has strong finite size effects for all q values. The variations of χ with P shown in Fig.3.11 are obtained for $h_0 = 1.0$ and $T = 1.80, 1.50$ and 1.24. In Fig.3.11(a), (b) and (c) χ is plotted for $q = 0, 0.1$ and 0.2 respectively on different system sizes $L = 64(\bigcirc)$, $L = 128(\diamond)$, $256(\triangle)$ and $512(\square)$. There is a peak around the phase transition point. The peak is the manifestation of the fact that the system goes through huge fluctuation near the phase transition. In other words, the peak in susceptibility indicates the phase transition point. The largest χ value is corresponding to the largest system size in each case as the larger lattice consists of more amount of spins and contributes to maximum fluctuation. The other observation is that the maximum of χ increases for the largest lattice ($L = 512$) as the dilution q increases. This observation is exactly opposite to what we saw while studying DPT varying temperature in Fig.3.7. In that case, we saw the maximum of χ decreases for the largest lattice ($L = 512$) as the dilution q increases. The χ/L^2 for different system sizes are not the same. It indicates the transition is not of the first order or discontinuous type.

Here, the slope of a least square fit straight line in a double logarithmic plot of χ versus L should give us γ/ν. χ at respective $P_c(q)$ is shown with L in double

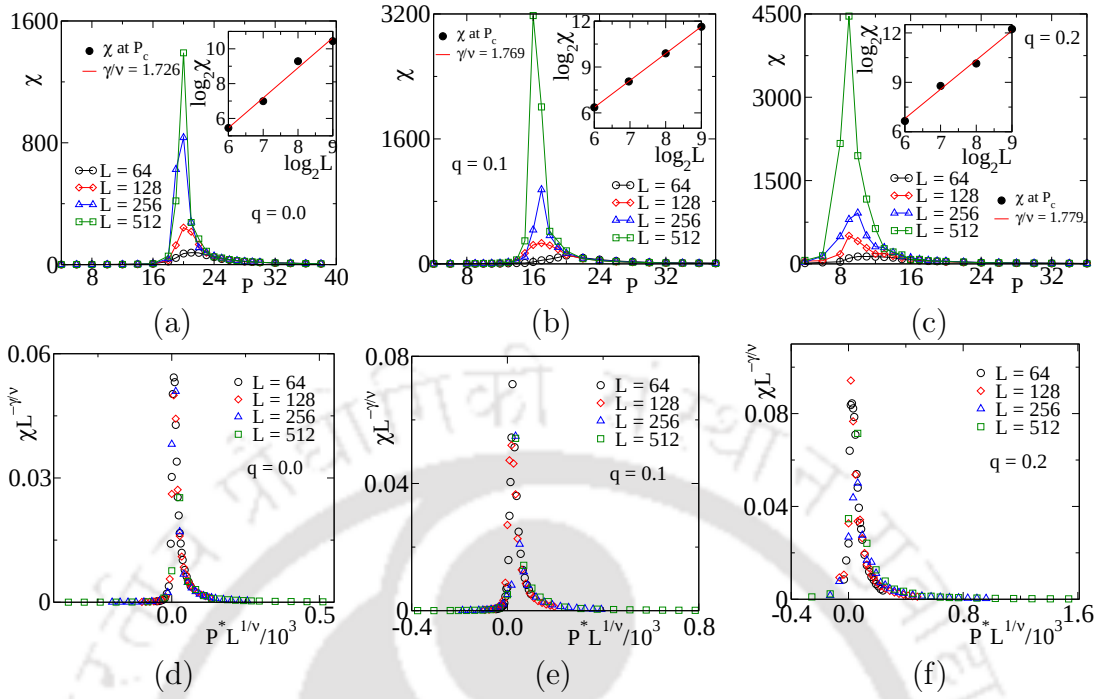

Figure 3.11: Plot of susceptibility χ with period P for $h_0 = 1.0$ and $T = 80\%$ of respective $T_c(q)$, $T = 1.80, 1.50$ and 1.24 for (a) regular lattice, (b) $q = 0.1$, and (c) $q = 0.2$ on system sizes $L = 64(\bigcirc)$, $L = 128(\diamond)$, $256(\triangle)$ and $512(\square)$. Critical exponents γ is estimated from the double logarithmic plot of χ at $P_c(q)$ with system size L for different q values shown in each inset. The bottom rows (d), (e) and (f) shows the data collapse for each χ versus P plot in top row when plotted scaled susceptibility $\chi L^{-\gamma/\nu}$ with scaled variable $P^* L^{1/\nu}$ for different q with respective critical exponents.

logarithmic plots for different q values in the inset of Fig.3.11(a), (b), and (c). The slope gives us the γ/ν at different q values. $\gamma/\nu = 1.73 \pm 0.03, 1.77 \pm 0.01$, and 1.78 ± 0.02 for regular lattice, $q = 0.1$, and 0.2 which are also very close to the static phase transition exponent reported values [110] on 2d diluted Ising model. The FSS forms of χ is verified with the same set of critical exponents as described above for different disorders q according to weak universality hypothesis description. The scaled susceptibility $\chi L^{-\gamma/\nu}$ are plotted against the scaled variable $P^* L^{1/\nu}$ in Fig.3.11(d), (e), (f) for different q. A reasonably good collapse of data occurred with the chosen respective values of the critical exponents. The U_L is plotted against period P of the external field in Fig.3.12 for (a) regular lattice, (b) $q = 0.1$, and (c) $q = 0.2$, respectively, for different values of L. In each case U_L corresponding to the different system sizes L cross each other at the period $P_c(q)$. The crossing points are found to be $P_c(q) = 19$, 15, and 8 for regular lattice, $q = 0.1$, and 0.2 respectively, which are very close to the estimated $P_c(q)$ from the order parameter in Fig.3.10. The period $P_{c\infty}$ at which such crossing occurs indicates the critical

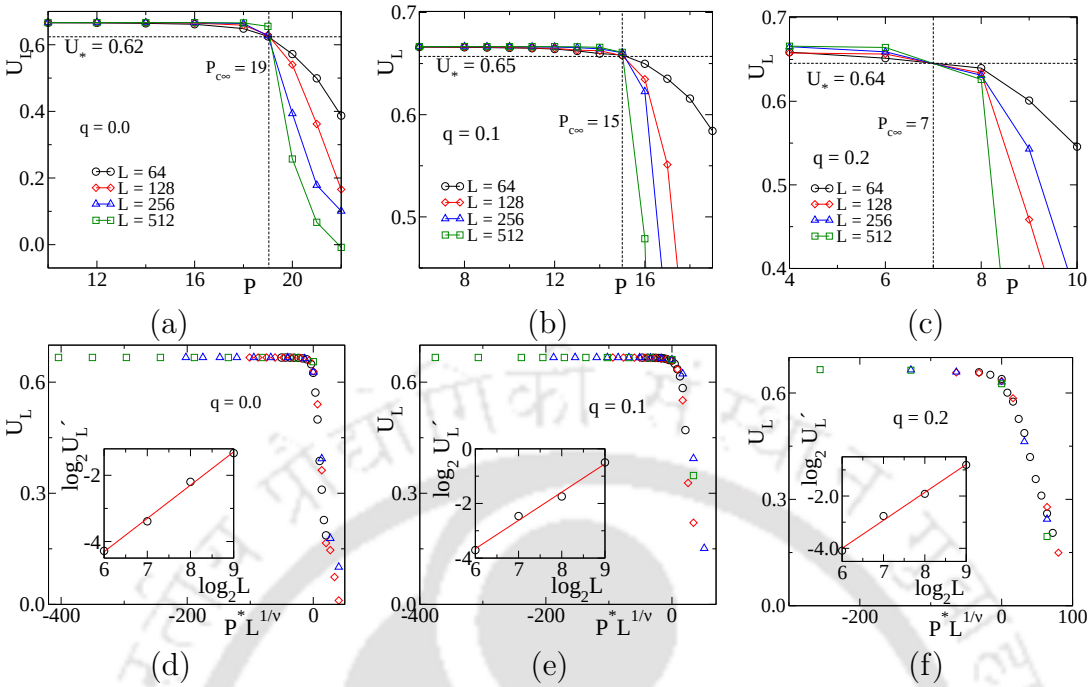

Figure 3.12: Plot of Binder cumulant U_L with period P for $h_0 = 1.0$ and $T = 80\%$ of respective $T_c(q)$, $T = 1.80, 1.50$ and 1.24 for (a) regular lattice, (b) $q = 0.1$, and (c) $q = 0.2$ on system sizes $L = 64(\bigcirc)$, $L = 128(\diamond)$, $256(\triangle)$ and $512(\square)$. The bottom rows (d), (e) and (f) shows the data collapse for each U_L versus P plot in top row when plotted scaled susceptibility U_L with scaled variable $P^*L^{1/\nu}$ for different q with respective critical exponents. The each inset in the bottom row shows variation of U_L' at $P_c(q)$ with L in double log plot. The exponent ν is estimated approximately 1 for different q.

period of the system in the thermodynamic limit. The value of U_L at the crossing is found to be $U^* \approx 0.62, 0.65$ and 0.64 for $q = 0, 0.1$, and 0.2, close to the already known estimates for the 2d the equilibrium zero field Ising model [24, 88, 89, 110]. It is also as per the U^* value for the DPT reported in Ref.[24]. The FSS forms of U_L is verified with exponent $\nu = 1$ for all disorders. The U_L are plotted against the scaled variable $P^*L^{1/\nu}$ in Fig.3.12(d), (e), (f) for different q. A good collapse of data occurred. The U_L' at $P_c(q)$ is plotted with system size L in double logarithmic scale for regular lattice, $q = 0.1$, and 0.2 in the inset of Fig.3.12(d), (e) and (f) in symbols. The solid red line shown in each inset represents the $\nu = 1$ line.

q	$P_c(q)\|_{L=512}$	$P_{c\infty}(q)$	U^*
0.0	19 ± 1	19 ± 1	0.62
0.1	15 ± 1	15 ± 1	0.65
0.2	8 ± 1	8 ± 1	0.64

Table 3.3: Critical periods for different dilution for fixed field amplitude $h_0 = 1.0$, and temperature $T = 1.80, 1.50$ and 1.24 for regular lattice, $q = 0.1$, and $q = 0.2$ respectively.

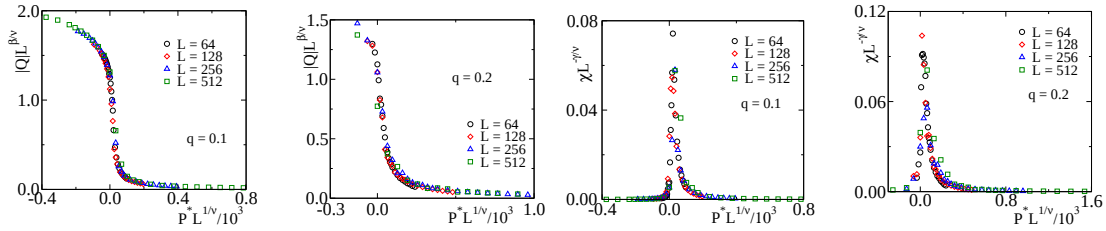

Figure 3.13: Data collapse of order parameter $|Q|$ and magnetic susceptibility χ with the respective FSS variables for $q = 0.1$, and $q = 0.2$ under the strong universality hypothesis in period varied DPT.

We have already found data collapse for $|Q|$, χ, and U_L plotting the respective FSS variables with slightly modified scaling exponents from that of the exact values for 2d Ising equilibrium for the period varied DPT at the fixed temperature. Here, we also verify the FSS forms of these quantities under the strong universality hypothesis. The critical exponents of a diluted system do not change with the addition of disorder in a pure system as per the strong universality hypothesis. The period variation of $|Q|$ and χ at fixed T for several q and system size L are shown in top rows of Fig.3.10 and 3.11 respectively. The corresponding FSS variables $|Q|L^{\beta/\nu}$ and $\chi L^{-\gamma/\nu}$ are plotted with a variable $P^*L^{1/\nu}$ using the 2d equilibrium Ising critical exponents $\beta = 1/8, \gamma = 7/4$, and $\nu = 1$ in Fig.3.13 for $q = 0.1$ and 0.2. Satisfactory data collapse has occurred. The quality of collapse deteriorates slightly as the q increases. The data collapse under the weak universality hypothesis is still better. The weak universality hypothesis seems to fit better in the case of period varied DTP too.

3.4 Magnetic time series and distribution of order parameter

The study of magnetization time series and the order parameter distribution can help to comprehend the system dynamics in DOP, DPT, and DDP in a more insightful manner. In Fig.3.14, selected portion of the magnetization time series $m(t)$ (solid line) and the order parameter distribution are plotted at different temperatures (a) $T = 0.66$, (b) $T = 0.7 \approx \theta_c(q)$ and (c) $T = 0.74$ corresponding to DOP, DPT and DDP on a system of size $L = 512$ for $h_0 = 0.75$, $P = 512$ and $q = 0.1$. A similar set of figures are plotted for $q = 0.2$ in Fig.3.15. The $\langle\tau\rangle$ is always larger than the half period $P_{1/2}$ in DOP in all the cases. As a result, the system can not come

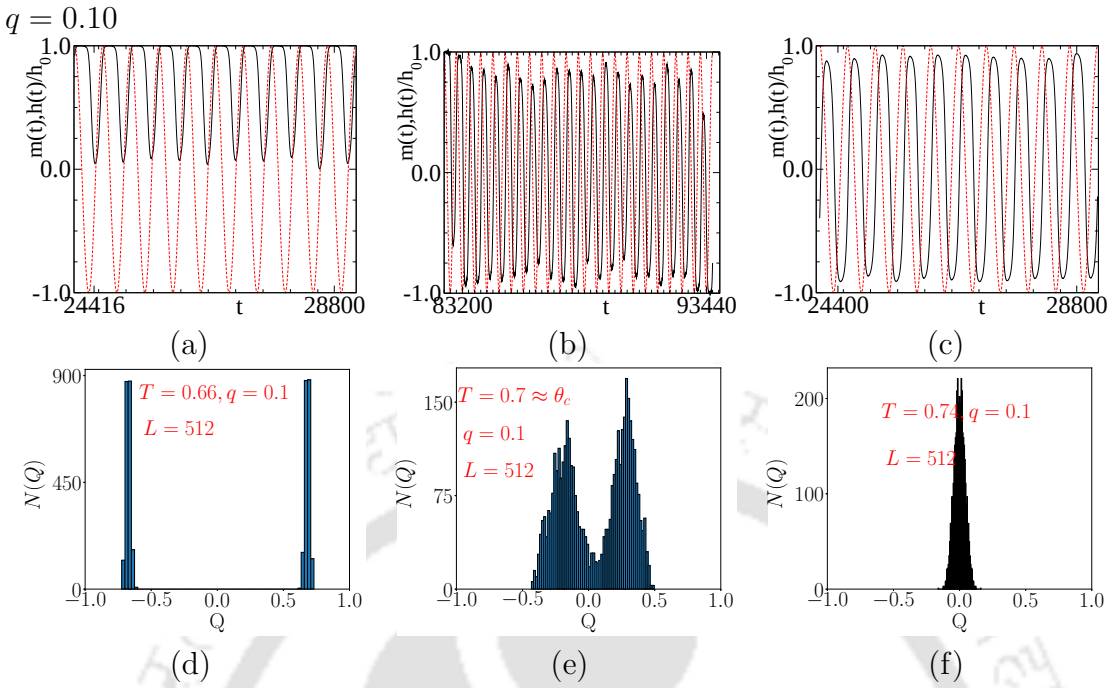

Figure 3.14: Magnetization time series $m(t)$ against MCS (t) at different temperatures (a) $T = 0.66$ (DOP), (b) $T = 0.70$ (DPT) and (c) $T = 0.74$ (DDP) on a system of size $L = 512$ for $h_0 = 0.75$, $P = 512$ and $q = 0.10$. The corresponding distribution of order parameter Q are shown in (d), (e) and (f) respectively over 60 equispaced bins.

out from the metastable well it is already in, and $m(t)$ shows a small fluctuation about a finite non-zero value (see Fig.(a) of each figure) but does not cross zero. The corresponding distribution (histogram) of the order parameter Q is shown in Fig.(d). It is evident from the distribution that the system remains trapped in either of the wells. As temperature increases, the average metastable lifetime $\langle \tau(T, h_0) \rangle$ becomes comparable with the half period of the external field $P_{1/2}$ and DPT occurs. The situation is described in Fig.(b) and (e). The $m(t)$ varies from a positive value to a negative value (or negative to positive) and crosses zero, as shown in Fig.(b). Note that $m(t)$, however, does not reach a value $+1$ or -1. The distribution of Q (Fig.(e)) have peaks around $\pm|Q|_c$. At this point, when the cycle average magnetization is still finite, the external field can move the system from one well to the other smoothly. Usually, in large systems, it corresponds to the MD regime [34, 36, 90]. In DDP, $\langle \tau \rangle$ is smaller than the $P_{1/2}$, $m(t)$ follows the external field with certain phase lag changes from close to $+1$ to close to -1 as shown in Fig.(c). Most of the states arise at $Q = 0$ and the distribution $N(Q)$ has a single peak around zero Q, as it can be seen in Fig.(f). For dilution $q = 0.1$ and 0.2, field intensity $h_0 = 0.75$, $P = 512$ the systems of size $128, 256$ and 512 found to exhibit continuous DPT.

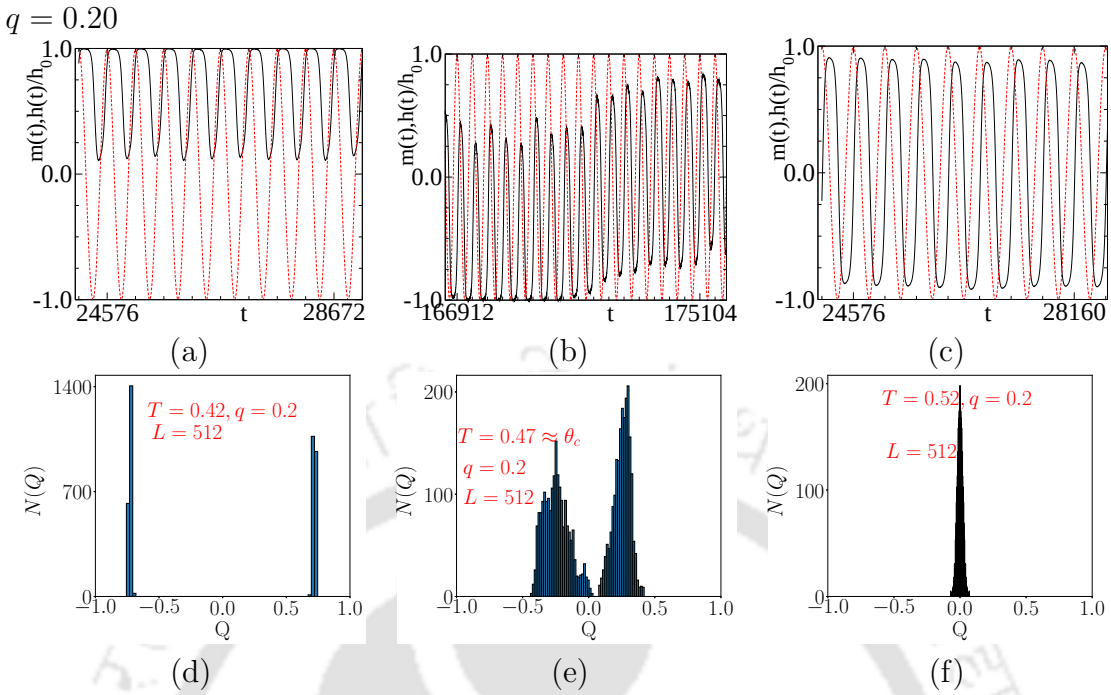

Figure 3.15: Magnetization time series $m(t)$ against MCS (t) at different temperatures (a) $T = 0.42$ (DOP), (b) $T = 0.47 \approx \theta_c(q)$ (DPT) and (c) $T = 0.52$ (DDP) on a system of size $L = 512$ for $h_0 = 0.75$, $P = 512$ and $q = 0.20$. The corresponding distribution of order parameter Q are shown in (d), (e) and (f) respectively over 60 equispaced bins.

3.5 Summary and Discussion

The nonequilibrium DPT is studied on the 2d site diluted Ising ferromagnet by an extensive Monte Carlo study on several system sizes $L = 64, 128, 256$, and 512. Below the zero field ferro to paramagnetic transition temperature $T_c(q)$, the diluted Ising ferromagnet found to be a bistable system with two equivalent ferromagnetic ground states corresponding to all spin up and all spin down configuration. The values of $T_c(q)$ depend on the amount of dilution q, decreases with increasing q. Nonequilibrium DPT is studied far below the respective $T_c(q)$ for each dilution $q = 0.1$, and 0.2 tuning the temperature T at fixed field amplitude h_0 and period P. The system is also studied by tuning the period P of the external sinusoidal oscillating field, keeping the T and h_0 fixed. The DPT occurs when metastable lifetime $\tau(h_0, T)$ becomes comparable to half period of the external field. Indeed, we change τ by changing T of the system in case of temperature varied DPT for a fixed P and h_0 and found a critical temperature $\theta_c(q)$. In case of period varying DPT study at constant T (i.e., fixed τ), we directly vary P and observe DPT at a critical period $P_c(q)$. The DPT results show that both the $\theta_c(q)$ and $P_c(q)$ value

decreases with increasing q in case of temperature varied and period varied DPT, respectively. The diluted ferromagnetic systems undergo a dynamic phase transition with hysteresis loss as the $m(t)$ follows $h(t)$ with a certain phase lag. Below θ_c or P_c, the hysteresis loops remain asymmetric, and above, they become symmetric. The hysteresis loop related properties, such as loop area A, orientation α, aspect ratio Φ of the loop and dynamic correlation C is evaluated from the geometry of the loops. The dilution has nontrivial effects on the spin system. The rate of increase of A and Φ with T decreases for larger q values. As the dilution increases, the spin-spin correlation becomes weak, and the field effects become stronger on the system; consequently, the value of C increases. The finite size effect on the hysteresis loop properties becomes higher and higher as the dilution increases. The DPT on different diluted Ising ferromagnets found to be of continuous type for both temperature varied DPT (fixed $h_0 = 0.75$, $P = 512$) and period varied DPT (fixed $h_0 = 0.75$, and $T = 0.8T_c(q)$). A detailed FSS analysis is performed on both the DPTs on diluted ferromagnets. The order parameter $|Q|$ and susceptibility χ obey the finite size scaling. A plot of Binder cumulant U_L shows the crossing point of different L at the respective $P_c(q)$ for different q. The corresponding value of U^* is also in agreement with the existing reported values. The β/ν and γ/ν are extracted, which comes out very close to that of equilibrium critical exponents reported for different q under weak scaling hypothesis [110]. Good data collapse is observed for FSS variables using those scaling exponents. The strong scaling hypothesis is also verified. The DPT in the 2d diluted Ising model under external sinusoidal field seems to follow the weak scaling hypothesis as we found comparatively better data collapse with q dependent scaling exponents.

Chapter 4

DPT in Ising ferromagnet on random fractals

As the site dilution reaches percolation threshold $q_c = 1 - p_c \approx 0.41$ ($p_c \approx 0.59$) for a 2d diluted Ising model on a square lattice, the ferro to paramagnetic transition temperature $T_c \to 0$ [119–121]. A study of the highly diluted spin system morphology reveals that the Ising spins form several small islands disconnected from the other spins in the system surrounded by empty sites. As a result, the spontaneous magnetization in a highly diluted system never becomes finite above $T = 0$. As a result, the transition temperature $T_c(p_c) \to 0$. However, two highly ramified but connected random fractals viz., spanning percolation and percolation backbone, can be extracted at $p = p_c$. These random fractals have connectivity throughout the lattice and are very highly ramified [119], unlike random dilution increased up to p_c in diluted Ising model. A fractal Ising ferromagnet can be formed by placing Ising spins on an above said random fractal. Some theoretical predictions [122–124] indicate the criticality still occurs in the limit $p \to p_c$ and $T \to 0$. Can the fractal ferromagnets exhibit ferromagnetic order at a non-zero small finite temperature as the spins on a random fractal have excellent connectivity throughout the lattice? If such a ferromagnetic state exists, it will be interesting to know the nature of DPT and hysteresis loops on such a random fractal ferromagnet. The criticality and scaling exponents for DPT on a random fractal is another aspect worth studying.

In this chapter, we will perform a Monte Carlo study of DPT on two such random fractals, namely spanning percolation cluster (SPC) and spanning percolation backbone (SPB). First, we will develop the models and search for T_c for both models. Next, DPT will be observed in detailed Monte Carlo studies tuning the temperature T of the system below the respective equilibrium ferro to paramagnetic transition

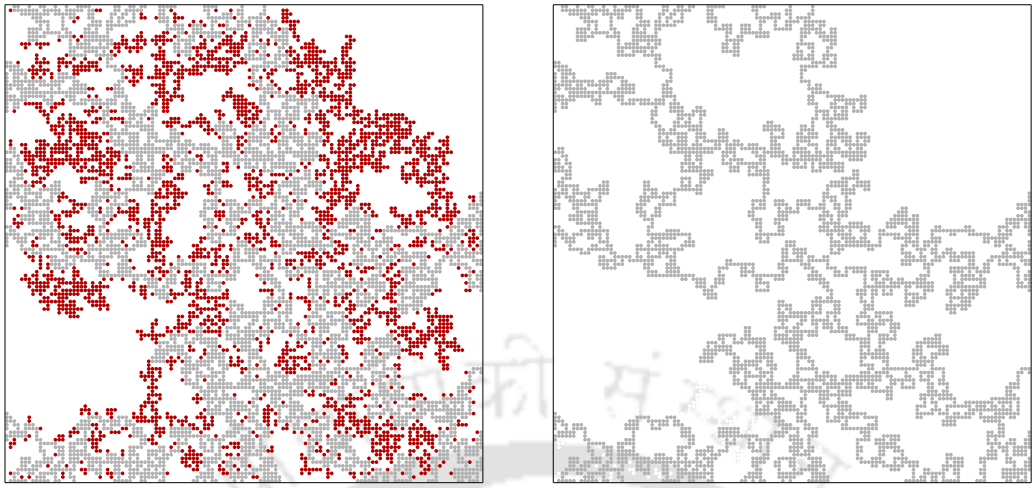

(a) (b)

Figure 4.1: (a) The SPC morphology on a square lattice of size $L = 128$, the dangling ends of the SPC are shown in red. (b) SPB is extracted from the SPC, chopping off the dangling ends.

temperature T_c where the systems are bistable. The models, details of numerical simulations, and results are described as following.

4.1 Ising model on random fractal

The Ising model on random fractal can be generated in two steps; first, to produce the fractal itself, and then replace the occupied sites in the cluster with Ising spins. We are going to generate two different types of random fractals, SPC and SPB. A cluster is a collection of occupied sites connected by nearest neighbor bonds. A spanning percolation cluster [76–78] is developed at the percolation threshold $p_c = 0.59278$ on a square lattice of size L using the Leath algorithm [79] where p is the probability with which a lattice site is occupied. Several spanning percolation clusters are carefully chosen from a distribution spanning clusters with a mass little above their mean values. It ensures that the spanning cluster has a certain amount of mass present in it. A percolation backbone is only the connecting path on a spanning percolation cluster. It can be obtained by chopping off the dangling ends of a spanning percolation cluster at p_c. The detailed percolation backbone extraction algorithm from a spanning percolation cluster can be found in the Ref. [80]. A SPC and its corresponding SPB morphologies are shown in Fig.4.1 on a square lattice of size $L = 128$. The percolation backbones are also chosen with a mass little above

the mean value of the mass distribution of the percolation backbones for a given system size L. The fractal dimension of the spanning percolation cluster and the percolation backbone are $d_f = 1.89$ and $d_f^B = 1.64$ respectively. Finally, we have a 2d Ising ferromagnet on a random fractal by replacing all the occupied sites of a random fractal with Ising spin variables $S = \pm 1$ corresponding to two states up and down, respectively.

The Hamiltonian for the spin-1/2 Ising model on the random fractal with nearest neighbor interaction on a square lattice of size L is given by

$$\mathcal{H} = -J \sum_{\langle ij \rangle} c_i c_j S_i S_j - h \sum_i c_i S_i \tag{4.1}$$

The occupation index $C_i = 1$ for the ith Ising spin S_i on the fractal and $C_i = 0$ for a site that does not belong to the random fractal. Each spin can interact with its nearest neighbor spins, if available, under periodic boundary condition with ferromagnetic interaction strength $J(> 0)$. h is an external magnetic field.

It is essential to know the T_c on these random fractals before the DPT study on them. The DPT can only be observed below the T_c of a system with two metastable ferromagnetic phases corresponding to all spins up and all spins down.

4.2 Equilibrium phase transition and T_c

Zero field ($h = 0$) Ferro to paramagnetic phase transition is studied using Monte Carlo simulations on both the fractal magnets on a square lattice of size $L = 128, 256$ and 512. The fractal magnet is kept in contact with a heat bath of constant temperature T. The spins are evolved using Metropolis single spin flip dynamics [72, 74] at T. The spin flip acceptance ratio W is given by

$$W(S_{i,j} \to -S_{i,j}) = \begin{cases} e^{-\Delta E/k_B T} & \text{if } \Delta \mathrm{E} > 0 \\ 1 & \text{Otherwise} \end{cases} \tag{4.2}$$

Where ΔE is the change in energy, both the J and the Boltzmann constant k_B are considered 1. The temperature is expressed in energy units J/k_B. One MC step includes checking and updating all the spins on the fractal once on average. The equilibrium configurations are achieved after 10^6 MC steps or iterations starting from all spin up configurations at a given temperature T under zero external field $h = 0$. The system's thermal equilibrium at a given temperature T is identified by

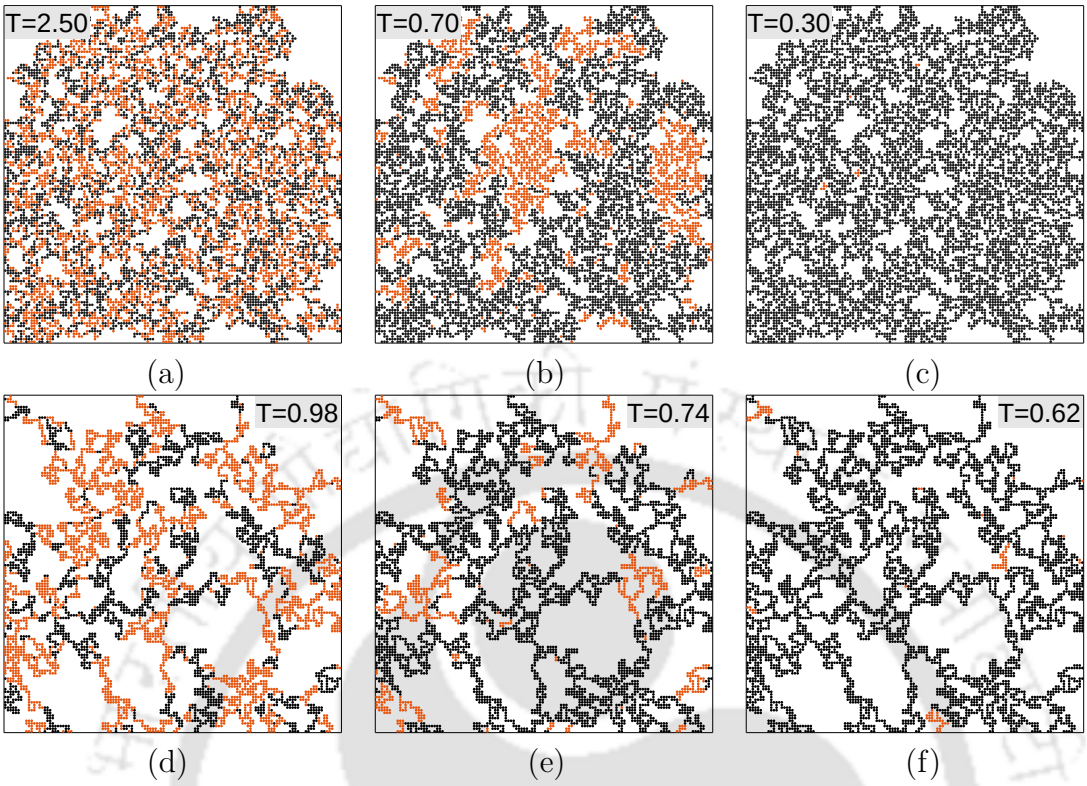

Figure 4.2: Ising spin configurations on SPC with nearest neighbour interaction in (a) paramagnetic phase $T > T_C$, (b) around T_c, and (c) ferromagnetic phase $T < T_c$ and on SPB in (d) paramagnetic phase $T > T_C$, (e) around T_c, and (f) ferromagnetic phase $T < T_c$ in the absence of external magnetic field on a square lattice of size $L = 128$. The black and saffron dots represent up and down spins, respectively. White denotes the absence of Ising spin on the lattice.

constant magnetization over a period of 10^5 MC steps. After equilibrium, another 10^6 iterations are performed. Data are collected at every 100 MC steps to avoid correlation in the Markov chain of states. Per spin magnetization m is averaged over 10^4 configurations on 16 different fractals, tolling to a total of 16×10^4 ensemble averages for both random fractals.

Final spin configurations on a SPC are shown in Fig.4.2 (a), (b) and (c) on a square lattice of size $L = 128$ at three different temperatures $T = 2.50$, $T = 0.70$ and $T = 0.30$. The black dots represent the up spins, and the saffron dots represent the down spins. At a higher temperature ($T = 2.50$), the spin orientation is found to be random, corresponding to a paramagnetic phase. As the temperature is lowered, a critical temperature $T_c \approx 0.70$ is found where a finite magnetization appears in the system. At a further lower temperature ($T = 0.3$), the fractal magnet is found to have almost all spins up configuration corresponding to a ferromagnetic phase. A similar evolution of Ising spins on a SPB is shown in Fig.4.2 (d), (e), and (f) at

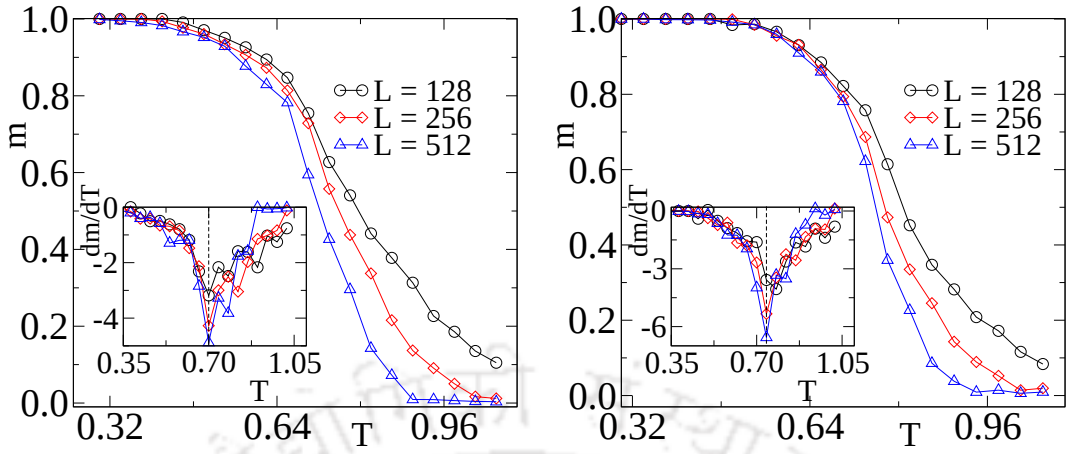

Figure 4.3: Plot of average per spin magnetization m with temperature T for 2d Ising ferromagnet developed on (a) spanning percolation, and (b) percolation backbone on system sizes $L = 128(\bigcirc)$, $256(\diamond)$ and $512(\triangle)$. In the inset of both plots, variation of dm/dT is shown with temperature T, the minima correspond to respective transition temperatures $T_c = 0.70 \pm 0.04$ and 0.74 ± 0.04, respectively.

$T = 0.98, 0.74$, and 0.62 in paramagnetic, near phase transition, and in ferromagnetic phase, respectively. It is important to note that long range correlation appears in both of these fractal magnets below a non-zero small finite critical temperature T_c.

The average spontaneous magnetization per lattice site m at a given T is estimated as

$$m = \frac{1}{N_e}\sum_{s=1}^{N_e} m_s \quad \text{where,} \quad \mathrm{m_s} = \frac{1}{\mathrm{N}}\sum_{\mathrm{i}=1}^{\mathrm{N}} \mathrm{S_i} \tag{4.3}$$

where $N_e = 16 \times 10^4$ is the number of ensembles, N is the total number of spins on the fractal. The variations of $m(T)$ with temperature T on a square lattice of system sizes $L = 128(\bigcirc)$, $256(\diamond)$ and $512(\triangle)$ for Ising ferromagnet on both spanning percolation and percolation backbone are shown in Fig.4.3(a) and (b) respectively. The m in the ferromagnetic phase at very low temperature is found close to the saturation value $m = 1$ when most of the spins in the cluster are in the same direction. The m continuously goes to zero in the paramagnetic phase at a higher temperature when the ferromagnetic order is destroyed by thermal agitation. There is a finite system size dependence on the variation of m at different L. The critical temperature T_c is determined from the point of inflection, where the change in the value of m is maximum with respect to T. The dm/dT is plotted in the inset for both systems. T_C is determined from the position of the deeps. The value of T_c comes out to be 0.70 ± 0.04 and 0.74 ± 0.04 for Ising ferromagnet on SPC and SPB. This result implies that the fractal Ising magnets developed on a SPC and SPB in

2d square lattice have long range order at a non-zero finite temperature below T_c. The values of T_c are found to be much smaller than that of a regular Ising system $\frac{2}{\ln\left(1+\sqrt{2}\right)} \approx 2.269185$ on the square lattice. An interesting observation is that the T_c in the percolation backbone is slightly larger than that of a spanning percolation cluster. In contrast, the backbone has a comparatively lesser amount of spins. This behavior can be explained by looking at the system morphologies. There are lots of dangling ends in the spanning percolation cluster. The spins at the dangling ends are very weakly connected, and they have disorders or empty sites as their neighbors. As these spins have weak ferromagnetic order, they flip very quickly at a comparatively lower temperature, contributing to the spanning percolation cluster's early transition. On the other hand, the percolation backbone is prepared specially by chopping off these dangling ends of a spanning percolation cluster, leaving the backbone with high ferromagnetic order. So, T_c on the backbone found to be a little higher.

4.3 Dynamic phase transition

Ising ferromagnets on a spanning percolation cluster and percolation backbone is a bistable system with two equivalent symmetry broken metastable phases far below the respective T_c. An external field can take a system resting in one metastable phase to the other if it gets enough time. Thus, fractal Ising ferromagnets can undergo nonequilibrium DPT. This section deals with DPT under external sinusoidal field in Ising ferromagnet on a SPC and SPB. The fractal Ising ferromagnets are strongly diluted systems with fractal space dimensions. It is expected to reveal novel behavior in a DPT study.

4.3.1 Model and Simulation

The kinetic Ising model is generated on two different random fractals following the same methodology described in the previous section - Ising model on random fractal. The Hamiltonian of the random fractal kinetic Ising model (RFKIM) can be obtained by replacing the static external field h with a time dependent external field $h(t)$ in random fractal Ising model Hamiltonian in Eq. 4.1

$$\mathcal{H} = -J \sum_{\langle ij \rangle} c_i c_j S_i S_j - h(t) \sum_i c_i S_i \tag{4.4}$$

Here, an external time t varying sinusoidal oscillating magnetic field $h(t)$ given by

$$h(t) = h_0 \sin(2\pi t/P) \tag{4.5}$$

is applied on the system, where h_0 is the amplitude and P is the time period of the oscillating field. h_0 is measured in the units of J.

The system is kept in contact with a heat bath at temperature T. The Glauber Monte Carlo (MC) single spin-flip dynamics [73] is used to evolve the spins at a particular T and $h(t)$. A spin is chosen randomly and updated from S_i to $-S_i$, each attempted spin flip is accepted with probability,

$$W(S_i \to -S_i) = \frac{e^{-\Delta E/k_B T}}{1 + e^{-\Delta E/k_B T}} \tag{4.6}$$

where $\Delta E = 2S_i\Sigma + 2S_i h(t)$ is the change in energy due to spin flip. The value of J and the Boltzmann constant k_B is taken to be 1, and the temperature T is measured in the unit of J. The time unit is one MC step per spin (MCSS). We increase one MCSS after checking all the spins in the system once on average.

Extensive Monte Carlo (MC) simulation is carried out on two dimensional random fractal Ising system of size $L = 128, 256$ and 512. The initial state is taken as either all spins up $S_i = +1$ state or all spins down $S_i = -1$ state. The system is iterated for 10^6 MC time steps to thermalize it at a given temperature T in the absence of the external field. A number of equilibrium states with constant magnetization are then generated at a given T in the absence of the external field. The external time-dependent magnetic field $h(t)$ is applied on a randomly chosen equilibrium state at a given temperature T. The system is further evolved to achieve the stable dynamic states in the presence of the applied field over 256 cycles, i.e., $\mathcal{O}(10^5)$ MC steps, before collecting data. The data is collected over the next 10^6 MC steps over the stable cycles. Eight randomly chosen equilibrium configurations are taken as initial samples, and measurements are made on the 1024 stable cycles selected from all over the time series for each sample. All the simulations are performed for different temperatures T on random fractals in square lattices of size $L = 128, 256$ and 512 for fixed field amplitude $h_0 = 0.75$ and period $P = 512$.

4.3.2 Hysteresis

There is a phase lag between the per spin instantaneous magnetization and the applied field due to the delay in response of the spins. The ensemble average instan-

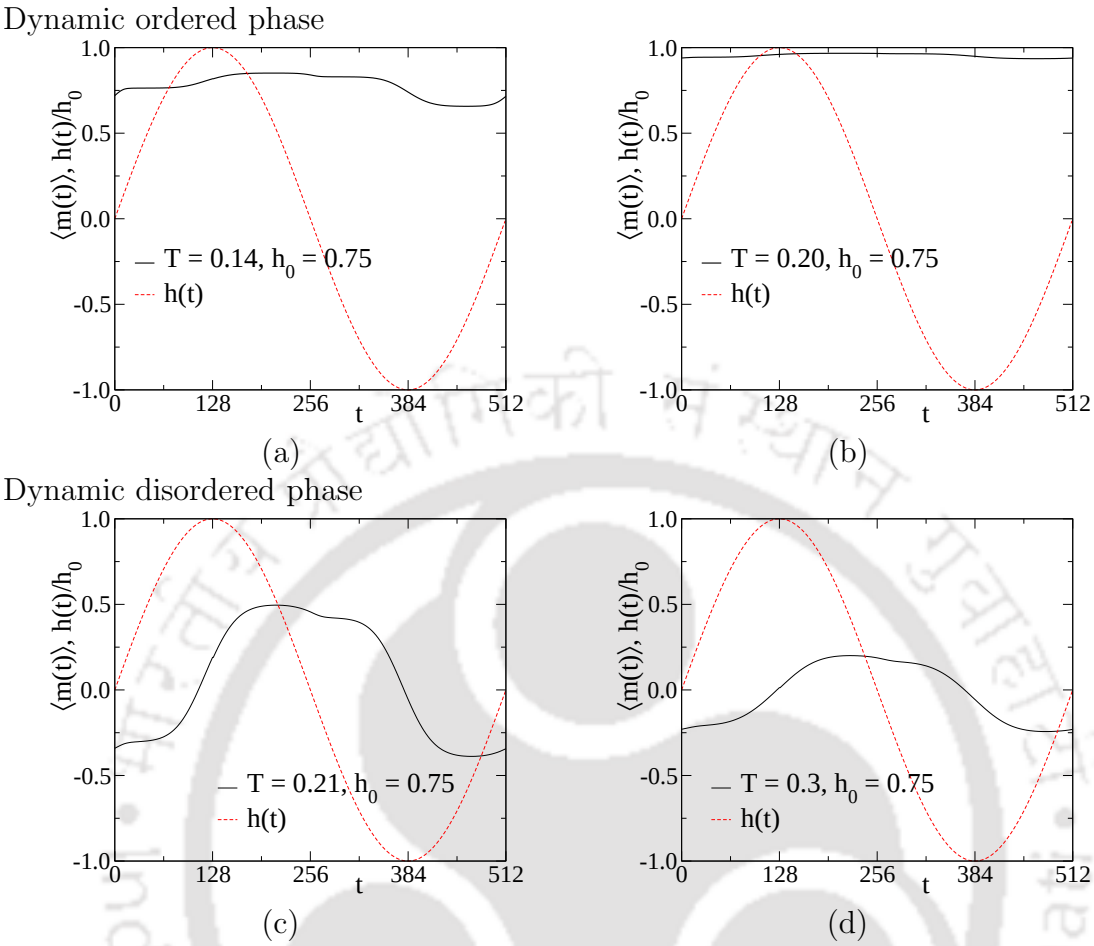

Figure 4.4: Instantaneous magnetization $\langle m(t)\rangle$ with MC step t over a complete cycle of the magnetic field $h(t) = h_0 \sin(2\pi t/P)$ for $h_0 = 0.75, P = 512$ on SPC and SPB for (a) $T = 0.14$, (b) $T = 0.20$ in DOP and (c) $T = 0.21$, (d) 0.30 in DDP respectively on a square lattice of size $L = 512$. The dashed line in red represents the external sinusoidal field.

taneous magnetization for a given cycle is defined as

$$\langle m(t)\rangle = \langle \frac{1}{N_s} \sum_{i=1}^{N_s} S_i(t)\rangle \tag{4.7}$$

where $S_i(t)$ represents the value of the spin at the ith lattice site at time t and $\langle \cdots \rangle$ represents the ensemble average. $N_s = \sum_{i=1}^{L^2} c_i$ is total number of spins. The variation of $\langle m(t)\rangle$ is plotted with MC time step t over a full period in Fig.4.4 on SPC and SPB for $h_0 = 0.75$ and the period $P = 512$. The systems presented in this plot are evolved starting from the all spins up ($S_i = +1$) configurations. Fig.4.4(a), and (b) have plots at lower temperatures whereas the plots in Fig.4.4(c), and (d) have the same in higher temperatures. There are few observations; first, the magnetization

lags behind the magnetic field at all temperatures. This leads to hysteresis loss in the system. Second, the magnetization remains near $+1$ (or -1 if started from the negative metastable phase) for most of the time at low temperatures. Whereas it is continuously varying from a positive to a negative value and vice versa at higher temperatures. Now, a period average magnetization Q can be defined as

$$Q = \frac{1}{P}\int_0^P \langle m(t)\rangle dt \tag{4.8}$$

where P is the time period of the external field. As a result, the system has a non-zero period average magnetization ($Q \neq 0$) (either +ve or $-$ve) at lower temperatures, but it will have a zero period average magnetization ($Q = 0$) at higher temperatures. The system then moves from a non-zero Q to $Q = 0$ as the temperature T is increased from a lower value to a higher value far below the respective zero field ferro-para transition temperature T_c. This observation indicates the existence of two distinct dynamical phases, one called dynamic ordered phase (DOP) with a finite period average magnetization and the other called dynamic disordered phase (DDP) with zero cycle average magnetization. A phase transition from DOP to DDP occurs at a temperature θ_c far below T_c.

The hysteresis loops ($\langle m(t)\rangle$ against $h(t)$) are shown in Fig.4.5(a) $T = 0.14$, and (b) 0.20, and in Fig.4.5(c) $T = 0.21$, and (d) 0.30 to visualize the hysteresis loop at different temperatures on SPC and SPB for fixed field amplitude $h_0 = 0.75$ and $P = 512$. It can be seen that the hysteresis loops about the zero magnetization line are asymmetric for lower temperatures, whereas they become symmetric at higher temperatures. The shape, orientation, and symmetry of the hysteresis loop change as temperature T is increased. The center of the loop moves from a positive finite value to zero with the increase in T. The phase corresponding to the asymmetric hysteresis loop, finite cycle average magnetization (represented by the center of the loop) is the DOP and the phase corresponding to symmetric hysteresis loop, zero cycle average magnetization is the DDP, the transition to DDP from DOP occurs at a temperature θ_c. The evolution of hysteresis loops with T is shown in Fig.4.6 for fractal Ising magnet on spanning percolation cluster on $L = 512$ for fixed $h_0 = 0.75$ and $P = 512$. The asymmetric hysteresis loops remain very flat, almost like a horizontal line parallel to the field axis at very low temperatures. As the T is increased in DOP, the loops acquire some width along the magnetization axis, and the area gradually increases. Near the DPT, hysteresis loops become symmetric for the first time. The hysteresis loop area keeps on increasing even after the DPT. The

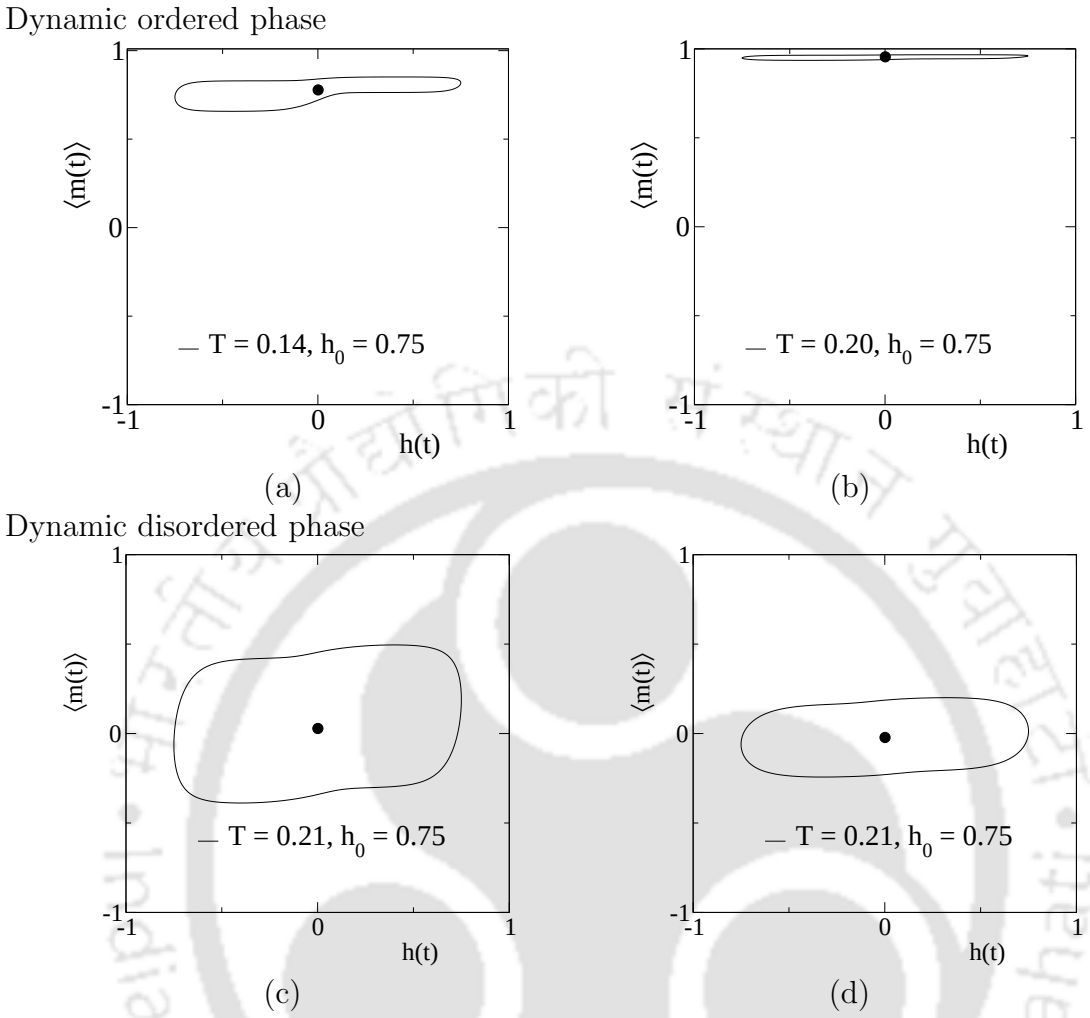

Figure 4.5: Hysteresis loops over a complete cycle of field (time period $P = 512$) on a square lattice of size $L = 512$ on SPC and SPB at temperatures (a) $T = 0.14$, (b) $T = 0.20$ in DOP and (c) $T = 0.21$, (d) 0.30 in DDP respectively. The solid circles represent the centers of the hysteresis loops.

loops rotate while changing their area and shape with increasing temperature. A similar change in the hysteresis loops can be observed in the case of dynamic phase transition in fractal ferromagnet on percolation backbone when the T is varied from a small value in DOP to a high value in DDP.

We can construct a hysteresis loop tensor $\overleftrightarrow{T}$ to describe the hysteresis loops' geometric properties quantitatively such as, hysteresis loops area, shape, and orientation. Here, we will follow the same method to construct $\overleftrightarrow{T}$ as already described in the previous chapters. The hysteresis loop area A of the loop, the average loss in

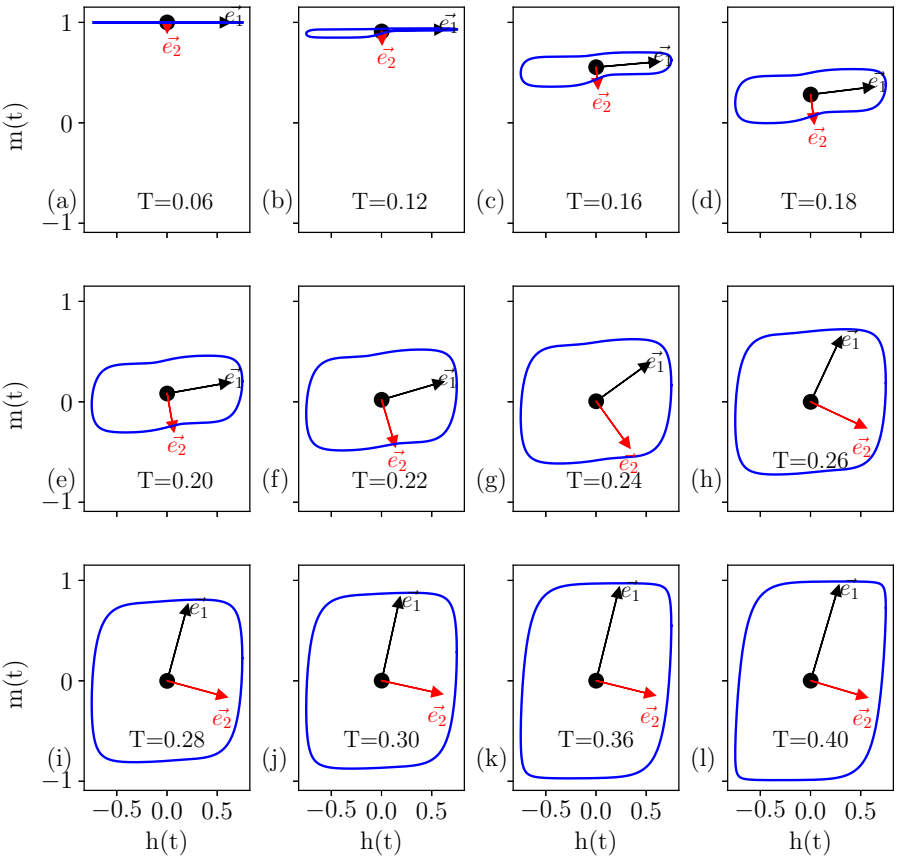

Figure 4.6: Evolution of average hysteresis loops with temperature T over a complete cycle of field on fractal Ising magnet on spanning percolation cluster on $L = 512$ for fixed $h_0 = 0.75$ and $P = 512$. The two eigenvectors are shown in each sub figure, in black and red corresponding to larger (λ_1) and smaller (λ_2) eigenvalues, respectively. The hysteresis loop area, shape, and orientation change as the temperature of the system increases.

magnetic energy over a cycle, is given by

$$A = -\oint m(t)dh(t) \tag{4.9}$$

However, an approximate loop area A can be obtained in terms of the eigenvalues of the hysteresis loop as $A \approx 4\sqrt{\lambda_1\lambda_2}$. The dynamic correlation C is defined as

$$C = \langle m(t)h(t)\rangle - \langle m(t)\rangle\langle h(t)\rangle \tag{4.10}$$

The orientation α can be defined as the angle made by $|e_1\rangle$ corresponding to the eigenvalue λ_1 with the horizontal axis corresponding to field amplitude. The orientation α of the loop with respect to the field axis is then given by

$$\alpha = \tan^{-1}\left(\frac{e_m}{e_h}\right) \tag{4.11}$$

where e_h and e_m are the components of $|e_1\rangle$ along magnetic field and magnetization axes respectively. The shape of the loop can be studied by measuring the aspect ratio of the loop. The aspect ratio Φ of the loop is defined as

$$\Phi = \sqrt{\frac{\lambda_2}{\lambda_1}} \tag{4.12}$$

in terms of eigenvalues λ_1 and λ_2.

The variation of hysteresis loop area A is shown in top row of Fig.4.7 for SPC and SPB in Fig.(a) and (b) for $h_0 = 0.75$, $P = 512$, on different system sizes $L = 128(\bigcirc)$, $256(\diamond)$ and $512(\triangle)$. A does not have any finite size dependence on SPC, but in the case of SPB, it shows a small finite size dependence near the θ_c. The A of asymmetric loops remains very small in DOP, which increases with T and reaches a maximum in DDP [45]. The rate of area increase with T is maximum near the θ_c. A is plotted with reduced temperature $\varepsilon = (T - \theta_c)/\theta_c$ for both SPC and SPB on the largest lattice $L = 512$ for a comparison between the two cases in Fig.(c). As the temperature range slightly different for the SPC and SPB, ε is used. $\varepsilon = 0$ refers to the DPT temperature θ_c. It can be seen that the rate of increase in hysteresis loop areas or loss with T is higher in the case of SPB, but the rate of loss is lower for SPC. The spin-spin correlation becomes weak on SPC due to dangling ends present in it, but spins have better correlations in SPB. Thus a field can more easily alter the spin orientations in the case of SPC, and the rate of loss decreases. When the spin correlation opposes the field, the loss increases.

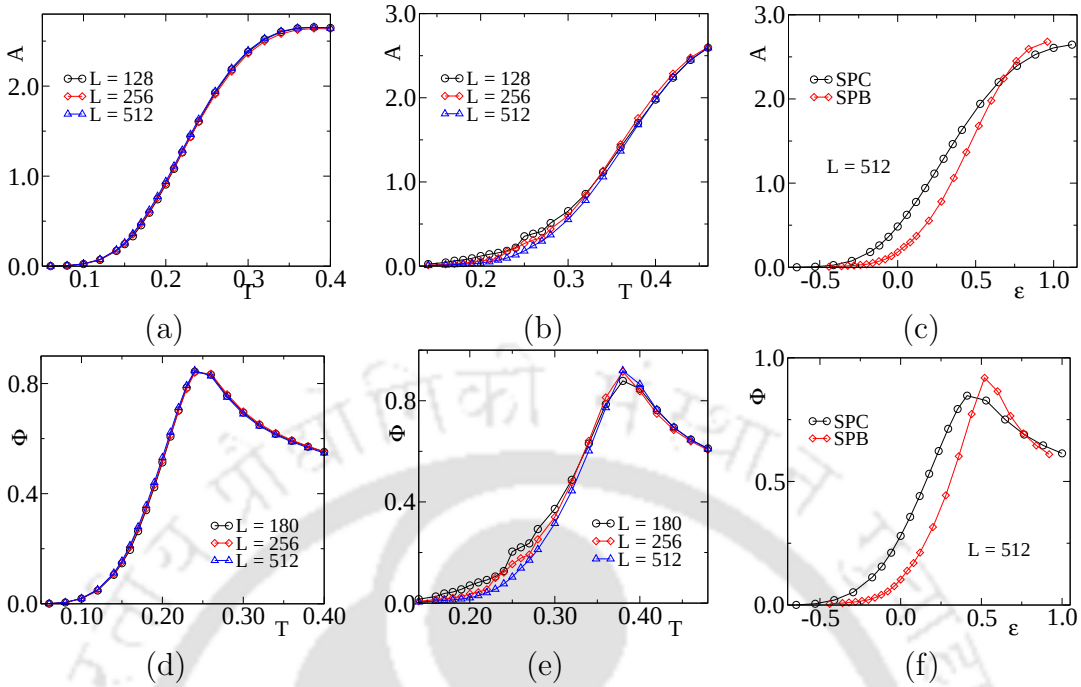

Figure 4.7: Hysteresis loop area A with T is shown on different L for (a) SPC, and (b) SPB. (c) A is plotted with reduced temperature ϵ for the two different cases. In the bottom row, aspect ratio Φ with T is shown on different L for (d) SPC, and (e) SPB. (f) Φ is plotted with reduced temperature ϵ for two different cases.

In Fig. 4.7 (c) and (d) the aspect ratio Φ is shown against T for SPC and SPB, respectively for $h_0 = 0.75$, $P = 512$, on different system sizes $L = 128(\bigcirc)$, $256(\diamond)$ and $512(\triangle)$. The Φ also shows no finite size effects in the case of SPC but has some small finite size effects for PCB near its θ_c. The Φ is small in DOP, corresponding to asymmetric hysteresis loops. Φ increases as the loop area increases with T in DOP. The aspect ratio increases with T even after θ_c, and then starts going down with a further increase in T in DDP. The aspect ratio ϕ with ε is shown in Fig.(e) for SPC and SPB on the largest lattice $L = 512$. The rate of increase of Φ with T as well as the rate of decrease $-d\Phi/d\varepsilon$ is higher in the SPB. The peak value of Φ is taller for SPB. The variation of dynamic correlation C is shown in top row of Fig.4.8 for SPC and SPB in Fig.(a) and (b) for $h_0 = 0.75$, $P = 512$, on different system sizes $L = 128(\bigcirc)$, $256(\diamond)$ and $512(\triangle)$. C does not have any finite size dependence on SPC, but in the case of SPB, it shows a small finite size dependence near the θ_c. The C depicts the effect of the field on the spin system. In the kinetic Ising model on a regular lattice, the C starts from a slightly positive value in DOP and becomes negative near the DPT due to strong spin correlations. After that, with a further rise in T it becomes positive when the field starts dominating overs spins

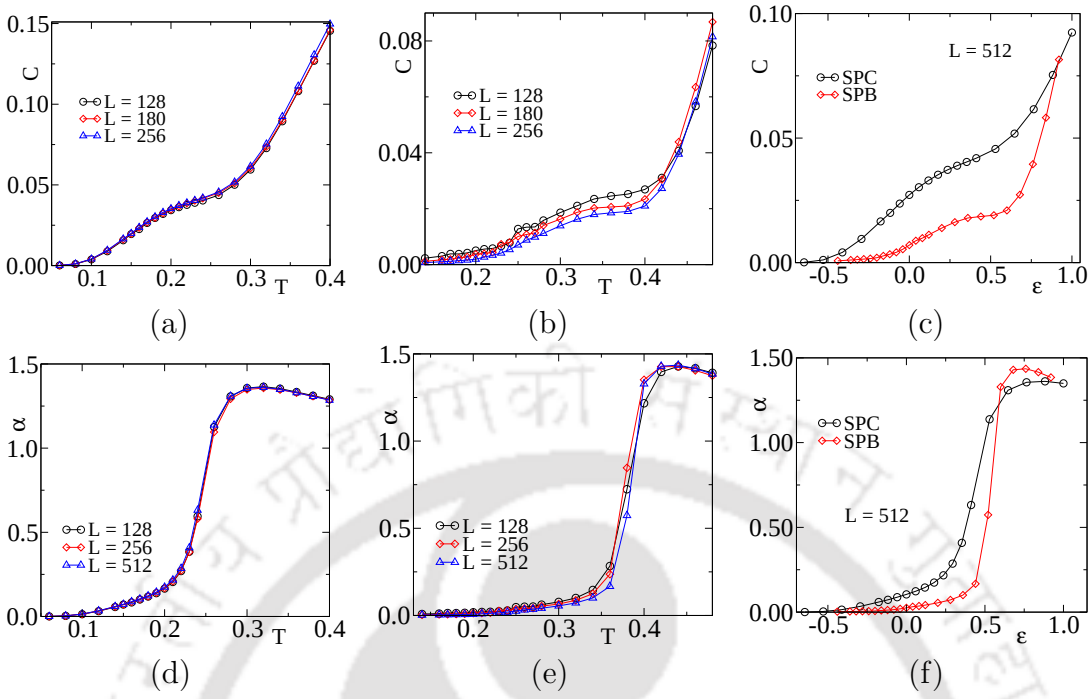

Figure 4.8: Dynamic correlation C with T is shown on different L for (a) SPC, and (b) SPB. (c) C is plotted with reduced temperature ϵ for the two different cases. In the bottom row, hysteresis loop orientation α with T is shown on different L for (d) SPC, and (e) SPB. (f) Φ is plotted with reduced temperature ϵ for two different cases.

as the spin correlations are destroyed due to thermal agitation. Here, we do not see the C assume a negative value. It implies that the field always dominates. The value of C is smaller in DOP due to small but finite ferromagnetic order, which gets destroyed with the increase in T and C value increases with T. The C is plotted with reduced temperature ε for both SPC and SPB on the largest lattice $L = 512$ for a comparison between the two cases in Fig.(c). It can be seen that the C is always higher on SPC. This is the effect of dangling ends present on a SPC, which further helps the field to affect the spins in the system. In Fig. 4.8 (c) and (d) the hysteresis loop orientation α is shown against T for SPC and SPB, respectively for $h_0 = 0.75$, $P = 512$, on different system sizes $L = 128(\bigcirc)$, $256(\diamond)$ and $512(\triangle)$. The α does not show any considerable finite size effects for both SPC and PCB. The α is small in DOP, corresponding to asymmetric tiny hysteresis loops. α increases at the same time when the loop area increases with T in DOP. The α has a sharp rise with T when the field dominance increases further. The loop orientation α with ε is shown in Fig.(e) for SPC and SPB on the largest lattice $L = 512$. The peak value of α is higher for SPB.

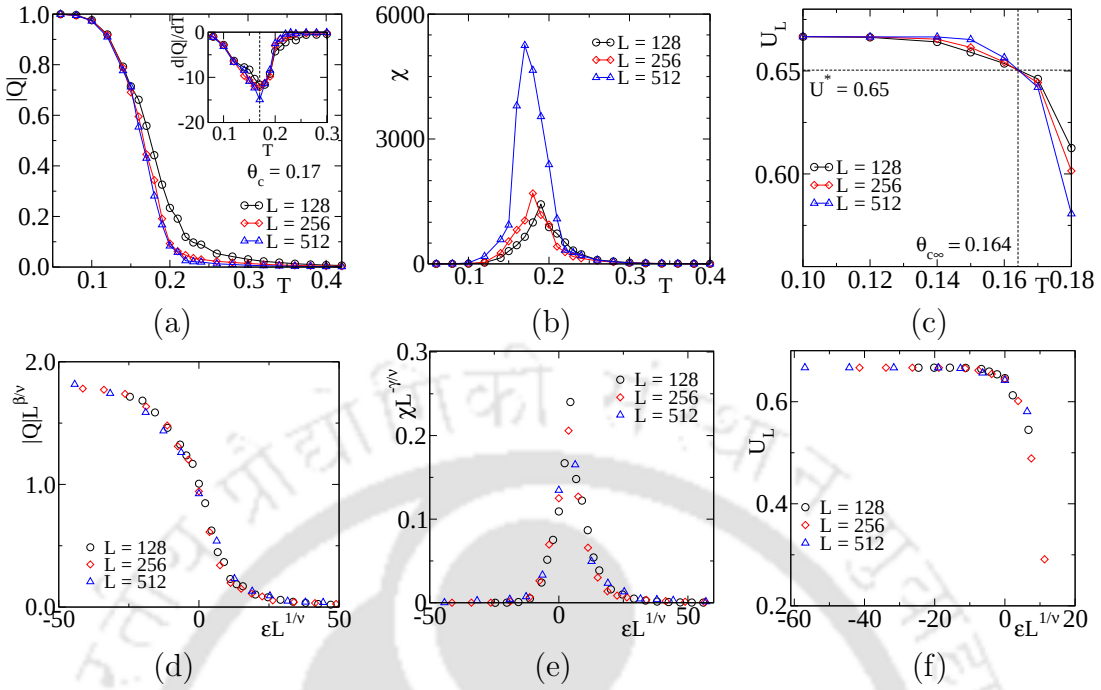

Figure 4.9: Plot of dynamic order parameters $|Q|$, (b) susceptibility χ and (c) Binder cumulant U_L against temperature T for $h_0 = 0.75$ and $P = 512$ on SPC with system sizes $L = 128(\bigcirc)$, $256(\diamond)$ and $512(\triangle)$. $d|Q|/dT$ is plotted with T in the insets of (a). The scaled order parameters, $|Q|L^{\beta/\nu}$, scaled susceptibility $\chi L^{-\gamma/\nu}$, and U_L are plotted against the scaled variable $\varepsilon L^{1/\nu}$ in (d), (e) and (f), respectively.

4.4 Finite size scaling study

We have already seen that the magnetization and the hysteresis loops are different under an external time dependent field while tuning the temperature T of the system for fixed h_0 and P. The system moves from an asymmetric dynamic phase (or DOP) to a symmetric dynamic phase (or DDP) as the temperature T of the system (below the critical temperature T_c) is increased from below θ_c to above θ_c. There is a critical temperature at which DPT occurs. In DOP, the system remains in one of the metastable states, whereas, in DDP, the system moves from one metastable state to the other in a complete cycle. The period average magnetization Q

$$Q = \frac{1}{P}\int_0^P m(t)dt \tag{4.13}$$

is taken as the dynamic order parameter of DPT. The Q could have both positive and negative values in DOP corresponding to two metastable states. We describe a finite size scaling (FSS) theory here considering absolute order parameter $|Q|$. Following the theory of thermal critical phenomena [5, 7], the finite size scaling

(FSS) form of $|Q|$ is assumed to be

$$|Q| = L^{-\beta/\nu}\widetilde{Q}[\varepsilon L^{1/\nu}] \tag{4.14}$$

where $\widetilde{Q}$ is a scaling function, β and ν are the order parameter and correlation length exponents, respectively. The susceptibility χ of the system then can be estimated from the fluctuation of dynamic order parameter $|Q|$ as

$$\chi = L^{d_f}(\langle|Q|^2\rangle - \langle|Q|\rangle^2) \tag{4.15}$$

where $\langle|Q|^n\rangle = \int |Q|^n P_L(|Q|)d|Q|$ and $d_f = 1.89$, and 1.64 for SPC and SPB respectively. The FSS form of χ is then given by

$$\chi = L^{\gamma/\nu}\widetilde{\chi}[\varepsilon L^{1/\nu}] \tag{4.16}$$

where $\widetilde{\chi}$ is a scaling function. γ is the susceptibility exponent. The fourth order Binder cumulant is defined as,

$$U_L = 1 - \frac{\langle Q^4\rangle}{3\langle Q^2\rangle^2} \tag{4.17}$$

and its FSS form is given by

$$U_L = \widetilde{U}[\varepsilon L^{1/\nu}] \tag{4.18}$$

where $\widetilde{U}$ is a universal scaling function.

The temperature variation of dynamic order parameter $|Q|$, susceptibility χ, and Binder cumulant U_L is plotted against T in top row of Fig.4.9 and Fig.4.10 for SPC and SPB, respectively on different system sizes $L = 128(\bigcirc)$, $256(\diamond)$ and $512(\triangle)$ for fixed $h_0 = 0.75$ and $P = 512$. The $|Q|$s shown in Fig.(a) have strong finite system size dependence and change almost similarly both on the SPC and SPB, except they have different θ_c. The value of θ_c is estimated from the temperature where the change of Q with T *i.e.*, $d|Q|/dT$ is maximum. The $d|Q|/dT$ is plotted with T in both cases in the inset, and the θ_cs are determined from the trough in each plot. The values of θ_c found to be 0.17 ± 0.01, and 0.25 ± 0.01 for SPC, and SPB respectively. The θ_c is little higher in the case of SPB in comparison with SPC. The dangling ends surrounded by empty lattice sites in SPC get flipped at a lower T. As a result, T_c becomes a little less on the SPC. Next, we verify the FSS forms of $|Q|$ by plotting the scaled order parameters $|Q|L^{\beta/\nu}$ are plotted against the scaled variable $\varepsilon L^{1/\nu}$ in Fig.(d) for both SPC and SPB. The kinetic Ising model

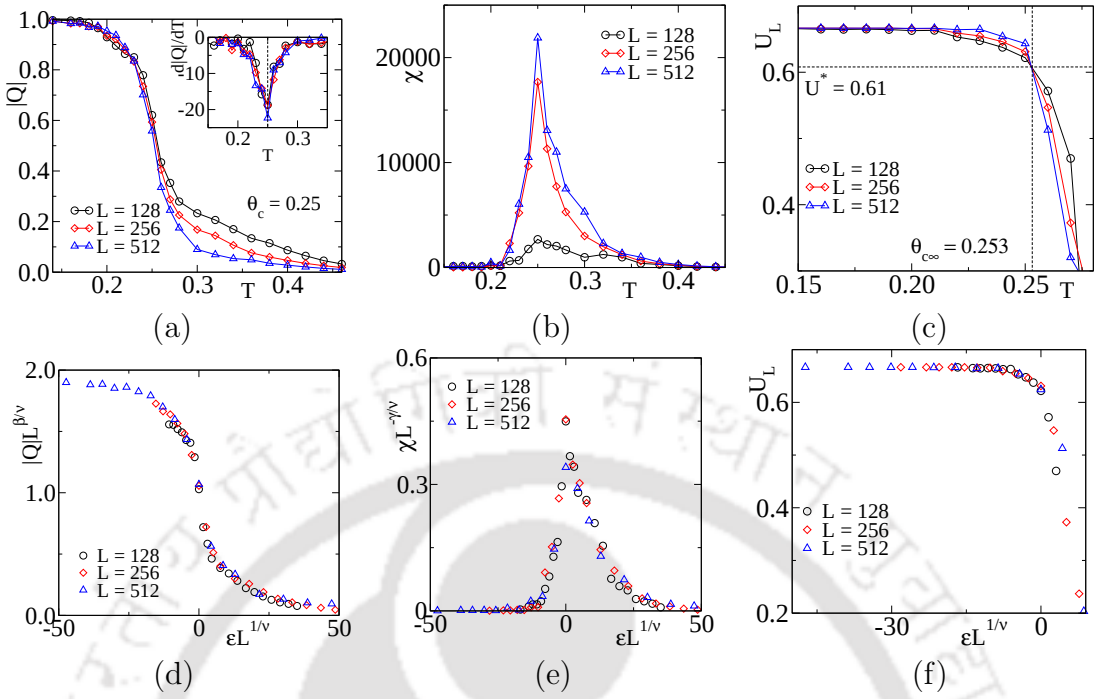

Figure 4.10: Plot of dynamic order parameter $|Q|$, (b) susceptibility χ and (c) Binder cumulant U_L against temperature T for $h_0 = 0.75$ and $P = 512$ on SPB with system sizes $L = 128(\bigcirc)$, $256(\diamond)$ and $512(\triangle)$. $d|Q|/dT$ is plotted with T in the insets of (a). The scaled order parameters, $|Q|L^{\beta/\nu}$, scaled susceptibility $\chi L^{-\gamma/\nu}$, and U_L are plotted against the scaled variable $\varepsilon L^{1/\nu}$ in (d), (e) and (f), respectively.

critical exponents are identical with the equilibrium Ising universality class on 2d regular lattice. However, a good data collapse occurs when the random percolation class's critical exponents are used, $\beta = 5/36$, and $\nu = 4/3$. It is worth mention that the decay of a metastable phase involving nucleation and coalescence mechanism produces transient percolation clusters. There are some past efforts to establish a one to one correspondence between the random percolation model and Ising spin dynamics [125, 126]. In the case of DPT on a SPC and SPB the percolation effects seem predominant.

The susceptibility χ plotted against T shows a peak around the phase transition point θ_c for both SPC and SPB in Fig.(b). The peak is the manifestation of the fact that the system goes through huge fluctuation near the phase transition. The χ has strong finite size effects in both systems. The largest χ value is corresponding to the largest system size in each case as the larger lattice consists of more amount of spins and contributes to maximum fluctuation. The maximum of χ is greater in the case of SPB in comparison with SPC for the largest lattice ($L = 512$). The χ/L^2 for different system sizes are not the same for both SPC and SPB. It indicates the

transition is not of the first order or discontinuous type. The FSS forms of χ are verified with the same set of critical exponents as described above for both different cases. The scaled susceptibility $\chi L^{-\gamma/\nu}$ are plotted against the scaled variable $\varepsilon L^{1/\nu}$ in Fig.(e) of both Fig.4.9 and Fig.4.10. Here, a good collapse of data occurred with critical exponents of the random percolation class ($\gamma = 43/18 \approx 2.39$) while Ising exponents did not show good results.

The U_L is plotted against temperature T in Fig.(c) of Fig.4.9 and Fig.4.10 for SPC and SPB, respectively for different values of L. In each case, U_L corresponding to the different system sizes L cross each other at a temperature. The crossing points are found to be ≈ 0.17, and 0.25 for SPC and SPB, respectively, which are very close to the estimated θ_c from the order parameter in the inset of Fig.(a). The temperature $\theta_{c\infty}$ at which such crossing occurs indicates the phase transition temperature of the system in the thermodynamic limit. The value of U_L at the crossing is found to be $U^* \approx 0.65$ and 0.61 for SPC and SPB. The U_L are plotted against the scaled variable $\varepsilon L^{1/\nu}$ in Fig.(f) in Fig.4.9 and Fig.4.10 for SPC and SPB. The FSS forms of U_L is verified with critical exponent $\nu = 4/3$ of the random percolation class. A good collapse of data is observed.

4.5 Magnetization time series

The study of magnetization time series and the order parameter distribution can help to comprehend the system dynamics in DOP, DPT and DDP in a more insightful manner. In Fig.4.11, selected portion of the magnetization time series $m(t)$ (solid line) and the order parameter distribution are plotted at different temperatures (a) $T = 0.12$, (b) $T = 0.18 \approx \theta_c$ and (c) $T = 0.22$ corresponding to DOP, DPT and DDP on a system of size $L = 512$ for $h_0 = 0.75$, $P = 512$ on SPC. A similar set of magnetization time series are plotted for the SPB in Fig.4.12 (a) $T = 0.20$, (b) $T = 0.26 \approx \theta_c$ and (c) $T = 0.30$ corresponding to DOP, DPT and DDP on a system of size $L = 512$ for fixed $h_0 = 0.75$, $P = 512$. The $\langle\tau\rangle$ is always larger than the half period $P_{1/2}$ in DOP in all the cases. As a result, the system can not come out from the metastable well it is already in and $m(t)$ shows a small fluctuation about a finite non-zero value (see Fig.(a) of both figures) but does not cross zero. The corresponding distribution (histogram) of the order parameter Q is shown in Fig.(d). It is evident from the distribution that the system remains trapped in either of the wells. As temperature increases, the average metastable lifetime $\langle\tau(T, h_0)\rangle$ becomes comparable with the half period of the external field $P_{1/2}$ and DPT occurs.

The situation is described in Fig.(b) and (e). The $m(t)$ varies from a positive value to

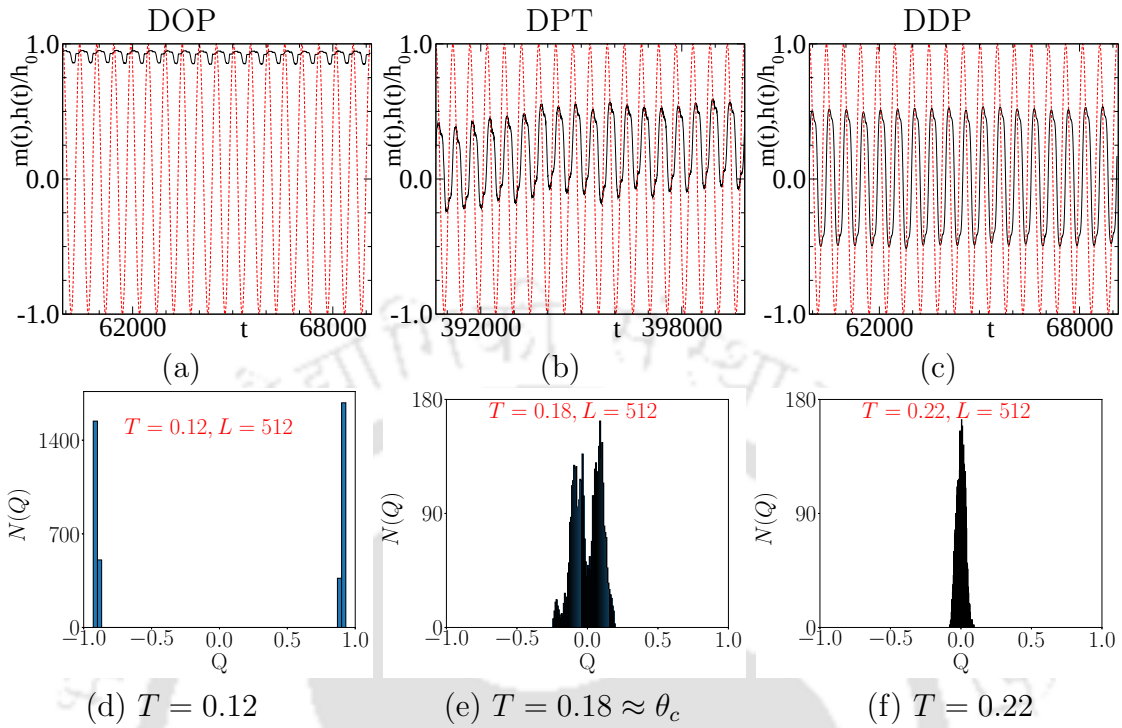

Figure 4.11: Plot of magnetization time series $m(t)$ against MCS (t) at different temperatures (a) $T = 0.12$ (DOP), (b) $T = 0.18$ (around DPT) and (c) $T = 0.22$ (DDP) on a SPC of size $L = 512$ for $h(t) = h_0 \sin(2\pi t/P)$, with $h_0 = 0.75$ and $P = 512$. The corresponding distribution of Q are given in (d), (e) and (f) respectively. Histograms are obtained for 2048 order parameters Q over 60 equispaced bins.

a negative value (or negative to positive) and crosses zero, as shown in Fig.(b). Note that $m(t)$, however, does not reach a value $+1$ or -1. The distribution of Q (Fig.(e)) have peaks around $\pm|Q|_c$. At this point, when the cycle average magnetization is still finite, the external field can move the system from one well to the other smoothly. Usually, in large systems, it corresponds to the MD regime [34, 36, 90]. There is one remarkable difference in the fractal magnets compared to the regular kinetic Ising system is the value of $|Q|_c$. The fractal magnets are strongly diluted and highly dominated by the external field having a very weak ferromagnetic order. So, the peak of $m(t)$s around θ_c is small compared to the regular Ising system. As a result, the $|Q|_c$s are also very small, and the peak to peak separation ($\Delta_p = 2|Q|_c$) is quite small in the fractal Ising model than a regular kinetic Ising model. The Δ_p is the smallest at θ_c in a SPC due to its dangling ends. The value of Δ_p improves a little in SPB.

In DDP, $\langle\tau\rangle$ is smaller than the $P_{1/2}$, $m(t)$ follows the external field with certain phase lag changes from close to $+1$ to close to -1 as shown in Fig.(c). Most of

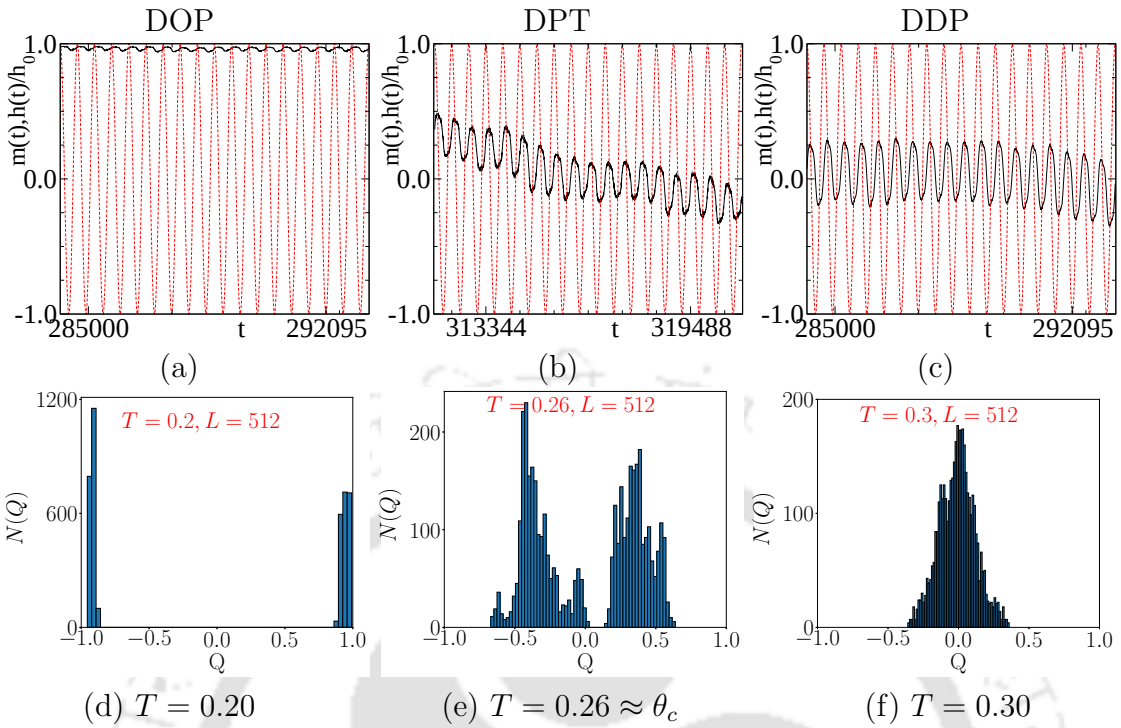

Figure 4.12: Plot of magnetization time series $m(t)$ against MCS (t) at different temperatures (a) $T = 0.20$ (DOP), (b) $T = 0.26$ (around DPT) and (c) $T = 0.30$ (DDP) on a SPB of size $L = 512$ for $h(t) = h_0 \sin(2\pi t/P)$, with $h_0 = 0.75$ and $P = 512$. The corresponding distribution of Q are given in (d), (e) and (f) respectively. Histograms are obtained for 2048 order parameters Q over 60 equispaced bins.

the states arise at $Q = 0$, and the distribution $N(Q)$ has a single peak around zero Q as shown in Fig.(f). Both the DPT on a SPC and SPB at fixed field intensity $h_0 = 0.75$, $P = 512$ on the systems of size $128, 256$ and 512 are found to exhibit continuous DPT.

4.6 Summary and Discussion

The nonequilibrium DPT is studied on the 2d kinetic Ising ferromagnet developed on two random fractals - spanning percolation cluster (SPC) and percolation backbone (SPB) on several system sizes $L = 128, 256$, and 512 using Monte Carlo methods. A small finite transition temperature T_c is observed for both SPC and SPB. The value of T_c in SPB is slightly higher than that of SPC as the dangling ends surrounded by empty sites of SPC can be easily flipped with little thermal energy or external field, whereas SPB has no such dangling ends. Nonequilibrium DPT is studied below respective T_cs on SPC and SPB tuning the temperature T at fixed field amplitude $h_0 = 0.75$, and period $P = 512$. The $m(t)$ follows the field $h(t)$ with a

certain phase delay. As a result, hysteresis loops too appear in fractal Ising systems. Below respective θ_c, the hysteresis loops remain asymmetric in DOP, which becomes symmetric in DDP with an increase in T. The θ_c of SPB, $\theta_c = 0.25$ is slightly higher than that of SPC $\theta_c = 0.17$. The hysteresis loop properties, such as loop area A, dynamic correlation C, orientation α, and aspect ratio Φ are evaluated from the geometry of the loops. The hysteresis loops transform from asymmetric in DOP to symmetric in DDP while hysteresis loop area A, aspect ratio Φ and orientation α increase with T. The rate of change of A and Φ with T are enhanced in SPB due to a stronger spin correlation than SPC. The dynamic correlation C always remains positive, unlike the regular Ising system or even system with random spin dilution up to $q = 0.1$ and 0.2. It is the manifestation of strong external field dominance in SPC and SPB. The C is found to be further higher in SPC. The α shows a jump at a higher T value where spin-spin correlations are lost. The values of Q_c around θ_c in SPC and SPB come out small compared to a regular lattice as the maximum value of $m(t)$ in either metastable well is smaller due to weak ferromagnetic order. The peak-to-peak separation Δ_p in the distribution of order parameters around θ_c becomes smaller in the case of fractal Ising systems. The Δ_p is even smaller in SPC than SPB. A detailed FSS study shows that the order parameter $|Q|$, susceptibility χ, and Binder cumulant U_L obey the finite size scaling. Reasonably good data collapse is observed for FSS variables using the scaling exponents of the random percolation class (not the Ising class) for both SPC and SPB. In the limit $p \to p_c$ and $T \to 0$, it is known that the percolation exponents replace all critical exponents of the Ising model [120]. However, the existence of finite low T_c of SPC and SPB and its critical behavior needs to be verified by a detailed numerical study on larger systems.

Chapter 5

Summary and Conclusion

The nonequilibrium dynamic phase transition (DPT) and hysteresis are studied on 2d Ising ferromagnet on the regular square lattice, random diluted disordered lattice, and random fractals. Phase transitions are studied either varying the temperature T of the system for fixed field amplitude h_0 and period P or varying the period P of the external field at fixed field amplitude h_0 and T. A new methodology is described to study the geometrical aspects of the hysteresis loops as well as DPT. Extensive numerical work with a detailed finite-size study (FSS) is carried out to explore nonequilibrium DPT using the Monte Carlo technique on systems of size L varying from 64 to 1024. A brief review of the equilibrium phase transition in the Ising model, features of dynamic phase transition, and hysteresis in bistable Ising ferromagnet is described in Chapter 1. A thorough survey of existing literature on DPT in the magnetic system is made in the introduction chapter before posing the thesis problems with appropriate motivations. Below we summarize the effect of an external field, temperature, and dilution on DPT in the ferromagnetic Ising model on different square lattices in 2d.

In Chapter 2, we study temperature varied DPT in 2d regular kinetic Ising ferromagnet through an extensive Monte Carlo study under an external sinusoidal external field for different field amplitudes $h_0 = 1.0, 2.0$, and 3.0 on several system sizes. The period of the field $P = 512$ is kept constant throughout the study. The DPT occurs when the average metastable lifetime becomes comparable to the half-period of the external field. We have estimated the average τ at different T for a fixed h_0 of sinusoidal a field and estimated θ_c, the critical temperature of DPT (below T_c), corresponding to a given h_0. Both the asymmetric hysteresis loops in DOP and symmetric loops in DOP change their area, shape, and orientation as the system evolves from DOP to DDP. We quantify the hysteresis loop related quantities

in a newly developed methodology to study the DPT from the changing geometry of the hysteresis loops. The known DPT related quantities are also recalculated using the new method. The nature of DPT remained ambiguous for a long time, whether the DPT is a continuous type phase transition or not. We observed stochastic resonance behavior at the high field regime on the smaller system size. However, a similar study on higher system size shows the DPT under sinusoidal field is indeed a second-order phase transition. Finite-size scaling analysis, the variation of fourth order Binder cumulant at several system sizes, and distribution of order parameters are reported to support the findings. We conclude that the DPT under sinusoidal external field on 2d is a second-order phase transition with the critical exponents belonging to the 2d equilibrium Ising model. The stochastic resonance behavior at high field regime was just a finite system size effect on smaller lattices that do not persist on larger systems.

Spin diluted systems are abundantly found in nature. DPT on a diluted Ising ferromagnet is rarely reported. We study the nonequilibrium DPT on the 2d site diluted Ising ferromagnet on several system sizes varying the T for fixed h_0 and P as well as varying P of the external field keeping T and h_0 constant in Chapter 3. The dilution q has nontrivial effects on the spin system. The critical temperature of DPT $\theta_c(q)$ and the critical period $P_c(q)$ of DPT are found to reduce with increasing dilution. The hysteresis loops below θ_c or P_c remain asymmetric in DOP, and above, they become symmetric as moved to DDP. As q increases, the rate of change in hysteresis loop area A and aspect ratio Φ reduces as the spin-spin correlation diminishes. The dynamic correlation C, which manifests the external field's influence on a correlated spin system, increases with higher dilution. A detailed FSS analysis on the diluted system shows continuous phase transition from DOP to DDP for both the DPT varied temperature and period. The scaling exponents in FSS variables are verified under the weak universality hypothesis and the strong universality hypothesis. The diluted Ising model's DPT seems to belong to the same universality class as the equilibrium diluted Ising system. The exponents vary slightly from that of a regular system. Scaled variables show good data collapse with these scaling exponents.

The work on Ising ferromagnet on random fractal is described in Chapter 4, where we study DPT on Ising ferromagnet in two different random fractals, spanning percolation cluster (SPC) and spanning percolation backbone (SPB). Assigning Ising spins to the fractal lattice sites, we obtain the random fractal Ising model. Though it is expected that as $p \to p_c$, T_c should tend to zero, a small finite transition

temperature T_c is found in the equilibrium ferro to paramagnetic phase transition for both SPC and SPB when studied numerically. The T_c of SPB is found to be a little higher than SPC. Expecting that a ferromagnetic phase exists below this low T_c, DPT and hysteresis analysis has been performed on these fractal lattices. A few new features are obtained. However, a further detailed numerical study should be carried out on larger system sizes to conclude the existence of ferromagnetic phase at finite T and the precise nature of the DPT on the fractal Ising models.

The researches reported in this thesis can be further be extended in several directions. For example, DPT on a binary mixture Ising spins having two different kinds of spins interaction strength can be studied. The variation of relative interaction strength can lead to novel behavior.

Bibliography

[1] N. Ashcroft and N. Mermin, *Solid state physics*, Saunders College, 1976.

[2] J. M. D. Coey, *Magnetism and Magnetic Materials*, Cambridge University Press, 2010.

[3] N. A. Spaldin, *Magnetic Materials: Fundamentals and Applications*, Cambridge University Press, 2010.

[4] S. Kaul, J. Magn. Magn. Mater **53**, 5 (1985).

[5] H. Stanley, *Introduction to Phase Transition and critical Phenomena*, Oxford University Press, New York, 1987.

[6] J. M. Yeomans, *Statistical Mechanics of Phase Transition*, Oxford University Press, New York, 1997.

[7] M. N. Barber, Finite-size scaling, in *Phase Transitions and Critical Phenomena, Vol. 8*, edited by C. Domb and J. L. Lebowitz, Academic Press, New York, 1988.

[8] C. Domb and J. L. Lebowitz, *Phase Transitions and Critical Phenomena*, Academic Press, New York, 1972 onwards.

[9] J. J. Binney, N. J. Dowrick, A. Fisher, and M. E. J. Newman, *The Theory of Critical Phenomena*, Oxford University Press, New York, 1992.

[10] L. Onsager, Phys. Rev. **65**, 117 (1944).

[11] M. Henkel, H. Hinrichsen, and S. Lübeck, *Non-Equilibrium Phase Transitions, Volume 1: Absorbing Phase Transitions*, Springer Netherlands, 2008.

[12] G. Ódor, *Universality in Nonequilibrium Lattice Systems*, World Scientific, 2008.

[13] B. Schmittmann, R. K.-p. Zia, J. L. Lebowitz, and C. Domb, *Phase transitions and critical phenomena Volume 17, Statistical mechanics of driven diffusive systems*, Academic Press, New York, 1995.

[14] G. L. Daquila and U. C. Täuber, Phys. Rev. Lett. **108**, 110602 (2012).

[15] I. Mayergoyz, Foreword, in *Hysteresis in Magnetism*, edited by G. Bertotti, Electromagnetism, page xi, Academic Press, San Diego, 1998.

[16] J. A. Ewing, Proc. R. Soc. London **33**, 21 (1881).

[17] E. Warburg, Annalen der Physik und Chemie (Neue Folge) **13**, 141 (1881).

[18] J. A. Ewing, Proc. R. Soc. London **34**, 39 (1882).

[19] C. P. Steinmetz, Trans. Am. Inst. Electr. Eng. **9**, 3 (1892).

[20] A. Aharoni, *Introduction to the Theory of Ferromagnetism*, Clarendon Press, Oxford, 1996.

[21] H. M. Duiker and P. D. Beale, Phys. Rev. B **41**, 490 (1990).
[22] M. Rao and R. Pandit, Phys. Rev. B **43**, 3373 (1991).
[23] A. Cheng and M. Caffrey, The Journal of Physical Chemistry **100**, 5608 (1996).
[24] S. W. Sides, P. A. Rikvold, and M. A. Novotny, Phys. Rev. E **57**, 6512 (1998).
[25] M. Acharyya and B. K. Chakrabarti, Phys. Rev. B **52**, 6550 (1995).
[26] B. K. Chakrabarti and M. Acharyya, Rev. Mod. Phys. **71**, 847 (1999).
[27] M. Acharyya and D. Stauffer, Eur. Phys. J. B **5**, 571 (1998).
[28] J. D. Gunton and M. Droz, *Introduction to the Theory of Metastable and Unstable States*, Springer-Verlag Berlin Heidelberg, 1983.
[29] R. Becker and W. Döring, Ann. Physik (5th sequence, Leipzig) **24**, 719 (1935).
[30] D. Stauffer, A. Coniglio, and D. W. Heermann, Phys. Rev. Lett. **49**, 1299 (1982).
[31] K. Binder, Phys. Rev. A **25**, 1699 (1982).
[32] K. Binder and H. Müller-Krumbhaar, Phys. Rev. B **9**, 2328 (1974).
[33] H. Tomita and S. Miyashita, Phys. Rev. B **46**, 8886 (1992).
[34] P. A. Rikvold, H. Tomita, S. Miyashita, and S. W. Sides, Phys. Rev. E **49**, 5080 (1994).
[35] S. W. Sides, R. A. Ramos, P. A. Rikvold, and M. A. Novotny, Journal of Applied Physics **79**, 6482 (1996).
[36] S. W. Sides, R. A. Ramos, P. A. Rikvold, and M. A. Novotny, Journal of Applied Physics **81**, 5597 (1997).
[37] S. W. Sides, P. A. Rikvold, and M. A. Novotny, Phys. Rev. E **59**, 2710 (1999).
[38] T. Tomé and M. J. de Oliveira, Phys. Rev. A **41**, 4251 (1990).
[39] M. Acharyya, Int. J Mod Phys. C **16**, 1631 (2005).
[40] M. Rao, H. R. Krishnamurthy, and R. Pandit, Phys. Rev. B **42**, 856 (1990).
[41] W. S. Lo and R. A. Pelcovits, Phys. Rev. A **42**, 7471 (1990).
[42] D. Dhar and P. B. Thomas, Journal of Physics A: Mathematical and General **25**, 4967 (1992).
[43] M. Acharyya, Phys. Rev. E **56**, 1234 (1997).
[44] M. Acharyya, Phys. Rev. E **56**, 2407 (1997).
[45] M. Acharyya, Phys. Rev. E **58**, 179 (1998).
[46] Muktish Acharyya, Physica A: Statistical Mechanics and its Applications **253**, 199 (1998).
[47] M. Acharyya, Phys. Rev. E **58**, 174 (1998).
[48] G. M. Buendía and P. A. Rikvold, Phys. Rev. E **78**, 051108 (2008).
[49] G. Korniss, C. J. White, P. A. Rikvold, and M. A. Novotny, Phys. Rev. E **63**, 016120 (2000).
[50] G. Korniss, P. A. Rikvold, and M. A. Novotny, Phys. Rev. E **66**, 056127 (2002).
[51] L. Gammaitoni, P. Hänggi, P. Jung, and F. Marchesoni, Rev. Mod. Phys. **70**, 223 (1998).
[52] M. Acharyya, Phys. Rev. E **59**, 218 (1999).
[53] H. Park and M. Pleimling, Phys. Rev. Lett. **109**, 175703 (2012).
[54] H. Park and M. Pleimling, Phys. Rev. E **87**, 032145 (2013).

[55] E. Vatansever and H. Polat, Dynamic phase transitions in a ferromagnetic thin film system: A monte carlo simulation study, 2015.
[56] E. Vatansever and N. G. Fytas, Phys. Rev. E **97**, 062146 (2018).
[57] O. Idigoras, P. Vavassori, and A. Berger, Physica B: Condensed Matter **407**, 1377 (2012), 8th International Symposium on Hysteresis Modeling and Micromagnetics (HMM 2011).
[58] R. A. Gallardo, O. Idigoras, P. Landeros, and A. Berger, Phys. Rev. E **86**, 051101 (2012).
[59] H. Fujisaka, H. Tutu, and P. A. Rikvold, Phys. Rev. E **63**, 036109 (2001).
[60] D. T. Robb and A. Ostrander, Phys. Rev. E **89**, 022114 (2014).
[61] B. O. Aktas, U. Akinci, and H. Polat, Phys. Rev. E **90**, 012129 (2014).
[62] G. M. Buendía and E. Machado, Phys. Rev. E **58**, 1260 (1998).
[63] S. W. Sides, P. A. Rikvold, and M. A. Novotny, Phys. Rev. Lett. **81**, 834 (1998).
[64] Y.-L. He and G.-C. Wang, Phys. Rev. Lett. **70**, 2336 (1993).
[65] Q. Jiang, H.-N. Yang, and G.-C. Wang, Phys. Rev. B **52**, 14911 (1995).
[66] J.-S. Suen and J. L. Erskine, Phys. Rev. Lett. **78**, 3567 (1997).
[67] B. C. Choi, W. Y. Lee, A. Samad, and J. A. C. Bland, Phys. Rev. B **60**, 11906 (1999).
[68] D. T. Robb et al., Phys. Rev. B **78**, 134422 (2008).
[69] A. Berger, O. Idigoras, and P. Vavassori, Phys. Rev. Lett. **111**, 190602 (2013).
[70] P. Riego, P. Vavassori, and A. Berger, Phys. Rev. Lett. **118**, 117202 (2017).
[71] G. M. Buendía and P. A. Rikvold, Phys. Rev. B **96**, 134306 (2017).
[72] N. Metropolis, A. W. Rosenbluth, M. N. Rosenbluth, A. H. Teller, and E. Teller, The Journal of Chemical Physics **21**, 1087 (1953).
[73] R. J. Glauber, Journal of Mathematical Physics **4**, 294 (1963).
[74] M. E. J. Newman and G. T. Barkema, *Monte Carlo Methods in Statistical Physics*, Oxford University Press, New York, 2001.
[75] K. Binder and D. Heermann, *Monte Carlo Simulation in Statistical Physics*, Springer-Verlag Berlin Heidelberg, 2010.
[76] D. Stauffer and A. Aharony, *Introduction To Percolation Theory: Second Edition*, Taylor & Francis, 1992.
[77] A. Bunde and S. Havlin, *Fractals and Disordered Systems*, Springer-Verlag Berlin Heidelberg, 1996.
[78] K. Christensen and N. R. Moloney, *Complexity and Criticality*, Imperial College Press and World Scientific Publishing Co., 2005.
[79] P. L. Leath, Phys. Rev. B **14**, 5046 (1976).
[80] W.-G. Yin and R. Tao, Physica B: Condensed Matter **279**, 84 (2000).
[81] T. Tomé and M. J. de Oliveira, Phys. Rev. A **41**, 4251 (1990).
[82] K. Binder and D. Heermann, *Monte Carlo Simulation in Statistical Physics*, Springer-Verlag Berlin Heidelberg, 2010.
[83] J.-C. Walter and G. Barkema, Physica A: Statistical Mechanics and its Applications **418**, 78 (2015).

[84] A. Ghosh and B. K. Chakrabarti, Journal of Statistical Mechanics: Theory and Experiment **2013**, P11015 (2013).
[85] G. Bertotti and I. Mayergoyz, The science of hysteresis, pages ix – x, Academic Press, Oxford, 2006.
[86] G.-P. Zheng and M. Li, Phys. Rev. B **66**, 054406 (2002).
[87] A. D. Bruce and N. B. Wilding, Phys. Rev. Lett. **68**, 193 (1992).
[88] G. Kamieniarz and H. W. J. Blote, Journal of Physics A: Mathematical and General **26**, 201 (1993).
[89] K. K. Mon, Phys. Rev. B **55**, 38 (1997).
[90] H. L. Richards, M. A. Novotny, and P. A. Rikvold, Phys. Rev. B **54**, 4113 (1996).
[91] H. G. Ballesteros et al., J. Phys. A: Math. Gen. **30**, 8379 (1997).
[92] H. G. Ballesteros et al., Phys. Rev. B **58**, 2740 (1998).
[93] P. H. L. Martins and J. A. Plascak, Phys. Rev. E **76**, 012102 (2007).
[94] J.-K. Kim and A. Patrascioiu, Phys. Rev. Lett. **72**, 2785 (1994).
[95] R. Kenna and J. J. Ruiz-Lorenzo, Phys. Rev. E **78**, 031134 (2008).
[96] B. Shalaev, Physics Reports **237**, 129 (1994).
[97] C. Jayaprakash, E. K. Riedel, and M. Wortis, Phys. Rev. B **18**, 2244 (1978).
[98] Y. L. Loh and E. W. Carlson, Phys. Rev. Lett. **97**, 227205 (2006).
[99] M. Hasenbusch, F. P. Toldin, A. Pelissetto, and E. Vicari, Phys. Rev. E **78**, 011110 (2008).
[100] A. R. Rivera, G. A. Perez Alcazar, and J. A. Plascak, Phys. Rev. B **41**, 4774 (1990).
[101] W. Zhong, G. T. Barkema, and D. Panja, Phys. Rev. E **102**, 022132 (2020).
[102] I. Syozi, Progress of Theoretical Physics **34**, 188 (1965).
[103] J. W. Essam and H. Garelick, Proceedings of the Physical Society **92**, 136 (1967).
[104] G. Mazzeo and R. Kühn, Phys. Rev. E **60**, 3823 (1999).
[105] V. V. Prudnikov and O. N. Markov, Eur. Phys. Lett. **29**, 245 (1995).
[106] R. B. Stinchcombe, in *Phase transitions and critical phenomena, Vol. 7*, edited by C. Domb and J. L. Lebowitz, Academic Press, London, 1983.
[107] W. Selke, L. N. Shchur, and A. L. Talapov, Monte carlo simulation of dilute ising model, in *Annual Reviews of Computational Physics I*, edited by D. Stauffer, World Scientific, 1995.
[108] D. P. Belanger, Brazilian Journal of Physics **30**, 682 (2000).
[109] A. B. Harris, J. Phys. C: Solid State Physics **7**, 1671 (1974).
[110] H.-O. Heuer, Phys. Rev. B **45**, 5691 (1992).
[111] H.-O. Heuer, Journal of Physics A: Mathematical and General **26**, L333 (1993).
[112] H.-O. Heuer, Phys. Rev. B **42**, 6476 (1990).
[113] Ümit Akıncı, Y. Yüksel, E. Vatansever, and H. Polat, Physica A Stat. Mech. Appl **391**, 5810 (2012).
[114] E. Vatansever, Ümit Ak nc, Y. Yüksel, and H. Polat, J. Magn. Magn. Mater **329**, 14 (2013).
[115] D. P. Landau, Phys. Rev. B **22**, 2450 (1980).
[116] N. G. Fytas and P. E. Theodorakis, Phys. Rev. E **82**, 062101 (2010).

[117] J. Marro, A. Labarta, and J. Tejada, Phys. Rev. B **34**, 347 (1986).
[118] V. V. Prudnikov, P. V. Prudnikov, A. N. Vakilov, and A. S. Krinitsyn, Journal of Experimental and Theoretical Physics **105**, 371 (2007).
[119] H. E. Stanley, R. J. Birgeneau, P. J. Reynolds, and J. F. Nicoll, J. Phys. C: Solid State Physics **9**, L553 (1976).
[120] W. Klein and A. Coniglio, Physics Letters A **84**, 83 (1981).
[121] A. Coniglio, Phys. Rev. Lett. **46**, 250 (1981).
[122] M. Kaufman and J. E. Touma, Phys. Rev. B **49**, 9583 (1994).
[123] C. L. Henley, Phys. Rev. Lett. **54**, 2030 (1985).
[124] Y. Gefen, B. B. Mandelbrot, and A. Aharony, Phys. Rev. Lett. **45**, 855 (1980).
[125] C.-K. Hu, Phys. Rev. B **29**, 5103 (1984).
[126] W. G. Wanzeller, T. Mendes, and G. A. Krein, Brazilian Journal of Physics **36**, 657 (2006).

List of Publications

1. *"Kinetic Ising model under sinusoidal oscillating external magnetic field: hysteresis and dynamic phase transition"*, Sourav Chattopadhyay and S. B. Santra, The Eur. Phys. J. B., **94**, 72 (2021).

2. *"Study of fractal Ising magnet with nearest and next nearest neighbour interactions"*, Sourav Chattopadhyay and S. B. Santra, AIP. Conf. Proc. **1953**, 040008 (2018).

3. *"Disorder induced hysteresis in diluted kinetic Ising model"*, Sourav Chattopadhyay and S. B. Santra, Journal of Physics: Conference Series **759**, 012011 (2016).

4. *"Hysteresis loop analysis to study dynamic phase transition"*, Sourav Chattopadhyay and S. B. Santra, AIP. Conf. Proc. **1731**, 030022 (2016).

5. *"Dynamic phase transition in diluted Ising model"*, Sourav Chattopadhyay, Gopal Gorai and S. B. Santra, AIP Conf. Proc. **1665**, 030017 (2015).

6. *"Hysteresis and dynamic phase transition in diluted kinetic Ising model"*, Sourav Chattopadhyay and S. B. Santra, manuscript under preparation.

7. *"Dynamic phase transition in Ising magnet on random fractals"*, Sourav Chattopadhyay and S. B. Santra, manuscript under preparation.

Conference attended

1. *International Conference on Condensed Matter and Applied Physics 2017*, **Bikaner**, Rajasthan, India.
2. *Statphys Kolkata IX 2016*, **SINP Kolkata**, India.
3. *XXVII IUPAP Conference on Computational Physics 2015*, **IIT Guwahati**, Assam, India.
4. *DAE Solid State Physics Symposium (DAE-SSPS-2015) BARC* - **Amity University**, Noida, India.
5. *DAE Solid State Physics Symposium (DAE-SSPS-2014) BARC* - **VIT**, Vellore, India.